DYNAMICS AND EVOLUTION OF PLANETARY NEBULAE

Stephen John Meatheringham

Mount Stromlo and Siding Spring Observatories,

The Australian National University

January, 1988

A thesis submitted for the degree of

Doctor of Philosophy

of The Australian National University

To my parents, whose support
and encouragement enabled me
to get this far.

And to Frances, for all her
precious love and support,
and patience throughout the
last three years.

CONTRIBUTION OF CANDIDATE

This thesis consists of five papers; one of which has been published, three that have been accepted for publication and are in press, and the final one submitted for publication. The contributions of the candidate to the content of these papers is described below. All sections not specifically mentioned are the work of the candidate alone.

Paper 1 The observations were carried out by the candidate with Drs. Dopita and Ford. Drs. Dopita, Ford and Webster made constructive suggestions with respect to the text of the paper.

Paper 2 Section IV, the discussion on the energy increase in the nebula is due to Dr. Dopita.

Paper 3 The observations were carried out by the candidate with Drs. Dopita and Webster. Both the candidate and Dr. Dopita contributed equally to the content of the paper.

Paper 4 The paper is the work of the candidate alone.

Paper 5 The observations were carried out by Drs. Wood and Faulkner, who both made constructive suggestions with respect to the text of the paper.

Stephen J. Meatheringham

ACKNOWLEDGEMENTS

I would firstly like to thank my supervisor *Michael Dopita* for the substantial scientific input he has injected into this thesis. Without his most welcome support and enthusiasm for this project the work would not have the value it does. I am also very grateful to my co-supervisor *Peter Wood* for his valuable insights and discussions.

I would like to thank the former director of the Mount Stromlo and Siding Spring Observatories (MSSSO) *Donald Mathewson*, and the present director *Alex Rodgers*, for allowing me the use of the excellent facilities of the observatories.

I thank the *Time Assignment Committee* of MSSSO for the allocation of observing time on the 1-metre and 2.3-metre telescopes at Siding Spring Observatories; and the *Australian Time Allocation Committee* of the *Anglo-Australian Observatory* for time on the 3.9-metre telescope, to pursue the observing requirements needed for this work.

Finally, I would like to thank the *academic staff members* of MSSSO, my *fellow students* and all the other *support staff* of the observatories for their help and friendship over the past four most enjoyable years.

Financial support for this work was provided by an Australian Commonwealth Postgraduate Research Award, for which I am grateful.

It is in the stillness of the midnight hour,
when all nature is hushed in repose,
when the hum of the world's on-going is no longer heard,
that the planets roll and shine,
and the bright stars, drooping through the deep heavens,
speak to the willing spirit that would learn their mysterious being.

O.M. Mitchell, 1862

ABSTRACT

A data-base of optical nebular information is presented for a large fraction of the population of planetary nebulae (PN) in the Small and Large Magellanic Clouds (SMC and LMC). Radial velocities and nebular expansion velocities measured from the [O III] λ5007 line have been determined for a total of 94 nebulae in the LMC. Expansion velocities and nebular electronic densities have been measured for a total of 44 nebulae in both Clouds from the [O II] $\lambda\lambda 3727, 3729$ doublet, and absolute Hβ nebular fluxes are presented for 97 objects.

A re-analysis of the H I survey by Rohlfs *et al.* (1984) is presented, taking into account the transverse velocity of the Large Magellanic Cloud, which is found to be 275 ± 65 km s^{-1}. The LMC is near perigalacticon, and this is consistent with a maximum Galactic mass of order $M_{gal} = 4.5 \times 10^{11} \mathcal{M}_{\odot}$. The H I rotation curve obtained after correction for the transverse velocity implies a mass of $M_{LMC} = (4.6 \pm 0.3) \times 10^{9} \mathcal{M}_{\odot}$, within a radius of 3 degrees of the centroid, or about $6 \times 10^{9} \mathcal{M}_{\odot}$ in total. Rotation solutions obtained from the PN and H I radial velocities are found to be identical, with the exception that the vertical velocity dispersion of the PN (19.1 km s^{-1}) is much larger than the H I (5.4 km s^{-1}). This increase in velocity dispersion is consistent with it arising from orbital heating and diffusion, and if this is the case it implies these processes occur in the LMC in a manner essentially the same as what is found for the solar neighbourhood.

New evolutionary correlations have been found to apply to the PN populations in the Magellanic Clouds. Firstly, a relationship between ionized mass and nebular density is seen to exist. For those objects which are expected to be optically thick $M_{neb} \propto n_e^{-1}$. This, together with a relationship between density and Hβ flux indicates at what density nebulae become optically thin. Optically thick nebulae follow a mass–radius relation of the form $M_{neb} \propto R^{3/2}$, while optically thin nebulae evolve at approximately constant ionized mass. Secondly, the age of the nebular shell is found to follow a relationship $\tau_{dyn} = 890(M_{neb}V_{exp})^{0.6}$ years. This is consistent with a model in which the total energy of the ionized and swept-up gas drives the nebular expansion down the density gradient in the precursor Asymptotic Giant Branch (AGB) star wind. Thirdly, a relationship is found between expansion velocity, and a combination of Hβ flux and excitation class, which appears to be determined by the mass of the PN nuclear star. These last two correlations provide strong evidence that PN shells are ejected initially at a low velocity during the AGB phase of evolution, and continually accelerated throughout their lifetimes. Fourthly, the PN populations of the Clouds lie in a sheet in dynamical age / excitation class / density space. This implies that the nebular parameters are entirely determined by properties of the central star, and as such may present a basis for a solution to the Galactic distance scale problem for PN.

Radial velocities and expansion velocities derived from the [O III] λ5007, [O II] $\lambda\lambda$3727,3729, and He II λ4686 lines are presented for a sample of 64 Southern Galactic planetary nebulae. Nebular densities are calculated for 23 of these objects from the [O II] doublet. The correlation between dynamical age, excitation class and density derived from the Magellanic

Cloud nebulae is used to determine distances and radii to 33 of these nebulae. The distances compare favourably with the Daub (1982) and Maciel (1984) scales. Ionized masses are derived and found to exhibit a large range between $10^{-3}\mathcal{M}_{\odot}$ and $0.6\mathcal{M}_{\odot}$. These objects cover the same area in the nebular mass–radius plane as their counterparts in the Magellanic Clouds and Galactic Center.

REFERENCES

Daub, C.T., 1982, *Ap. J.*, **260**, 612.

Maciel, W.J., 1984, *Astr. Ap. Suppl.*, **55**, 253.

Rohlfs, K., Kreitschmann, J., Siegmann, B.C., and Feitzinger, J.V. 1984, *Astr. Ap.*, **137**, 343.

TABLE OF CONTENTS

INTRODUCTION

As far back as 1785 William Herschel noted that the small, greenish nebulae appeared to form a distinct subset of diffuse nebulae, and due to their resemblance to planetary disks he named them planetary nebulae (PN). In 1928 Perrine, and separately Zanstra, were the first to point out that splitting of certain emission lines in the spectra of PN was due to an expansion of the nebula. This, together with measured radii gave an indication of the short lifetimes of PN and was the first evidence that this was a very brief stage of stellar evolution that a large majority of all stars probably passed through. Since then the idea that PN are approximately spherical expanding shells has been built-up by many authors (eg. Wilson 1950; Osterbrock *et al.* 1966).

Today, some 60 years after Perrine, we know quite well the overall evolution of a star from a red giant, through the Asymptotic Giant Branch phase, on to a planetary nebula, and finally to the realm of the white dwarfs. However, there are still a number of fundamental problems involved in the study of PN. A major reason for this is that dynamical studies of the nebular shell and associated central star have, in the past, been concerned solely with Galactic PN, with all the concomitant problems of uncertain distances, population type, and reddening. Unfortunately, very few PN are close enough to have their distances measured by methods not relying on certain assumptions about the properties of the nebula or central star (see Pottasch 1984 for a discussion of this problem). Distances to some Galactic PN are so poorly known that various authors quote and use distances often differing by factors of up to two or three. It is this uncertainty in distances that tends to mask and confuse true correlations and relationships between

the various nebular and stellar parameters. For example, no clear consensus has yet emerged on what is the trend of expansion velocity with nebular radius. Robinson, Reay, and Atherton (1982) suggest that high and low mass PN have different relationships; while Phillips (1984) finds basically a monotonic relationship, and yet other authors suggest a maximum in expansion velocity at radii of order 0.2 pc with a slow decline to larger sizes (eg. Sabbadin, Bianchini and Hamzaoglu 1984). Another problem concerns the masses of PN nuclei. Schonberner (1981) studied evolution from the Asymptotic Giant Branch and concluded it was possible to assign only a very narrow range about 0.58 $\mathcal{M}_{\odot}$ to the central stars, but Wood and Faulkner (1986) find theoretical evidence for masses up to 0.9 $\mathcal{M}_{\odot}$. The majority of known Galactic PN nuclei, when plotted on a Hertzsprung–Russell (HR) diagram fall in a region below 0.6 $\mathcal{M}_{\odot}$ (Pottasch 1983). However, placement of the stars on an HR diagram relies on a knowledge of their absolute luminosity, and this in turn on their distance, and reddening.

A possible solution to the problem of trying to deal with the uncertain distances involved in studying Galactic PN presents itself in the form of the Large and Small Magellanic Clouds (LMC and SMC). There are some 170 PN known in the LMC and 64 in the SMC. These two galaxies furnish us with a luminosity limited sample of PN. The Magellanic Clouds are at distances known to an accuracy of order 20%, or better, and have a low line-of-sight reddening. However, there is the drawback of nebular sizes. At the distance of the Clouds all but the largest few objects are unresolved from the ground, and hence, we must rely on indirect determinations of nebular radius (Wood, Dopita and Bessell 1986; Wood, Meatheringham, Dopita and Morgan 1987), or relationships not explicitly involving size.

This thesis has grown as the major part of a ground-based optical survey of the kinematics and internal dynamics of the planetary nebula populations in the Magellanic Clouds. The large observational data-base built-up during the course of this work is presented in the first four sections of the thesis. Other related papers in this study include : Dopita *et al.* (1985a, b), Wood *et al.* (1986, 1987).

This dissertation is organized into five papers, each of which has been published, is currently in press, or has been submitted for publication. The first paper studies the kinematics of the Large Magellanic Cloud, using the planetary nebula population. It compares the PN, an old population, to the H I, a young population. The H I survey of Rohlfs *et al.* (1984) is re-analyzed and the transverse velocity of the LMC calculated. Correction for this velocity allows a determination of the mass of the LMC from the H I rotation curve. The rotation solutions of the H I and PN are found to be identical, except that the PN have a much larger vertical velocity dispersion. This increase in velocity dispersion, if the result of diffusion, indicates these processes operate in a similar manner in the LMC to the solar neighbourhood. The second paper examines two evolutionary correlations found to apply to the PN in the Magellanic Clouds. The first shows that a correlation exists between the dynamical age and net momentum of the ionized gas. The second is between expansion velocity, Hβ flux, and excitation class, and this is determined by the mass of the central star. A discussion of the consequences of these correlations is presented. The third paper also deals with evolutionary correlations derived from the various nebular parameters. A fractional thickness of the ionized shell is determined from the ratio of [O III] to [O II] expansion velocities.

The population of PN lies in a sheet in dynamical age / excitation class / density space. As dynamical age and density are purely nebular quantities, and the excitation class is determined by the central star temperature, this implies the nebular parameters are determined by properties of the central star. This relation presents a basis for a possible solution to the Galactic distance scale problem for PN. The fourth paper presents the Hβ flux data, and examines the interrelationships between density, flux and mass. A critical density is found below which nebulae appear to become optically thin to Hydrogen ionizing radiation. The optically thick nebulae have a mass–radius relation of the form $M_{neb} \propto R^{3/2}$, while optically thin nebulae seem to evolve at constant, or decreasing ionized mass. The final paper looks at a sample of Southern Galactic PN and presents new radial velocities, expansion velocities and densities for them. These new data together with published fluxes and angular sizes allow a determination of distances, radii and masses using the correlation found in the third paper. These distances are found to be comparable to the Daub (1982) and Maciel (1984) scales. The ionized masses cover the same range as found for Galactic Centre and Magellanic Cloud objects.

REFERENCES

Dopita, M.A., Ford, H.C., Lawrence, C.J. and Webster, B.L. 1985a, *Ap. J.*, **296**, 390.

Dopita, M.A., Ford, H.C. and Webster, B.L. 1985b, *Ap. J.*, **297**, 593.

Daub, C.T. 1982, *Ap. J.*, **260**, 612.

Maciel, W.J. 1984, *Astr. Ap. Suppl.*, **55**, 253.

Osterbrock, D.E., Miller, J.S. and Weedman, D.W. 1966, *Ap. J.*, **145**, 697.

Phillips, J.P. 1984, *Astr. Ap.*, **137**, 92.

Pottasch, S.R. 1983, in *IAU Symposium 103, Planetary Nebulae*, ed. D.R. Flower, (Dordrecht : Reidel), p. 391.

Pottasch, S.R. 1984, in *Planetary Nebulae*, (Dordrecht : Reidel), p. 95.

Robinson, G.J., Reay, N.K. and Atherton, P.D. 1982, **199**, 649.

Rohlfs, K., Kreitschmann, J., Siegmann, B.C., and Feitzinger, J.V. 1984, *Astr. Ap.*, **137**, 343.

Sabbadin, F., Bianchini, A. and Hamzaoglu, E. 1984, *Astr. Ap.*, **136**, 200.

Schonberner, D. 1981, *Astr. Ap.*, **103**, 119.

Wilson, O.C. 1950, *Ap. J.*, **111**, 279.

Wood, P.R., Dopita, M.A., and Bessell, M.S. 1986, *Ap. J.*, **311**, 632.

Wood, P.R., and Faulkner, D.J. 1986, *Ap. J.*, **307**, 659.

Wood, P.R., Meatheringham, S.J., Dopita, M.A., and Morgan, D.H. 1987, *Ap. J.*, **320**, 178.

THE KINEMATICS OF THE PLANETARY NEBULAE IN THE LARGE MAGELLANIC CLOUD

Stephen J. Meatheringham, Michael A. Dopita

Mount Stromlo and Siding Spring Observatories,

Australian National University

Holland C. Ford

Space Telescope Science Institute,

Johns Hopkins University

B. Louise Webster

School of Physics,

University of New South Wales

Received: 1987 January 31

Accepted: 1987 October 10

To appear in *Astrophysical Journal*, 1988, April 15.

ABSTRACT

The radial velocities of a total of 94 planetary nebulae (PN) in the Large Magellanic Cloud (LMC) have been determined. This kinematics of the population of planetary nebulae is compared with the H I data in the context of a re-analysis of the survey by Rohlfs *et al.* (1984), taking into account the transverse velocity of the LMC. We find that the best solution for this transverse velocity is 275 ± 65 km s^{-1}, and that the LMC is near perigalacticon. This is consistent with a maximum Galactic mass of order $4.5 \times 10^{11} \mathcal{M}_{\odot}$ out to 51 kpc. The rotation curve obtained after correction for this velocity implies a mass of $(4.6 \pm 0.3) \times 10^{9} \mathcal{M}_{\odot}$ within a radius of 3 degrees, or about $6 \times 10^{9} \mathcal{M}_{\odot}$, total. The rotation solution for the PN population is essentially identical with that of the H I, but the vertical velocity dispersion of 19.1 km s^{-1} is much greater than the value of 5.4 km s^{-1} found for the H I. This increase in velocity dispersion is consistent with it being the result of orbital heating and diffusion operating in the LMC in a manner essentially identical with that found for the solar neighbourhood.

Subject Headings: galaxies : Magellanic Clouds, masses
nebulae : planetary

I. INTRODUCTION

The Magellanic Clouds hold the solution to many of the unanswered questions about planetary nebulae (PN) by furnishing us with a large luminosity limited sample at a common and known sample, with low reddening, and close enough that it can be observed in detail. Previous papers in our studies of the Magellanic Cloud PN have tended to concentrate on evolutionary problems of the PN themselves (Dopita *et al.* 1985; Dopita, Ford and Webster 1985; Dopita *et al.* 1987, 1988; Meatheringham *et al.* 1988; Wood, Bessell and Dopita 1985; Wood *et al.* 1987).

Both the SMC and the LMC are of considerable interest from a kinematical viewpoint. The tidal interaction of the Clouds with each other and with the Galaxy appears to have been quite significant in recent times (Murai and Fujimoto 1980). The SMC in particular appears to have been considerably disrupted by a recent close passage to the LMC (Mathewson and Ford 1984; Mathewson 1984; Mathewson, Ford and Visvanathan 1986). Our survey of the kinematics of the PN in the SMC suggests that the stellar component has certainly been randomized, but that gaseous tidal arms project from the stellar core of the SMC (Dopita *et al.* 1985). For the LMC, Freeman, Illingworth and Oemler (1983) report the enigmatic finding that the young and old populations have significantly different rotation solutions. The old population of clusters has its line of nodes rotated by some 49 degrees with respect to the younger clusters with ages less than 10^9 years. The data on the planetary nebulae were sparse but appeared to be in agreement with the 'young' solution.

The PN form a population with an age intermediate between the H I and young clusters and the old Population II clusters, and therefore a detailed study of their kinematics might be expected to cast new light on this problem. Previous to the results reported in this paper, there have been only three kinematic studies of the LMC PN, which together furnish radial velocities for some 35 objects. In this paper we present new kinematical data for a total of 95 objects. By combining this data with a re-analysis of the H I survey of Rohlfs *et al.* (1984), we have been able to estimate the transverse velocity of the LMC, generate a new rotation curve and mass estimate for the LMC, and have derived a typical age and precursor mass for the population of PN in the LMC.

II. OBSERVATIONS AND DATA REDUCTION

a) Selection of Objects

The majority of the objects we have observed appear in the list of Sanduleak, McConnell and Philip (SMP) (1978) which gives 102 PN in the LMC and 28 in the SMC. Many of these were previously known to be emission nebulae (Henize 1956; Lindsay and Mullen 1963) and a fair number had been positively identified as PN by Henize and Westerlund (1963). Throughout this paper we have identified objects by their SMP number, this being the the most comprehensive and unambiguous listing to date. The Jacoby (J) (1980) objects present a more difficult group. Many of these are faint, and could not be definitely confirmed as PN even with the AAT 3.9-metre telescope at the dispersion we were using. Only five objects gave data of sufficiently high quality to be included here. Recently

Morgan and Good undertook a search for LMC planetary nebulae using an objective prism on the UK Schmidt Telescope at Siding Spring. We observed, and confirmed, a total of seven new candidates in the northern part of the LMC in a list of 31.

The spatial distribution of the observed PN is shown in Figure 1, along with outer H I contours from Mathewson and Ford. There is little difference between the spatial locations of the PN and the H I in this diagram.

b) The Observations and Results

We have used three telescopes, two spectrographs and two photon-counting systems in this study. Observations in October and November 1983 and October 1984 were with the 1.0-metre telescope at Siding Spring Observatory, and observations in January 1985 used the 2.3-metre Advanced Technology Telescope at Siding Spring. Both of these telescopes are operated by the Australian National University. The spectrograph was a Perkin-Elmer échelle and the detector the Photon-Counting Array (PCA) (Stapinski, Rodgers and Ellis 1981). The faintest objects were observed in December 1983 using the 3.9-metre Anglo-Australian Telescope (AAT) with its Royal Greenwich Observatory spectrograph and the Image Photon Counting System (IPCS).

The instrumental parameters and the reduction procedures have already been described (Dopita *et al.* 1985) and will not be repeated here. The resolutions of both systems are very similar, 11.5 km s^{-1} FWHM for the échelle system, and 11.75 km s^{-1} FWHM for the AAT system. For objects with a high signal to noise, and with relatively narrow line profiles, our

Figure 1. The spatial distribution of the LMC planetaries. Filled circles represent the SMP (1978) objects, open circles the Morgan (1984) objects, and crosses the Jacoby (1980) nebulae. Outer H I contours from Mathewson and Ford (1984) are also shown (units of atoms cm^{-2} in line of sight).

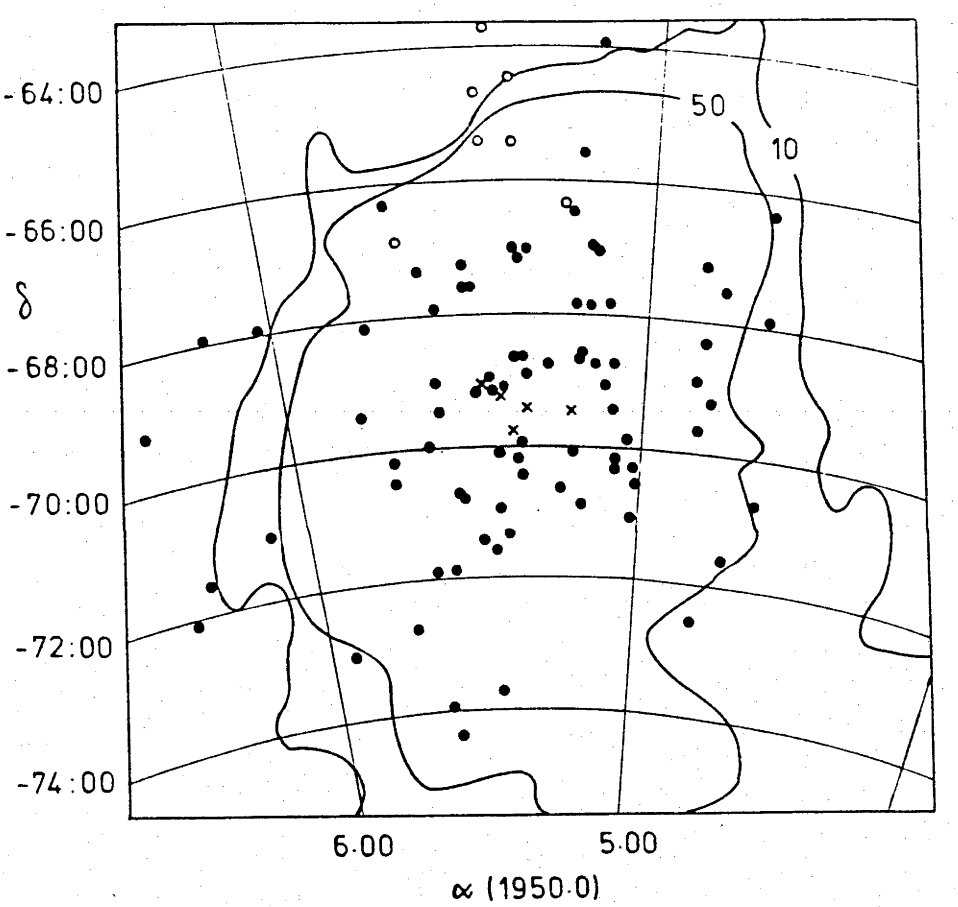
-64:00
-66:00
δ
-68:00
-70:00
-72:00
-74:00
50
10
6·00
5·00
α (1950·0)

estimated ultimate errors in the determination of radial velocities are ± 1.5 km s^{-1} for the 1.0-metre observations, ± 0.6 km s^{-1} for the 2.3-metre data, and ± 0.3 km s^{-1} in the case of the AAT measurements (see also Dopita *et al.* 1985). For those those objects with large expansion velocities measurement errors are greater, and can been estimated as $\pm\sigma/N^{1/2}$, where σ is the e-folding width of the gaussian fit and N is the number of photons in the profile (Bevington 1969). With this definition, we find that the maximum error could be as large as 4.8 km s^{-1}. This error can be checked for those objects for which repeated observations exist. In the following list, the difference between the individual determinations is given in units of km s^{-1}. Shown in parentheses is the error estimated in the manner given above. SMP 5, 0.03 (0.1); SMP 6, 0.09 (0.2); SMP 11, 2.42 (1.8); SMP 21, 1.35 (1.4); SMP 23, 0.4 (0.7); SMP 47, 0.72 (0.9); SMP 94, 3.33 (3.0); J 26, 3.83 (2.7); J 33, 1.72 (1.9). The mean ratio of the observed velocity difference to the expected error is 0.87, compared with a figure of 0.95 expected for a gaussian distribution of errors.

In Table 1 we present the measured radial velocities, corrected to Local Standard of Rest (LSR), positions the telescopes used in the observations and our estimated error for each object. The radial velocity given is the area weighted mean in the cases were more than one gaussian component was needed to fit the profile. It might be argued that, in the case of those objects which show two separated components, the simple mean might have been a more accurate representation of the radial velocity. In these cases the radial velocity given by this procedure is shown in parentheses.

TABLE 1

RADIAL VELOCITY DATA FOR LMC PLANETARY NEBULAE

Object Name[1]	RA (1950.0)	Dec	V_{lsr}	Telescope
SMP 1	4 38 59.9	-70 42 32	209.1 ± 0.2	b
SMP 2	4 41 00.4	-67 53 49	248.2 ± 0.2	b
SMP 3	4 42 12.8	-66 18 47	172.0 ± 0.2	b
SMP 4	4 43 57.6	-71 35 40	283.0 ± 1.1	b
SMP 5	4 48 08.3	-67 31 18	271.0 ± 0.1 (271.2)	a,b
SMP 6	4 48 27.7	-72 33 33	249.0 ± 0.2	a,b
SMP 7	4 48 43	-69 13 34	204.9 ± 1.9	a
SMP 8	4 50 31.3	-69 38 58	277.1 ± 0.8	a
SMP 9	4 50 35	-68 18 31	270.7 ± 1.1	a
SMP 10	4 51 20.6	-68 54 02	207.0 ± 1.4 (207.1)	a
SMP 11	4 51 35.8	-67 10 15	249.4 ± 1.8 (273.2)	a,c
SMP 13	5 00 34	-70 31 11	212.3 ± 1.5	a
SMP 14	5 00 54.5	-71 03 10	236.9 ± 2.6	c
SMP 15	5 01 19.4	-70 17 57	188.0 ± 1.2	a
SMP 16	5 02 24.8	-69 53 03	237.5 ± 1.5	a
SMP 18	5 04 13	-70 11 01	228.7 ± 1.4	a
SMP 19	5 04 16	-70 18 03	220.2 ± 0.8	a
SMP 20	5 04 59.3	-69 25 39	273.1 ± 1.7	a
SMP 21	5 05 05.1	-68 43 08	243.7 ± 1.4 (232.4)	a,c
SMP 23	5 06 15.0	-67 49 21	268.0 ± 0.7	a
SMP 24	5 06 34.0	-69 03 24	254.7 ± 3.5	c
SMP 27	5 08 00	-67 01 12	258.2 ± 2.2	a
SMP 28	5 08 11.9	-68 55 35	233.7 ± 2.4	c
SMP 29	5 08 17.4	-68 44 03	228.2 ± 0.8	a
SMP 30	5 09 18	-66 57 26	264.9 ± 1.0 (264.3)	a
SMP 31	5 09 26.4	-67 51 08	248.1 ± 0.4	a
SMP 32	5 10 11.7	-70 52 50	240.2 ± 1.7	a
SMP 33	5 10 26	-68 33 49	253.9 ± 1.0	a

TABLE 1 (Continued)

RADIAL VELOCITY DATA FOR LMC PLANETARY NEBULAE

Object Name[1]	RA (1950.0)	Dec	V_{lsr}	Telescope
SMP 35	5 10 45	-65 33 02	295.0 ± 1.0 (297.8)	a
SMP 36	5 10 51	-68 39 48	247.6 ± 2.6	a
SMP 37	5 11 14	-67 50 57	255.2 ± 1.5	a
SMP 38	5 11 51	-70 04 46	225.4 ± 0.9	a
SMP 40	5 12 11.7	-66 26 25	238.9 ± 1.9 (237.0)	a
SMP 41	5 13 59.1	-70 36 55	244.2 ± 1.9 (265.1)	a
SMP 42	5 16 02	-68 45 36	273.4 ± 1.7	a
SMP 45	5 19 22.2	-67 01 10	275.0 ± 1.0	a
SMP 46	5 19 45.6	-68 54 07	258.0 ± 1.0	c
SMP 47	5 20 17.8	-69 34 00	256.6 ± 0.9 (249.5)	a,b
SMP 48	5 20 35.5	-69 56 34	240.8 ± 0.2	a
SMP 49	5 20 30	-70 27 01	232.2 ± 1.2 (235.7)	a
SMP 50	5 20 54.5	-67 08 37	284.1 ± 1.2	a
SMP 51	5 21 22.0	-70 12 24	256.4 ± 0.5	a
SMP 52	5 21 38.8	-68 38 27	256.9 ± 1.0	a
SMP 53	5 21 37	-67 01 00	261.8 ± 0.7	a
SMP 54	5 21 58.6	-68 42 10	265.4 ± 1.7 (278.1)	a,b
SMP 55	5 23 22.8	-71 21 52	194.7 ± 0.3	a
SMP 56	5 23 50.4	-69 06 45	276.1 ± 0.4	c
SMP 57	5 24 01	-69 14 00	297.7 ± 1.1	a
SMP 58	5 24 36	-70 06 00	264.2 ± 0.3	a
SMP 60	5 24 53.7	-70 56 34	207.0 ± 4.8	a
SMP 61	5 25 48.8	-73 43 18	178.4 ± 0.9	a
SMP 62	5 25 40.6	-71 35 29	223.6 ± 0.5	a
SMP 63	5 25 44.3	-68 58 30	248.8 ± 0.4	a
SMP 65	5 28 13	-71 27 00	195.7 ± 0.9	a
SMP 66	5 28 49	-67 35 00	289.2 ± 1.1	a

TABLE 1 (Continued)

RADIAL VELOCITY DATA FOR LMC PLANETARY NEBULAE

Object Name[1]	RA (1950.0)	Dec	V_{lsr}	Telescope
SMP 67	5 29 22.7	-67 35 07	274.1 ± 0.9	a
SMP 69	5 29 24	-67 15 01	289.9 ± 2.9	a
SMP 71	5 30 48	-70 46 01	201.2 ± 0.5	a
SMP 73	5 31 36	-70 42 00	225.6 ± 0.4	a
SMP 74	5 33 54	-71 53 00	253.6 ± 1.1	a
SMP 76	5 34 06.1	-67 55 06	262.8 ± 0.9 (268.9)	a
SMP 77	5 34 29.8	-69 28 13	328.2 ± 0.3	a
SMP 78	5 34 39.6	-69 00 19	240.7 ± 1.1	a
SMP 79	5 34 55	-74 22 00	215.1 ± 0.8	a
SMP 81	5 36 07	-73 56 00	242.2 ± 1.1	a
SMP 82	5 36 26.5	-70 00 01	239.6 ± 0.9 (239.9)	c
SMP 83	5 36 25.8	-67 19 57	276.2 ± 0.5 (279.4)	a,b,c
SMP 84	5 37 13	-71 54 00	235.0 ± 0.2	a
SMP 85	5 40 29.7	-66 19 04	217.0 ± 0.3	a
SMP 87	5 42 06.6	-72 43 35	264.6 ± 1.0	a
SMP 88	5 43 08.5	-70 30 43	211.0 ± 2.0	a
SMP 89	5 43 07.5	-70 10 50	261.2 ± 0.6	a
SMP 91	5 45 12	-68 06 59	295.3 ± 1.5	b
SMP 92	5 47 27.8	-69 28 32	256.4 ± 0.7	a
SMP 94	5 55 15.9	-73 03 02	256.8 ± 3.0	a,b
SMP 95	6 01 57.3	-67 55 58	290.9 ± 0.9	b
SMP 96	6 06 46.7	-71 03 49	239.5 ± 2.0	a
SMP 97	6 10 36.5	-67 55 44	271.8 ± 0.6 (271.6)	b
SMP 99	6 19 45.9	-71 34 35	248.8 ± 0.3	b
SMP 100	6 24 08	-72 06 08	270.1 ± 0.8	b
SMP 101	6 23 52	-69 09 08	266.0 ± 1.0 (267.5)	b
SMP 102	6 29 41	-68 00 55	286.5 ± 1.2	b

TABLE 1 (Continued)

RADIAL VELOCITY DATA FOR LMC PLANETARY NEBULAE

Object Name[1]	RA (1950.0)	Dec	V_{lsr}	Telescope
J 5	5 12 07.9	-69 27 13	262.9 ± 0.6	b
J 26	5 20 22.6	-69 28 53	227.8 ± 2.7 (236.0)	a,b
J 33	5 21 42.3	-69 45 51	231.9 ± 1.9	a,b
J 38	5 24 55.7	-69 08 27	265.6 ± 1.2 (272.3)	b
J 41	5 26 29.6	-69 03 28	240.0 ± 1.1 (239.9)	b
A 0	5 25 46.0	-63 39 30	283.4 ± 0.5	a,b
A 3	5 21 46.9	-64 28 03	272.9 ± 0.5	b
A 4	5 26 30.8	-64 40 28	254.2 ± 2.0 (243.4)	a,b
A 22	5 21 36.7	-65 25 16	236.7 ± 0.9	a,b
A 24	5 26 10.8	-65 24 15	267.2 ± 1.3	b
A 46	5 13 23.8	-66 20 52	243.4 ± 1.3 (259.1)	b
A 54	5 39 17.3	-66 51 17	282.8 ± 1.9	b

Note — Velocities in km s^{-1}

[1] SMP = Sanduleak, McConnell, and Philip 1978;
J = Jacoby 1980; A = Morgan 1984

[2] a = 1-metre; b = 2.3-metre; c = 3.9-metre

c) Comparison with Earlier Results

There have been three earlier studies of the kinematics of the LMC planetary nebulae; that of Feast (1968) (25 PN), of Webster (1969) (14 PN) and of Smith and Weedman (1972) (27 PN). There is a substantial overlap of objects observed in these studies, which together yield radial velocities for a total of 35 objects. The earlier work was with low-dispersion spectrographs and photographic plates, but the Smith and Weedman study used a single-channel, photoelectric, pressure-scanned Fabry-Perot interferometer with a resolution almost identical to us (11 km s^{-1}, FWHM).

Table 2 compares our measurements with these three earlier determinations. The radial velocities are given in the Heliocentric System. As was found in our kinematical study of the SMC (Dopita *et al.* 1985), there is excellent agreement with the Feast (1968) results, the mean difference being only 1.39 km s^{-1} for the 23 objects in common. The Webster (1969) data appears to have a systematic error, in the sense that radial velocities are over-estimated by 8.5 km s^{-1}, both for the LMC and SMC. This is probably the result of the different conditions of illumination between the observations and the comparison lamp exposures. However, if this error is taken into account, then the scatter is very similar to the Feast (1968) data. As might have been expected, given the comparable resolutions, the agreement between our determinations and the Smith and Weedman (1972) measurements is excellent. The results differ by only 1.5 km s^{-1} in the mean, with an RMS scatter of only 3.0 km s^{-1}.

TABLE 2

A Comparison With Radial Velocities
Obtained In Earlier Studies

Object			Heliocentric Radial Velocity (km s^{-1})			
SMP	N	WS	This Study	Feast	Webster	Smith & Weedman
1	182	1	224.7	219	...	224
6	184	2	264.6	271	...	263
15	...	5	203.1	...	...	202
19	188	6	235.2	239	...	236
21	97	7	260.5	250	283	262
23	24	8	282.4	302	301	281
32	192	10	263.6	247	...	257
38	110	15	240.5	243	...	238
47	122	18	...	275	280	269
48	123	19	255.7	...	258	...
50	39	20	299.9	337	317	296
52	124	21	272.7	280	...	270
53	42	22	277.7	277	...	278
58	133	23	279.4	...	...	276
61	203	24	192.6	185	...	...
62	...	25	238.3	...	250	238
63	...	26	264.1	...	280	264
66	52	27	304.9	308	...	...
73	208	29	240.5	239	241	236
74	209	30	268.2	...	...	262
75	151	31	...	...	...	297
76	...	32	278.2	...	295	280
78	153	33	256.1	252	262	258
79	210	...	229.3	230	...	...
81	211	34	256.3	234	...	...
83	66	35	288.2	287	296	...
84	212	36	249.6	261	...	251
87	215	37	279.6	284	...	...
89	178	38	276.4	276	270	277
92	170	39	271.7	274	...	271
97	...	40	288.4	293	...	...
98	...	41	...	262	...	...
99	221	42	264.2	263	254	258
Mean Difference (km s^{-1}) (Other Study – This Study)				+1.39	+8.54	−1.50

III. THE KINEMATICS OF THE LMC

a) H I *Surveys*

Since the H I surveys of the LMC give a detailed and global coverage, the H I data gives a very useful (young) reference frame with which to compare and contrast the kinematics of the older PN population. The first extensive H I survey of the LMC was by McGee and Milton (1964, 1966a, b), but this has been supplanted, at least in the central six degrees or so, by the Rohlfs *et al.* (1984) work, hereafter RKSF. This gives H I velocities to a precision of ± 1 km s^{-1} in a regular grid spacing of $\Delta\alpha \approx$ 2m 20sec and $\Delta\delta = 12'$, over a total of 1023 points.

The derivation of both a reliable rotation curve and the orientation parameters from such data is not a staightforward task. First, the large angular diameter of the LMC and its large transverse velocity (of order 300 km s^{-1}; Mathewson, Schwartz and Murray 1977; Feitzinger, Isserstedt and Schmidt-Kaler 1977; Lin and Lynden-Bell 1982), ensure that there will be a substantial velocity gradient in the direction of motion. This probably accounts for the rotation between the geometrical line of nodes of $168 \pm 4°$ (Feitzinger, Isserstedt and Schmidt-Kaler 1977) and the kinematically determined value of 208° (RKSF). If the LMC is a rotating flat disk, the regular velocity gradient resulting from the transverse motion will be combined with the "spider" diagram of the rotation curve to both change the maximum velocity gradient and to twist the lines of constant velocity, particularly in the outer regions. This effect could, in some circumstances, simulate a warp in the H I disk.

A second problem is that the LMC is seen nearly face-on. The best estimates of its inclination are $31 \pm 8°$ derived from the the luminosity gradient of the Cepheids (de Vaucouleurs 1960) and a value of $33 \pm 3°$ estimated from both the H I and optical distributions (Feitzinger, Isserstedt and Schmidt-Kaler 1977). This ensures a relatively feeble projection of the rotation into radial velocities, and allows local perturbations in the vertical velocity distribution to confuse and mask rotation. Such effects are known to occur in regions of active star-formation such as 30Dor or in LMC Constellation III (Caulet *et al.* 1982; Dopita, Mathewson and Ford 1985).

The third complicating factor is the possibility of ram-pressure induced distortions in the velocity field, or ram-pressure stripping of the outer H I envelope caused by the passage of the LMC through the tenuous hot outer corona of our Galaxy. This may be the most plausible explanation for the origin of the Magellanic Stream (Mathewson *et al.* 1974; Mathewson, Schwartz and Murray 1977). Circumstantial evidence to support this viewpoint may be found in the displacement of the globular cluster system to the NE (Freeman, Illingworth and Oemler 1983), and the steep gradient in the H I column density in this sector of the LMC, in the presumed direction of motion (Mathewson *et al.* 1974). The RKSF data also suggests that the gas in this portion of the LMC has been considerably disturbed. This sector of the LMC displays split line profiles. One component merges into the H I disk of the rest of the LMC, and we identify this as relatively undisturbed disk H I, which we have used in our further analysis of the disk kinematics. However the other component, with higher radial velocity, appears to be a dynamically distinct entity, and may represent either a

grossly warped outer disk, or else a stream of ram-pressure stripped gas originating at the "leading" edge of the LMC.

b) The Transverse Velocity of the LMC

In principle, the magnitude of the transverse velocity of the LMC can be estimated from the transverse velocity gradient which it gives rise to across the face of the LMC provided that the orbital plane of the LMC is known. Previous workers (Mathewson *et al.* 1974; Mathewson, Schwartz and Murray 1977) have already noted that the Magellanic Stream holds the key to this problem. As seen from the sun, the Magellanic Stream defines a Small Circle in the sky. However, provided that the distance to the Stream is of order 50 kpc, it will define a Great Circle as seen from the Galactic Center, passing through the LMC at position angle $110 \pm 10°$.

Both the ram-pressure stripping models of the origin of the stream (Meurer *et al.* 1985) and the tidal interaction models (Lin and Lynden-Bell 1982; Fujimoto and Murai 1984) predict that, provided that the tail of the Stream is not too close, then the Stream will extend along the orbital plane of the Magellanic Clouds. This result is independent of whether the Stream leads or lags the Magellanic Clouds. Thus we can take the orbital plane to be defined as the Great Circle the Stream extends along as seen from the Galactic Center.

In order to estimate the magnitude of the transverse velocity of the LMC in this plane, we have investigated the effect of the transverse velocity gradient on the direction of the kinematical line of nodes as defined in the central two degrees of the LMC. The correct value of the transverse

velocity is found when, applying its inverse, rotates the kinematic line of nodes to lie in the same direction as the photometric line of nodes. The effect of this correction is shown of Figure 2, which implies that the correct transverse velocity of the LMC is 275 ± 65 km s^{-1}. The size of the error bar is defined principally by the uncertainty in the photometric line of nodes ($\pm 4°$), the uncertainty in the kinematic line of nodes ($\pm 1°$) is small but not negligible. Figure 3 shows the H I iso-velocity contour plot resulting from the application of this correction, adopting only the "disk" component of the H I in the region of split line profiles discussed above. This diagram bears a much closer resemblance to the classical "spider" diagram than does the "raw" H I data (RKSF). Perturbations in the iso-velocity plot reflect regions of star formation such as 30Dor, Constellation III, or other supergiant shells (Meaburn 1981). There also appears to be a perturbation associated with the bar of the LMC, which could be a result of the gas streaming motions expected on theoretical grounds (de Vaucouleurs and Freeman 1973).

c) The Orbit of the LMC and the Mass of the Galaxy

The total orbital energy of the LMC with respect to the Galaxy can now be calculated, provided that the Galactocentric distance can be computed and that the effect of the solar motion can be taken out. The distance modulus of the LMC has been estimated from a variety of methods to be 18.5 ± 0.1 (Feast 1984; Visvanathan 1985). In galactic coordinates, therefore, the position vector from the sun to the LMC, $\mathbf{L}$, is $\mathbf{L} = 50.1 \pm 2.3(0.153, -0.826, -0.540)$ kpc. Here the distance with its error is given, and the direction cosines are given in parentheses. This figure can be

Figure 2. Graph showing the effect of varying the transverse velocity (V_{trans}) on the mean position angle of the kinematic line of nodes.

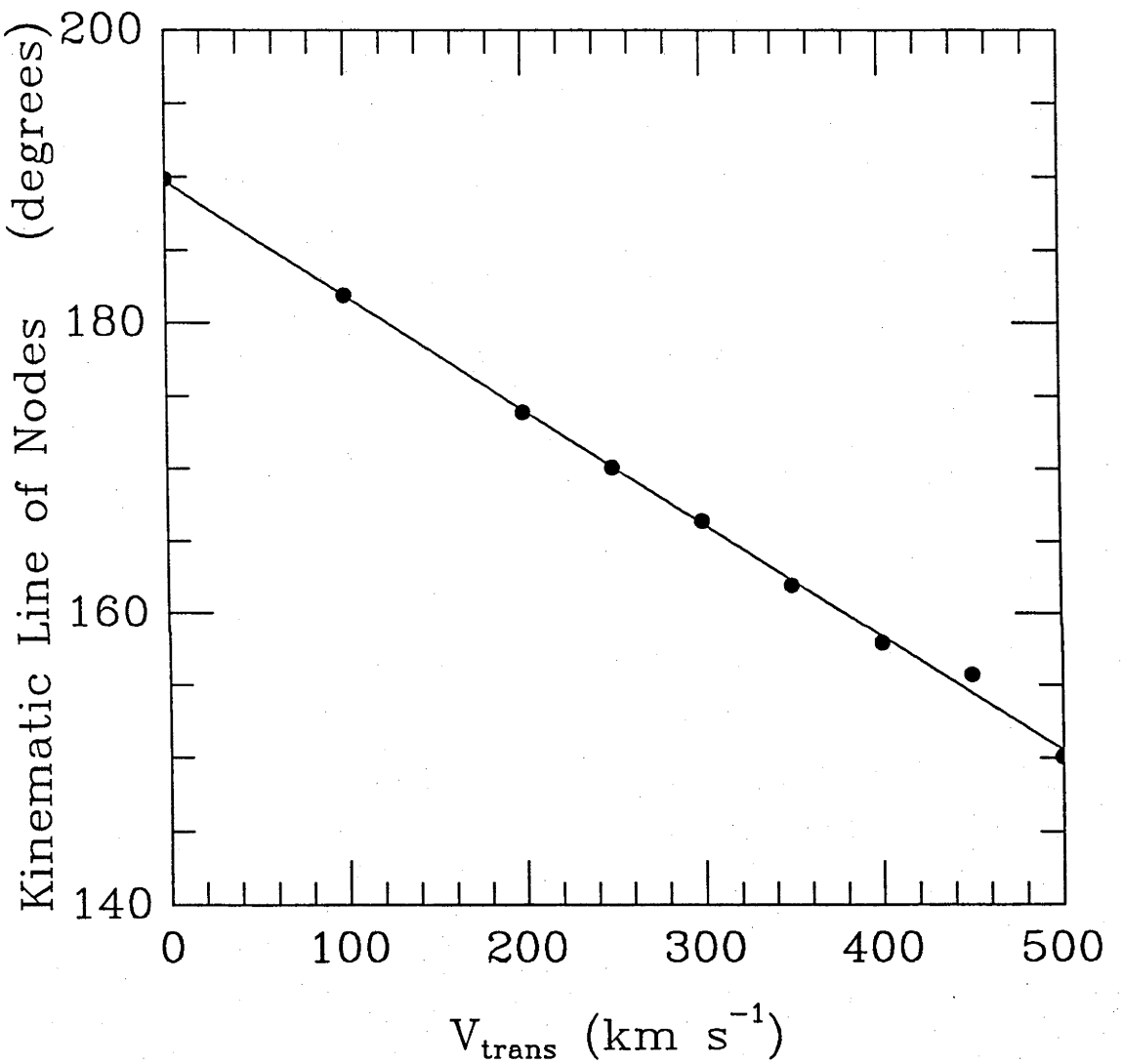
Kinematic Line of Nodes (degrees)
200
180
160
140
0
100
200
300
400
500
V_{trans} (km s^{-1})

Figure 3. Smoothed H I velocity contour map after subtracting the radial velocity component due to a transverse velocity of 275 km s^{-1}. The coordinate system is that due to Isserstedt (1975).

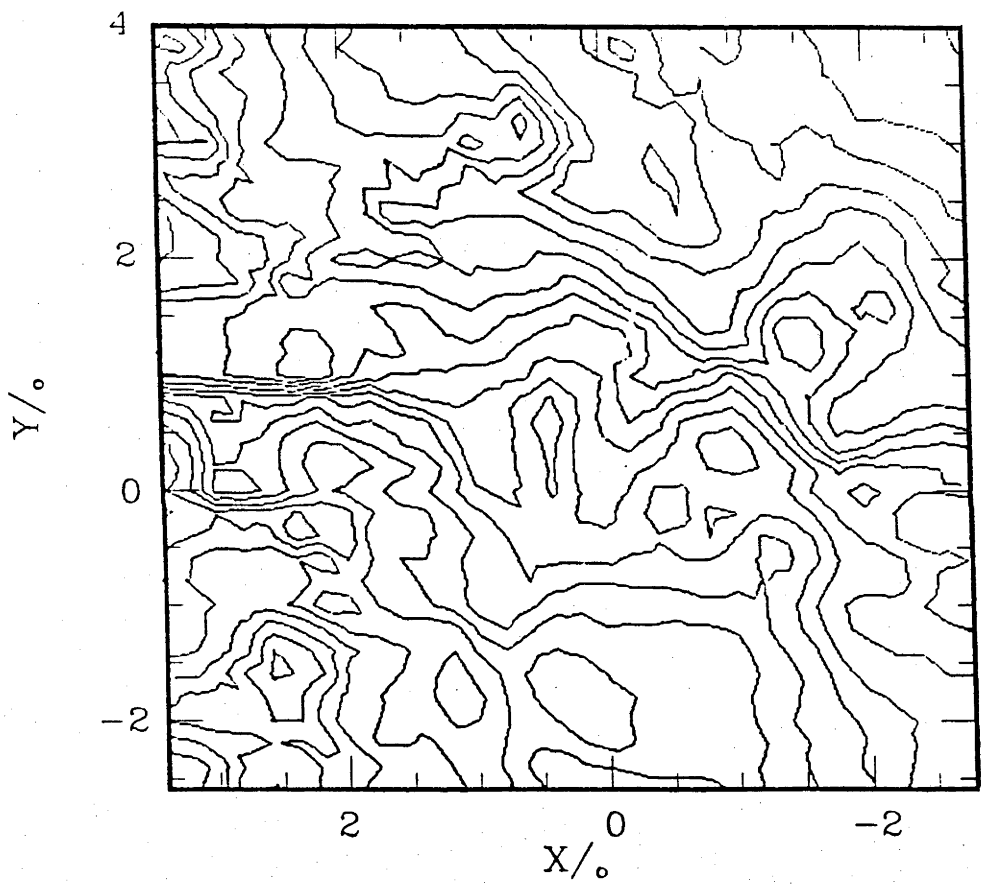
4
2
0
-2
Y/°
2
0
-2
X/°

compared with the value of 52 kpc adopted by Lin and Lynden-Bell (1982). The position vector of the sun with respect to the Galactic center is $\mathbf{S} = 8.7 \pm 1.0(1,0,0)$ (see review by Graham 1979). Hence, the distance from the Galactic center to the LMC is $|\mathbf{L} - \mathbf{S}| = 51 \pm 3$ kpc. The geometry of the situation ensures that the LMC–Galactic Center distance is always very similar to the adopted LMC–solar distance, and the errors are determined principally by the errors in this distance.

The radial velocity (LSR) of the LMC is 250 ± 5 km s^{-1}. We adopt 220 ± 7 km s^{-1} as the orbital motion of the sun about the Galactic center (Einasto, Hvad and Jeveer 1979). This geometry can now be used with the transverse velocity of the LMC as seen at the Sun of 275 ± 65 km s^{-1}, derived above, to derive the radial velocity of the LMC as seen from the Galactic center. This turns out to be very small, only 42 ± 10 km s^{-1}. We may therefore conclude that the LMC is very close to its perigalacticon, and that its space velocity with respect to the Galactic center is about 278 km s^{-1}. This agrees excellently with the value of 280 km s^{-1} for a perigalactic distance of 52 kpc claimed by Mathewson (1976) using a different approach to ours.

The fact that the LMC is near its perigalacticon allows us to put an indicative upper limit on the mass of the Galaxy out to 51 kpc, by assuming that the LMC has fallen from rest from infinity to its current distance. This gives $M_{gal} = 4.5 \times 10^{11} \mathcal{M}_{\odot}$. This is in good agreement with White and Frenk (1983), who obtained $5 \times 10^{11} \mathcal{M}_{\odot}$ out to 33 kpc, using systems in the outer halo of our Galaxy. The derived mass of the Galaxy would double if the Magellanic Clouds are in fact in a circular orbit, and could be reduced by an arbitrary factor if the LMC is in a hyperbolic orbit.

d) The Mass and Rotation Curve of the LMC

The rotation curve, obtained from a strip of ±15° in position angle passing through the centroid of the PN distribution (Sanduleak 1984) and deprojected for an inclination of 33° (Feitzinger, Isserstedt and Schmidt-Kaler 1977), is shown in Figure 4. Note that this curve is approximately symmetric about $r = +0.5°$ and not about the PN centroid. Note also that the central ±1.5° is strongly perturbed, possibly as a result of the gas streaming motions expected as a result of an asymmetric positioning of the bar (de Vaucouleurs and Freeman 1973; Feitzinger 1983). Folding this curve about its point of symmetry, which we adopt as the rotation center, gives the average rotation curve shown in Figure 5.

The rotation curve does not fit well to a Keplerian curve, even in the outer regions. Usually, an exponential disk is taken as giving acceptable fit to the rotation curve of Magellanic type galaxies (Freeman 1970). The mass is then given in terms of the maximum rotation velocity, V_{max}, by:

$$V_{max} = 0.623(GM_{exp}\alpha)^{1/2} \tag{3.1}$$

where α, the photometric scale length is taken as 0.010 per arc min, corresponding to a disk scale length of 1.6 kpc (de Vaucouleurs 1960). This gives $M_{exp} = (3.2 \pm 0.3) \times 10^9 \mathcal{M}_\odot$, where the uncertainty in the distance of the LMC has been taken into account. However, a better fit to the rotation curve would be obtained assuming solid-body rotation out to 2.0° from the center of symmetry, with an exponential disk outside that. Fitting this disk model gives our best estimate of the mass of the LMC out to 3°; $(4.6 \pm 0.2) \times 10^9 \mathcal{M}_\odot$. If the exponential disk continues out to 6°, which is about the largest acceptable value from H I observations (Mathewson and

Figure 4. LMC rotation curve derived from the H I survey, corrected for a transverse velocity of 275 km s^{-1}, obtained by taking a sector $\pm 15°$ wide along the photometric line of nodes.

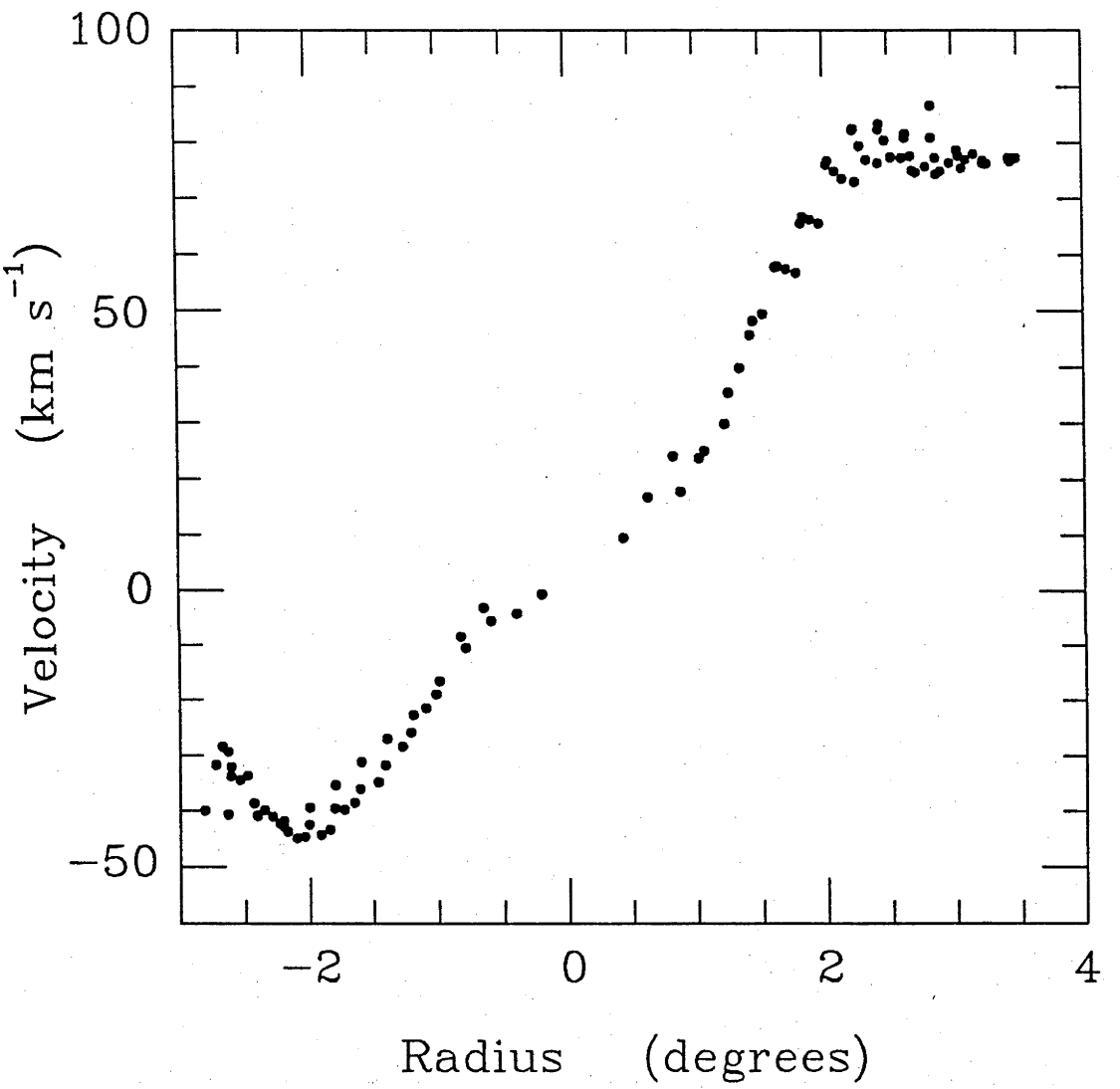
100
50
0
−50
Velocity (km s^{-1})
−2
0
2
4
Radius (degrees)

Figure 5. LMC rotation curve obtained after folding the H I data about the symmetrical point. The solid line represents the fitted theoretical curve comprising solid body rotation within the inner 2° together with an exponential disk outside that radius.

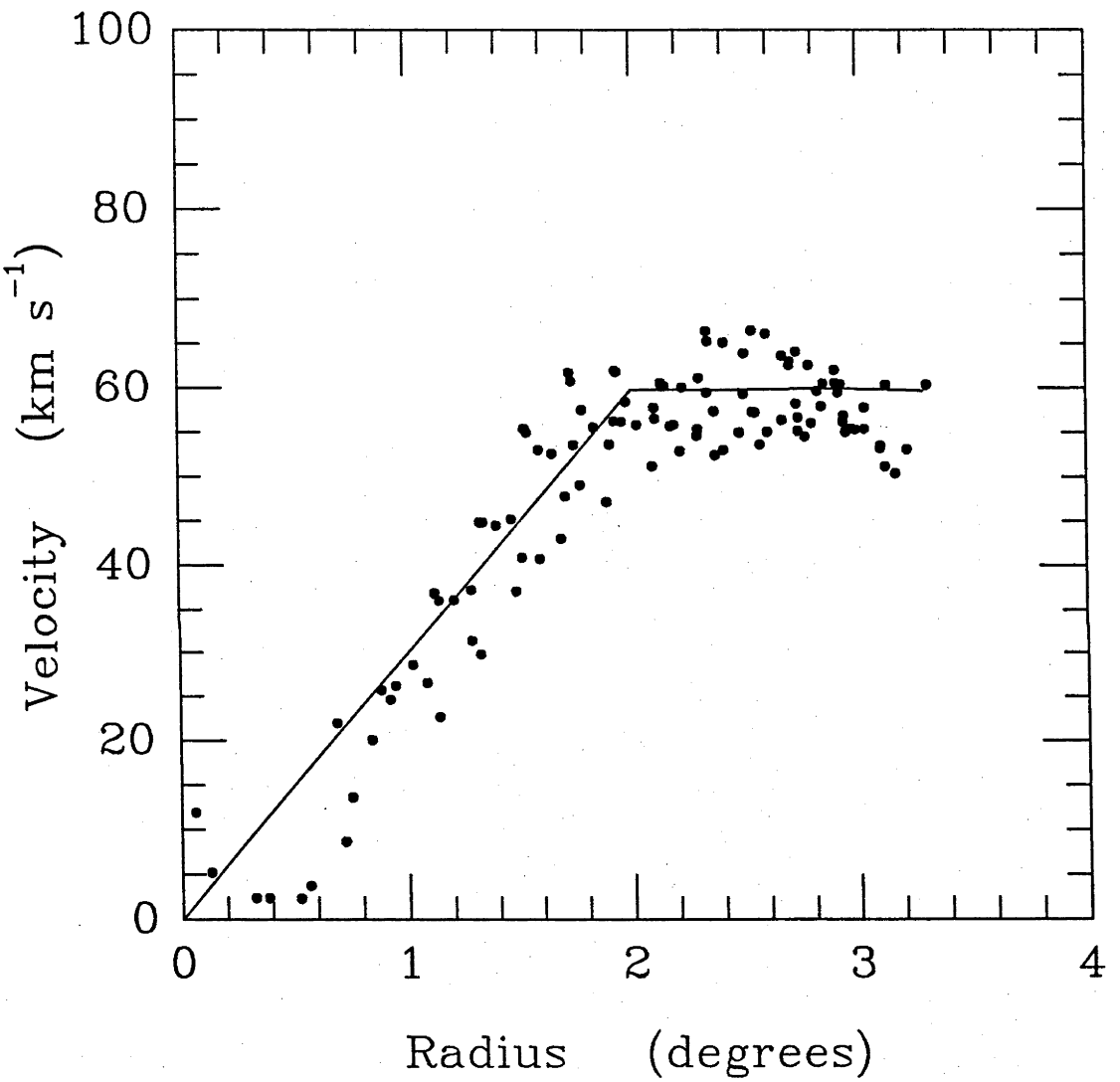
100
80
60
40
20
0
Velocity (km s^{-1})
0
1
2
3
4
Radius (degrees)

Ford 1984) or from photometry (de Vaucouleurs 1957), then a total mass of $(6.0 \pm 0.6) \times 10^9 \mathcal{M}_\odot$ is estimated. These figures are entirely consistent with the estimate of $(5 \pm 1) \times 10^9 \mathcal{M}_\odot$ for the total mass of the LMC estimated from a variety of mass models by Feitzinger (1979).

e) Rotation Solutions for the H I *and Planetary Nebulae*

The PN in the SMC present strong evidence for a considerable tidal disruption of this system (Dopita *et al.* 1985). Freeman, Illingworth and Oemler (1983) presented evidence from clusters to suggest that the same might well be true for the LMC. It is therefore of great interest to compare the PN and H I dynamics to search for such effects. The simplest exercise that can be done is to simply compare the radial velocity of each PN with the H I in its vicinity. This has been done in Figure 6, which should be compared with Figure 4 in Freeman, Illingworth and Oemler (1983). The diagram shows a correlation between the H I and PN with a dispersion of approximately 20 km s^{-1} about the line of slope unity. From this diagram it would appear that there may be an offset of about 5 km s^{-1} between the two. However, from Figure 7 the difference is less then 2 km s^{-1}. Hence, there is no evidence for the systematic offset in velocity claimed for the older population by Freeman, Illingworth and Oemler (1983).

Having obtained the form of the rotation curve, a more sophisticated means to analyse the velocity data is derived from that given by Freeman, Illingworth and Oemler (1983). The rotation solution is given by:

$$V(\theta, r) = V_m(r)\{1 \pm [\tan(\theta - \theta_0) \sec i]^2\}^{-0.5} + V_0 \qquad (0 \leq \theta \leq 2\pi) \quad (3.2)$$

where $V(\theta,r)$ is the rotational velocity projected onto the line of sight at

position angle θ and radial coordinate r. We minimized the residuals in this equation using a non-linear χ^2-minimization routine from the software package MINUIT. The two free parameters to be minimized with respect to the velocity residuals are: θ_0, the position angle of the line of kinematic line nodes for the whole of the LMC (as opposed to the central region, used in the estimation of the transverse velocity) and V_0, the systemic Galactocentric velocity of the LMC. We have adopted $V_m(r)$ as the measured H I rotation curve.

Our analysis gave $\theta_0 = 166°$ and $V_0 = 46$ km s^{-1} for the H I solution, and $\theta_0 = 170°$ and $V_0 = 42$ km s^{-1} for the PN population. These figures are identical to within the errors for the two populations. In Figure 7 we show, as a function of azimuthal angle, the velocity difference between the PN radial velocities, and the local H I radial velocities as compared with the rotation solution for the H I. Clearly, the velocity dispersion in the PN population is considerably higher than that of the H I. Notice also that the typical line-of-sight velocity dispersion in the H I is 10 km s^{-1}, but that there are clearly distinct local regions of increased velocity dispersion. These correspond closely in position to supergiant shells of star-forming activity, principally the 30 Doradus complex ($\theta = 100°$), the N206 region ($\theta = 240°$), and the region around N186 ($\theta = 320°$). This is further observational proof that star-formation has the effect of stirring up the gas in the plane and increasing the vertical velocity dispersion (Dopita, Mathewson and Ford 1985). By contrast, the PN velocity dispersion is constant and featureless with position angle.

Figure 6. The observed GSR velocity for each planetary nebula in km s^{-1} compared to the H I velocity at each PN's position. Equality is indicated by the line of slope unity. The error in the velocity measurement is no larger than the size of each symbol.

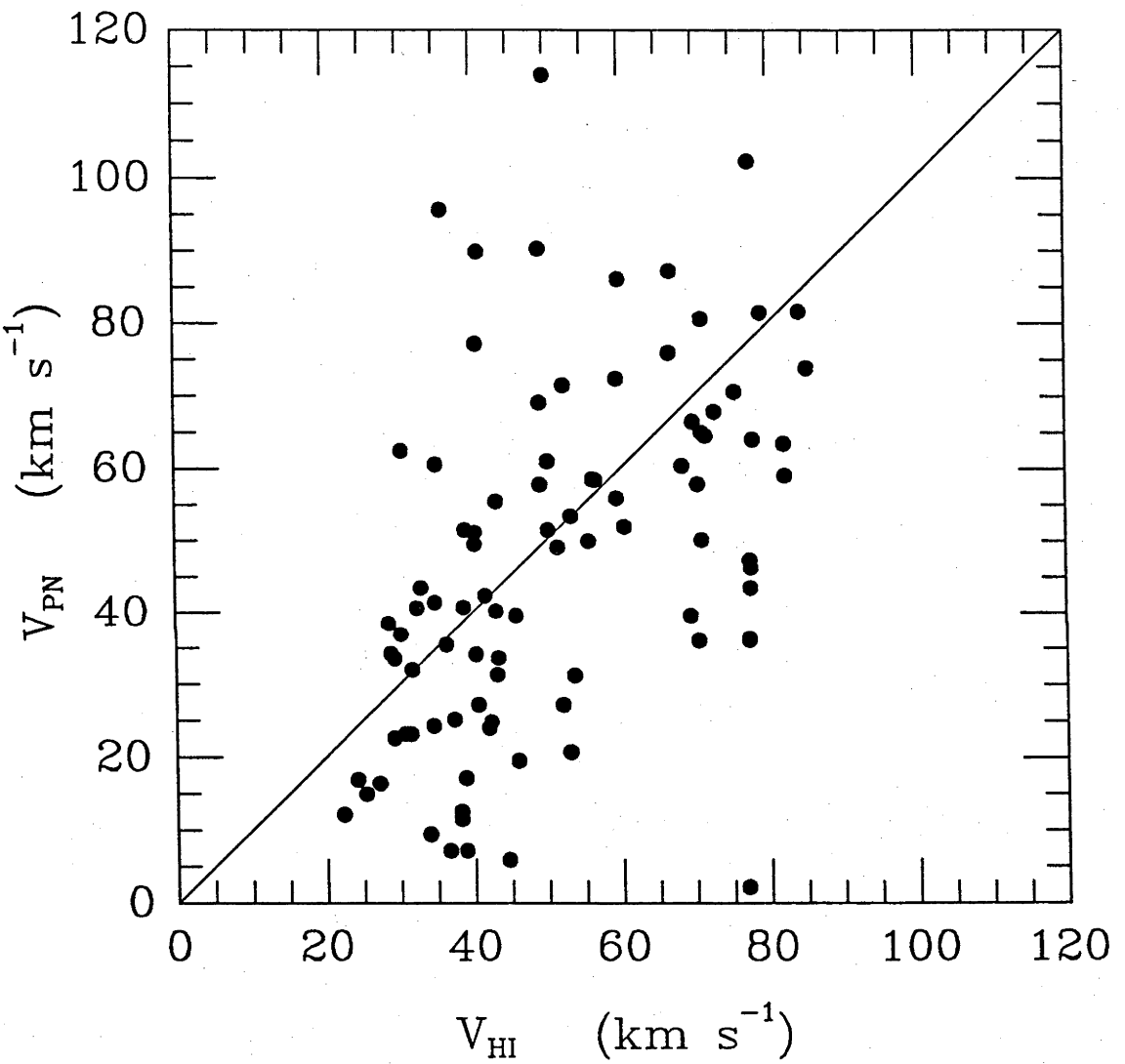
120
100
80
60
40
20
0
0
20
40
60
80
100
120
V_{PN} (km s^{-1})
V_{HI} (km s^{-1})

Figure 7. The velocity difference obtained from the H I data (filled circles) and the planetary nebulae (open circles). The 30 Doradus complex is clearly visible at position angle 100°, as are other star-forming regions near 240° and 320°.

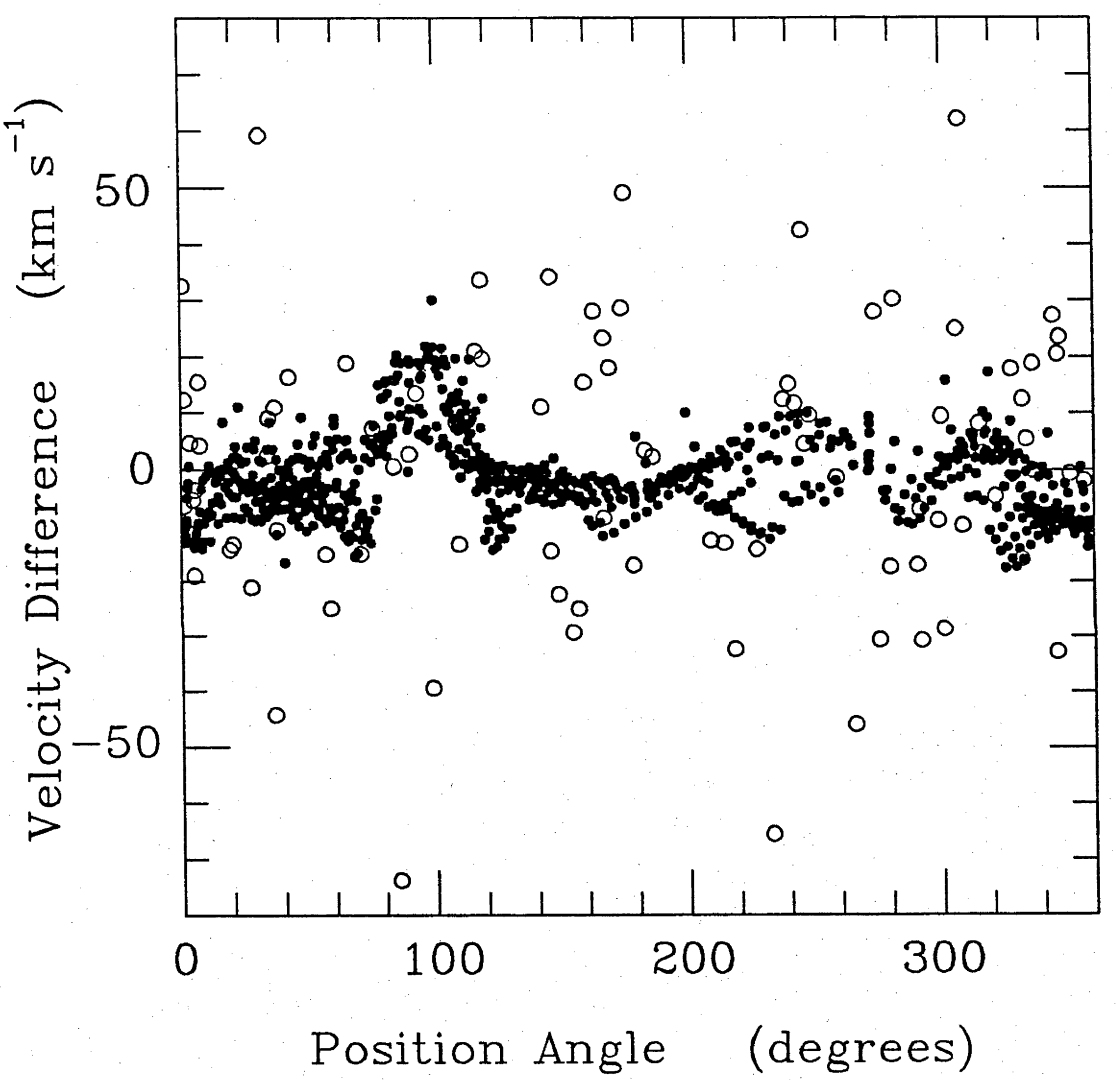
Velocity Difference (km s^{-1})
50
0
−50
0
100
200
300
Position Angle (degrees)

It is possible that the PN population might in fact be a halo population with a lower orbital velocity. To check this possibility, we divided the planetaries into two groups, those with projected radius from the center less than 2°, and the rest. If the PN rotate more slowly than the H I then this would show as a systematic modulation of the velocity residuals with position angle for the outer group. As shown in Figure 8, no such effect is found, implying that the PN population rotates just as fast as the H I.

We can therefore conclude that there is no significant difference between the H I and the PN kinematics other than an increase in velocity dispersion in the older PN population. This result confirms and amplifies that foreshadowed by Freeman, Illingworth and Oemler (1983), and poses an interesting conundrum. If, as claimed by Freeman, Illingworth and Oemler (1983), the old clusters have a rotation axis that differs from the young solution by about 50°, how then could this have occurred? As pointed out in that paper, such a tilt is not stable, and can persist only for a timescale of order 10^9 years, unless the older clusters define the form of the gravitational potential of the LMC, a hypothesis for which there is little supporting evidence. The most profound dynamical disturbance that may have been experienced by the LMC would have been a near-collision with the SMC that may have occurred about 2×10^8 years ago (Murai and Fujimoto 1980), resulting in profound tidal disturbance to the SMC (Mathewson and Ford 1984; Dopita *et al.* 1985; Mathewson, Ford and Visvanathan 1986). We can therefore conclude either the PN population is younger than 2×10^8 years old or that this collision did not result in the twisting of the rotation axes implied by the old clusters.

Figure 8. The velocity difference as a function of position angle for the planetary nebulae when they are split into two groups. Those inside $r = 2°$ (marked with filled circles) and those outside that radius (marked with open circles).

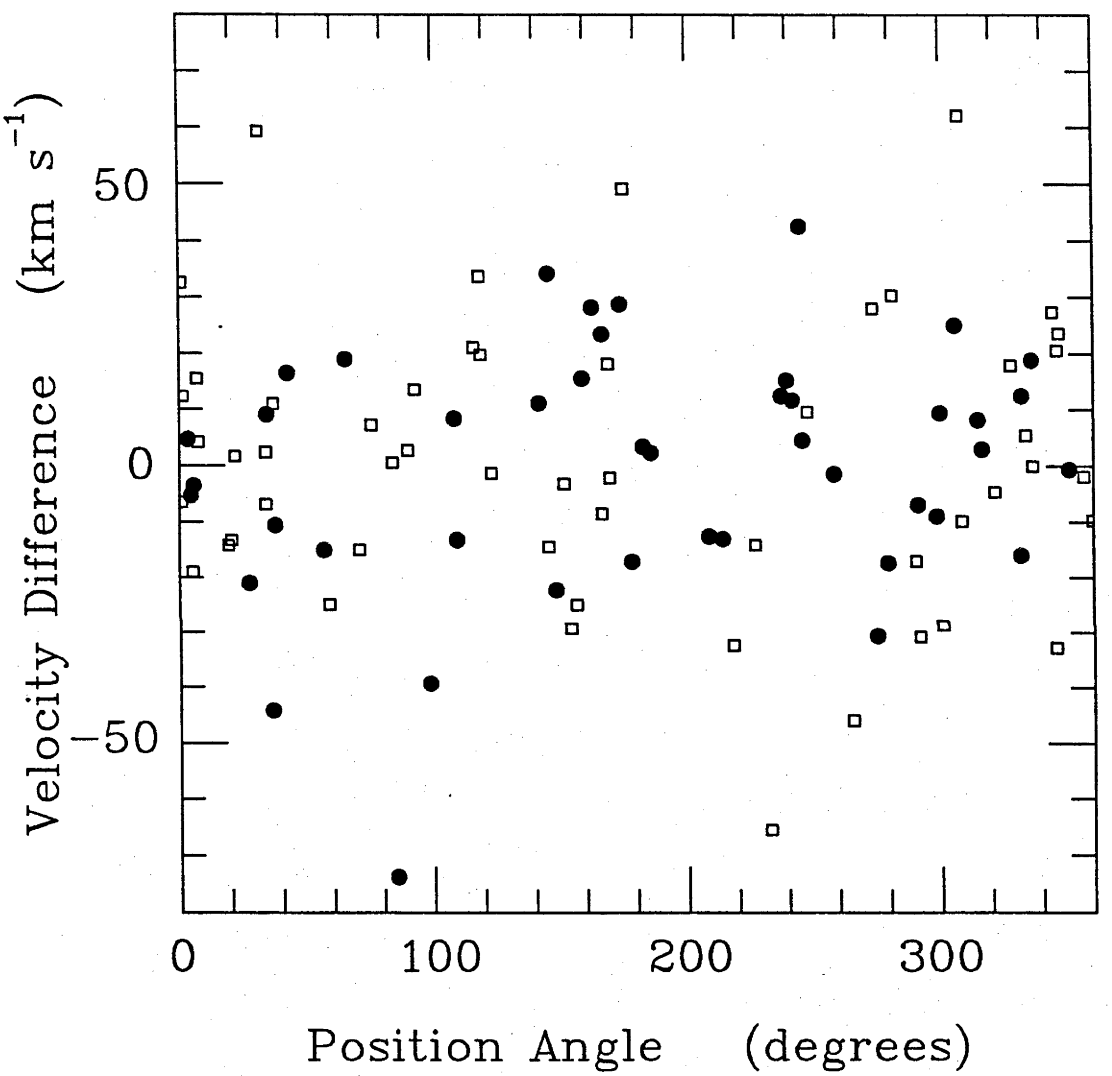
Velocity Difference (km s^{-1})
50
0
−50
0
100
200
300
Position Angle (degrees)

f) Orbital Diffusion and the Age of the Planetary Nebulae

We demonstrated in the previous section that there is no evidence that the PN represent a halo population. However, the PN population undeniably does have a much larger velocity dispersion than the H I. An increase in velocity dispersion is a natural consequence of a greater age. The process was examined by Spitzer and Schwartzschild (1951, 1953) who showed that orbital diffusion can occur as a consequence of "gravitational Fermi scattering", the encounter between stars and giant molecular clouds (GMCs). The relaxation time (10^8 years) for such encounters is much shorter than for star-star encounters (10^{14} years) as a consequence of the large characteristic mass of the GMCs, typically of order $10^5\mathcal{M}_\odot$. The relationship between total velocity dispersion at time t, $V(t)$, and the initial velocity dispersion, $V(0)$, of a stellar population is given by:

$$V(t) = V(0)[1 + (t/t_e)]^{1/3} \tag{3.3}$$

where the encounter timescale, t_e, is given in terms of the number of clouds per unit volume, n_c, their average mass, m_c, and an impact parameter function a (≈ 9.8) by:

$$t_e = 4V_m^3(0)/[3\pi^{3/2}G^2 n_c m_c^2 \ln a] \tag{3.4}$$

the accuracy of such a formula is determined both by the evolution of the disk GMC population, and by the reduction of interaction events when the orbits have diffused sufficiently to take them out of the region of the disk occupied by GMCs for a significant portion of the orbit. Both of these tend to reduce the rate of the diffusion with time. Wielen (1977) examined the diffusion rate by direct observation of populations of various ages in the solar neighbourhood. He found that an equation of similar form to

equation (3.3) gives an adequate description, but with an exponent of 1/2 and an encounter timescale of 5×10^7 years. Subsequent theoretical studies (Vader and de Jong 1981; Villumsen 1985) have tended to confirm the lower value for the exponent.

As dynamical evolution proceeds, the velocity ellipsoid does not remain spherical, because radial diffusion is more active than axial diffusion. Wielen finds that, for a dynamically old population, the ratio of axial to radial velocity dispersions, $\sigma_w : \sigma_r$, tends to 0.6 : 1.0. With this fact, we can transform the observed line-of-sight velocity differences to a histogram of the vertical (or axial) velocity dispersion in the LMC, assuming that the PN population is dynamically old, and that the H I is dynamically young. These are shown in Figures 9 and 10, from which we conclude that $\sigma_w(\mathrm{H\,I}) = 5.4$ km s^{-1} and $\sigma_w(\mathrm{PN}) = 19.1$ km s^{-1} (FWHM). These figures imply a total velocity dispersion of $\sigma_T(\mathrm{H\,I}) = 9.4$ km s^{-1} and $\sigma_T(\mathrm{PN}) = 37.1$ km s^{-1}, using the ratios of vertical to axial velocity dispersion given above. The vertical velocity dispersion of the H I is very similar to the values of $7 - 10$ km s^{-1} found by van der Kruit and Shostak (1984 and references therein) in other disk galaxies covering a wide variety of morphological types. The velocity dispersion in these galaxies does not appear to depend on radial coordinate, or vary much between arm and inter-arm regions, and can be understood as a consequence of self-regulating feedback in star formation activity (Dopita 1986).

Are the observations consistent with the hypothesis that the increase in velocity dispersion is the result of the operation of the stellar orbital diffusion process described above? The answer to this question requires a knowledge of the age distribution of the precursor stars.

Figure 9. Histogram of the derived vertical velocity dispersion (σ_w) for the H I data. The tail extending to +20 km s^{-1} is due to the 30 Doradus region. The full width at half maximum is 6 km s^{-1}.

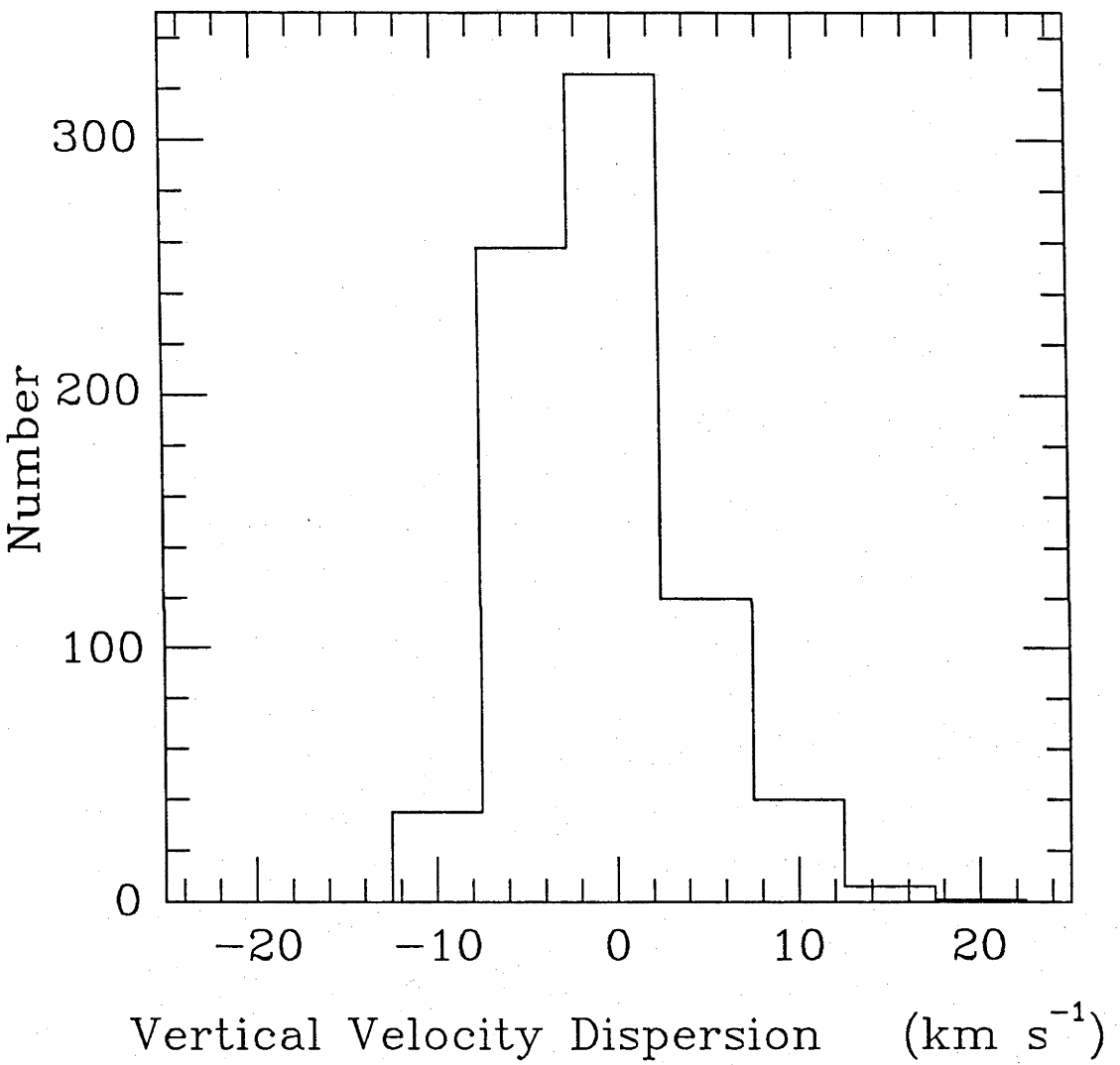
300
200
100
0
Number
−20
−10
0
10
20
Vertical Velocity Dispersion (km s^{-1})

Figure 10. Histogram of the derived vertical velocity dispersion (σ_w) for the planetary nebulae. The full width at half maximum is 19 km s^{-1}.

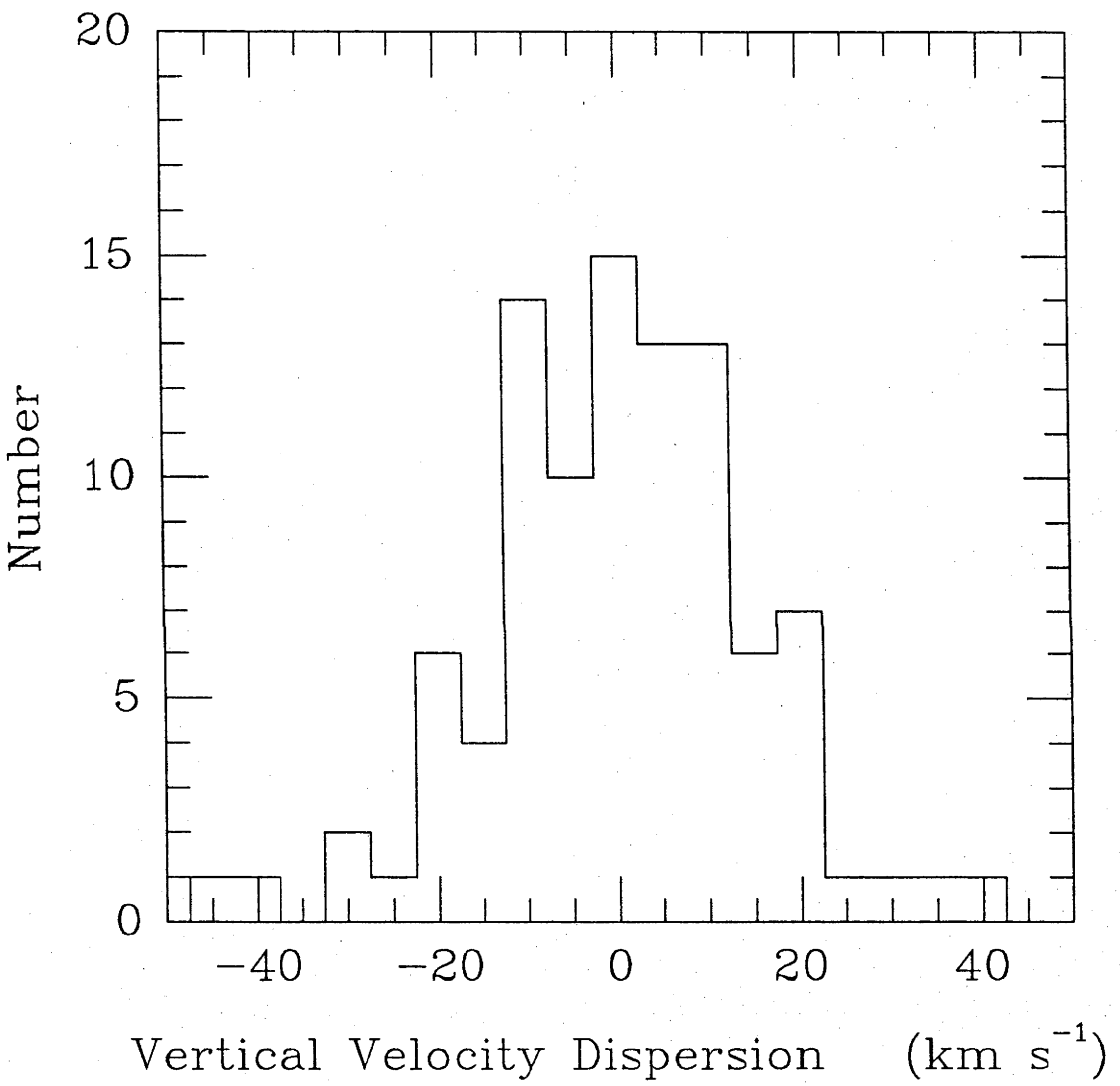
20
15
10
5
0
Number
−40
−20
0
20
40
Vertical Velocity Dispersion (km s^{-1})

Fortunately, the precursor mass of the stars giving rise to the PN can be estimated fairly accurately from existing observational and theoretical material. The mass distribution for LMC stars leaving the Asymptotic Giant Branch (AGB) has been computed by Weidemann (1987), using the luminosity function derived for these stars by Reid and Mould (1984). This is a very sharply peaked function with a maximum at $0.59\mathcal{M}_{\odot}$, and which is skewed to higher masses, with 80% of stars lying below $0.70\mathcal{M}_{\odot}$. The relationship between this mass and the initial mass depends on the mass-loss rate in the AGB phase of evolution, and has been determined for these same stars by Wood, Bessell and Fox (1983). From this work, we can conclude that most of the LMC planetaries had initial stellar masses near $0.88\mathcal{M}_{\odot}$, but there exists a tail in the distribution extending to about $1.4-1.6\mathcal{M}_{\odot}$. This is in good agreement with the figure obtained by simply adding the typical mass of the central star ($0.6\mathcal{M}_{\odot}$) to the largest ionized mass measured for optically thin nebulae ($0.5\mathcal{M}_{\odot}$, Wood *et al.* 1987).

The typical ages of these stars at the time of PN formation can be estimated from the main-sequence lifetimes given by Iben and Tutakov (1985), assuming that this occupies 90% of the total lifetime of the planetary nebula precursor star. This shows that the bulk of the PN have an age of near 3.5×10^{9} years, but there are also younger objects present down to an age of order $(0.5-1.3)\times10^{9}$ years. Thus, the PN population predates, by a considerable margin, any encounter between the LMC and SMC, but is insufficiently aged to have been formed during the initial collapse of the LMC.

These ages can now be substituted in either the Wielen (1977) diffusion coefficients or the Spitzer and Schwartzschild (1951, 1953) formulae,

equations (3.3) and (3.4) above. The principal uncertainty in the use of these equations is the mass appropriate for the giant H I clouds in the LMC.

The H I data does not have sufficient resolution to see these, and although these are seen in the CO data (Cohen, Montani and Rubio 1984), the low abundance of both C and O renders a mass calculation uncertain. Using a mass density of 3×10^{-24} g cm^{-3} in equations (3.3) and (3.4), the PN age derived above, and the observed velocity dispersions of the H I and the PN population, implies that the mass of the typical scattering cloud is about $1.6 \times 10^5 \mathcal{M}_\odot$. This should be compared with the value found for Galactic molecular clouds, $1.5 \times 10^5 \mathcal{M}_\odot$ (Liszt, Delin and Burton 1981). Thus, diffusive processes appear to work in the same way, and on the same timescale in the LMC as in the local region of our Galaxy.

This conclusion can be checked using Wielen's work. With the observed velocity dispersions, and using a constant diffusion coefficient of 6.0×10^{-7} (km s^{-1})^2 yr^{-1}, the indicative age of the PN population is 2.1×10^9 years. Using his velocity-dependent diffusion formulae gives ages of $(2.5-3.6) \times 10^9$ years. Both of these figures are sufficiently close to the ages given above to give us confidence that diffusive processes are very similar to those operating in our local region of the Galaxy.

IV. CONCLUSIONS

From radial velocity data for a very extensive sample of planetary nebulae in the LMC, we have established that the PN population forms a flattened disk with almost the same spatial distribution and rotation solution as the H I layer. The vertical velocity dispersion of the PN is

consistent with the action of orbital diffusion over the lifetime typical for the PN precursor stars. Whilst there may be a few objects in the sample sufficiently old to be considered halo objects, it is clear that the bulk of the PN cannot represent a halo population.

This result must be reconciled with the Freeman, Illingworth and Oemler (1983) finding that the rotation axis of old ($> (1-2) \times 10^9$ years) clusters have a rotation axis twisted by some 50° with respect to the younger. The age of the PN is sufficient that we can exclude the possibility that this twisting has been caused by tidal torques during a recent close encounter of the LMC with the SMC. On the other hand, there is no evidence to support the idea that the old clusters provide the gravitational potential in which the H I and younger stellar components move. The question of the reality and cause of the twisting of the cluster population remain open.

From a re-analysis of the H I data, we have also been able to derive a figure for the transverse velocity of the LMC, assuming that the LMC is moving along the Small Circle defined by the Magellanic Stream, and that the kinematic and photometric line of nodes agree. This gave a transverse velocity of 275 ± 65 km s^{-1}, which implies that the LMC is near perigalacticon. An indicative mass of the Galaxy out to 51 kpc is therefore $4.5 \times 10^{11} \mathcal{M}_\odot$, derived on the assumption that the LMC has fallen to its current position from rest at infinity. Finally, from our new rotation curve, we estimate the mass of the LMC to be $(4.5 \pm 0.3) \times 10^9 \mathcal{M}_\odot$ out to $r = 3°$; and of order $6 \times 10^9 \mathcal{M}_\odot$ in total.

REFERENCES

Bevington, P.R. 1969, *"Data Reduction and Error Analysis in the Physical Sciences"*.

Caulet, A., Deharveng, L., Georgelin, Y.M., and Georgelin, Y.P. 1982, *Astr. Ap.*, **110**, 185.

Cohen, R., Montani, J. and Rubio, M. 1984, *in IAU Symposium 108, "Structure and Evolution of the Magellanic Clouds"*, ed. S. van den Bergh and K.S. de Boer (Dordrecht : Reidel), p. 401.

de Vaucouleurs, G. 1957, *Astron. J.*, **62**, 69.

de Vaucouleurs, G. 1960, *Ap. J.*, **131**, 574.

de Vaucouleurs, G., and Freeman, K.C. 1973, *Vistas in Astronomy*, **14**, 163.

Dopita, M.A. 1986, *in "Nearly Normal Galaxies : From the Planck Time to the Present"*, ed. S.M. Faber, (Springer Verlag).

Dopita, M.A., Ford, H.C., Lawrence, C.J., and Webster, B.L. 1985, *Ap. J.*, **296**, 390.

Dopita, M.A., Ford, H.C., and Webster, B.L. 1985, *Ap. J.*, **297**, 593.

Dopita, M.A., Mathewson, D.S., and Ford, V.L. 1985, *Ap. J.*, **297**, 599.

Dopita, M.A., Meatheringham, S.J.,Wood, P.R., Ford, H.C., Webster, B.L., and Morgan, D.H. 1987a, *Ap. J. (Letters)*, **315**, L107.

Dopita, M.A., Meatheringham, S.J., Webster, B.L., and Ford, H.C. 1988, *Ap. J.*, (April 15).

Einasto, J., Hvad, U., and Jeveer, M. 1979, *in "The Large Scale Structure of the Galaxy"*, ed. W.D. Burton, (Dordrecht : Reidel), p. 231.

Feast, M.W. 1968, *M.N.R.A.S.*, **140**, 345.

Feast, M.W. 1984, South African Observatory Circ. #397.

Feitzinger, J.V., Isserstedt, J., and Schmidt-kaler, Th. 1977, *Astr. Ap.*, **57**, 265.

Feitzinger, J.V. 1979 Doctoral Thesis: Astronomisches Institut der Ruhr-Universitt, Bochum.

Feitzinger, J.V. 1983, *in IAU Symposium 100, "Internal Kinematics and Dynamics of Galaxies"*, ed. E. Athanassoula, (Dordrecht : Reidel), p. 214.

Freeman, K.C. 1970, *Ap. J.*, **160**, 811.

Freeman, K.C., Illingworth, G., and Oemler, A. 1983, *Ap. J.*, **272**, 488.

Fujimoto, M., and Murai T. 1984, *in "The Structure and Evolution of the Magellanic Clouds"*, eds. S. van den Bergh and K.S. de Boer, (Dordrecht : Reidel), p. 115.

Graham, J.A. 1979, *in "The Large Scale Structure of the Galaxy"*, ed. W.D. Burton, (Dordrecht : Reidel), p. 195.

Henize, K.G. 1956, *Ap. J. Suppl.*, **2**, 315.

Henize, K.G., and Westerlund, B.E. 1963, *Ap. J.*, **137**, 747.

Iben, I., and Tutakov, A.V. 1985, *Ap. J. Suppl.*, **58**, 661.

Isserstedt, J. 1975, *Astr. Ap.*, **41**, 21.

Jacoby, G.H. 1980, *Ap. J. Suppl.*, **42**, 1.

Kruit, van der, J.P., and Shostak, G.S. 1984, *Astr. Ap.*, **134**, 258.

Lin, D.N.C., and Lynden-Bell, D. 1982, *M.N.R.A.S.*, **198**, 707.

Lindsay, E.M., and Mullen, D.J. 1963, *Irish Astr. J.*, **6**, 51.

Liszt, H.S., Delin, X., and Burton, W.B. 1981, *Ap. J.*, **249**, 532.

McGee, R.X., and Milton, J.A. 1964 *in IAU Symposium 20, "The Galaxy and the Magellanic Clouds"*, eds. F.J. Kerr and A. W. Rodgers (Aust. Acad. Sci : Canberra), p. 289.

McGee, R.X., and Milton, J.A. 1966a, *Aust. J. Phys.*, **19**, 343.

McGee, R.X., and Milton, J.A. 1966b, *Aust. J. Phys. Astrophys. Suppl.*, No. 2.

Mathewson, D.S. 1976, *Roy. Greenwich Obs. Bull.*, No. 182.

Mathewson, D.S. 1984, *Mercury*, **13**, 57.

Mathewson, D.S., and Ford, V.L. 1984, *in IAU Symposium 108, "Structure and Evolution of the Magellanic Clouds"*, eds. S. van den Bergh and K.S. de Boer (Dordrecht : Reidel), p. 125.

Mathewson, D.S., Ford, V.L., and Visvanathan, N. 1986, *Ap. J.*, **301**, 664.

Mathewson, D.S., Schwarz, M.P., and Murray, J.D. 1977, *Ap. J. (Letters)*, **217**, L5.

Meaburn, J. 1981, *in "Investigating the Universe"*, ed. F.D. Kahn (Dordrecht : Reidel), p. 61.

Meatheringham, S.J., Dopita, M.A., and Morgan, D.H. 1988, *Ap. J.*, (April 15).

Meurer, G.R., Bicknell, G.V., and Gingold, R.A. 1985, *Proc. Astr. Soc. Aust.*, **6**, 195.

Morgan, D.H. 1984, private communication.

Murai, T., and Fujimoto, M. 1980, *Publ. Astr. Soc. Japan*, **32**, 581.

Reid, N. and Mould, J. 1984, *M.N.R.A.S.*, **284**, 98.

Rohlfs, K., Kreitschmann, J., Siegmann, B.C., and Feitzinger, J.V. 1984, *Astr. Ap.*, **137**, 343.

Sanduleak, N., McConnell, D.J., and Philip, A.G.D. 1978, *Pub. A.S.P.*, **90**, 621.

Sanduleak, N. 1984, *in IAU Symposium 108, "Structure and Evolution of the Magellanic Clouds"*, eds. S. van den Bergh and K.S. de Boer (Dordrecht : Reidel), p. 231.

Smith, H.C., and Weedman, D.W. 1972, *Ap. J.*, **177**, 595.

Spitzer, L., and Schwartzschild, M. 1951, *Ap. J.*, **114**, 385.

Spitzer, L., and Schwartzschild, M. 1953, *Ap. J.*, **118**, 106.

Stapinski, T.E., Rodgers, A.W., and Ellis, M.J. 1981, *Pub. A.S.P.*, **93**, 242.

Vader, J.P., and de Jong, T. 1981, *Astr. Ap.*, **100**, 124.

Villumsen, J.V. 1985, *Ap. J.*, **290**, 75.

Visvanathan, N. 1985, *Ap. J.*, **288**, 182.

Webster, B.L. 1969, *M.N.R.A.S.*, **143**, 79.

Weidemann, V. 1987, *in "Late stages of Stellar Evolution"*, eds. S. Kwok and S.R. Pottasch, (Dordrecht : Reidel), p. 347.

White, S.D.,and Frenk, C.S. 1983, *in "Kinematics, Dynamics and Structure of the Milky Way"*, ed. W.L. Shuter (Dordrecht : Reidel), p. 343.

Wielen, R. 1977, *Astr. Ap.*, **60**, 263.

Wood, P.R., Bessell, M.S. and Fox, M.W. 1983, *Ap. J.*, **272**, 99.

Wood, P.R., Bessell, M.S., and Dopita, M.A. 1985, *Proc. Astr. Soc. Aust.*, **6**, 54.

Wood, P.R., Meatheringham, S.J., Dopita, M.A., and Morgan, D.H. 1987, *Ap. J.*, **315**, L.107.

NEW EVOLUTIONARY RELATIONSHIPS FOR MAGELLANIC CLOUD PLANETARY NEBULAE

Michael A. Dopita, Stephen J. Meatheringham, Peter R. Wood

Mount Stromlo and Siding Spring Observatories,

Australian National University

B. Louise Webster

School of Physics,

University of New South Wales

David H. Morgan

Royal Observatory,

Edinburgh

Holland C. Ford

Space Telescope Science Institute,

Johns Hopkins University

Received: 1986 November 3

Accepted: 1987 January 16

Appeared in *Astrophysical Journal*, 1987, **315**, L107.

ABSTRACT

Two new evolutionary correlations have been discovered to apply to the population of planetary nebulae (PN) in the Magellanic Clouds. Firstly, the age of the nebular shell is found to follow a relationship $\tau = 890[(M_{neb}/\mathcal{M}_{\odot})(V_{exp}/\mathrm{km\ s^{-1}})]^{0.6}$ yr, which is shown to be consistent with a model in which the total energy of the ionized and swept up gas drives the expansion down the density gradient in the precursor AGB wind. Secondly, a tight correlation is found between the expansion velocity and a combination of the excitation class and the Hβ flux. This appears to be determined by the mass of the planetary nebula nuclear star. These correlations provide strong observational support for the idea that the PN shells are ejected at low velocity during the Asymptotic Giant Branch phase of evolution, and that they are continually accelerated during their nebular lifetimes.

Subject Headings: galaxies : Magellanic Clouds
nebulae : planetary
stars : evolution, white dwarfs

I. INTRODUCTION

Although there exists a substantial body of literature on the planetary nebula stage of stellar evolution, as yet there is no clear understanding of the relationship between the expanding nebular shell and the planetary nebula nuclear star (PNn) as it evolves from an asymptotic giant branch (AGB) star to a hot, dense white dwarf. The major reason for this is that dynamical studies have, in the past, been exclusively concerned with the study of the Galactic PNs, with all of the concomitant problems of uncertain distance scale, population type and reddening. For example, no clear consensus has emerged on what is the evolutionary trend of expansion velocity. Robinson, Reay and Atherton (1982) have suggested that the high- and low-mass PNs have different expansion velocity / radius relationships. Phillips (1984) finds a monotonic relationship, with a small subset of large-diameter, slowly expanding nebulae. Some authors have suggested that a maximum in expansion velocity is reached at a radius of about 0.2 pc, with a slow decline to larger sizes (Smith 1969; Bohuski and Smith 1974; Sabbadin, Bianchini and Hamzaoglu 1984). The recent series of papers by Sabbadin and his collaborators has provided a great detail of knowledge on the evolution of the nebular properties with age (Sabbadin and Hamzaoglu 1982; Sabbadin *et al.* 1984; Sabbadin 1986a, b).

The sample of planetary nebulae in the Magellanic Clouds offers notable advantages in evolutionary studies by furnishing us with a luminosity - limited sample at a known distance and with low line-of-sight reddening. In this paper we describe the discovery of a new evolutionary relationship for planetary nebulae using the results of our (almost) complete survey of the kinematics, internal dynamics and Hβ photometry of this population

(Dopita *et al.* 1985, 1988, Meatheringham *et al.* 1988a, b).

II. THE OBSERVATIONAL DATA BASE

The majority of the objects we have observed come from the list of Sanduleak, McConnell and Philip (1978), which includes many objects previously known as planetary nebulae (Henize and Westerlund 1963). This list was supplemented by a few objects from the Jacoby (1980) list, many of which are exceedingly faint and difficult to observe, and from the Morgan and Good (1985) list. One or two (unpublished) identifications by these same workers were also observed. The excitation classifications were made on the basis of UK Schmidt objective prism material by Morgan (1984) and are good to about one class.

The observations of the internal expansion velocities were made using the Cassegrain échelle spectrograph on the ANU 1-metre and 2.3-metre telescopes at Siding Spring and the RGO spectrograph on the Anglo-Australian 3.9-metre telescope also at Siding Spring. The observational techniques and reduction procedures are fully described elsewhere (Dopita *et al.* 1985).

The Hβ fluxes were measured using narrow-band interference filters in conjunction with the two dimensional Photon Counting Array (Stapinski, Rodgers and Ellis 1981) on the ANU 1-metre telescope, with supplementary determinations by speckle-mode Hβ imaging using the IPCS on the Anglo-Australian telescope (Meatheringham *et al.* 1988b).

Physical sizes for some PN have been measured by two techniques, speckle interferometry for the smallest and brightest objects (Wood, Bessell

and Dopita 1985), and by high time resolution imaging to remove the effects of translational seeing (Wood *et al.* 1987). The first technique gives angular diameters for those objects less than 0.4 arc seconds in diameter, whereas the second is good for objects larger than 0.7 arc seconds across. In a few cases, both measurements have been made, and the diameter is constrained between these two limits.

Given the Hβ flux and the angular diameter, the ionized mass of the PN can be derived. This mass is found to increase, roughly as the diameter, until a radius of about 0.1 pc is reached, and thereafter remain about constant in the range $0.15 - 0.5\mathcal{M}_{\odot}$, as the nebula becomes optically thin (Wood 1986).

III. EVOLUTIONARY CORRELATIONS

a) Expansion Velocity / Excitation Class / Flux Correlation

A recent study of expansion velocities of the SMC planetary nebulae has shown that a good correlation exists between the expansion velocity and the excitation class (Dopita *et al.* 1985). This correlation has also been found to apply to the LMC population (Dopita *et al.* 1988). However, it is apparent from the Hβ flux determinations (Meatheringham *et al.* 1988b), that a somewhat poorer correlation also exists between this quantity and the expansion velocity and/or excitation class. We were therefore encouraged to investigate the possibility that the expansion velocity, V_{exp}, is determined by a combination both of the excitation class and Hβ flux. A relationship of the form:

$$V_{exp} = a + bE - c\,[14.0 + \log F_{\mathrm{H}\beta}] \qquad (3.1)$$

was adopted, where E refers to the excitation class and a, b and c are constants. The parameters a, b and c were adjusted to minimize the RMS velocity difference between the expansion velocities given by equation (3.1) and those observed. The best fit correlation for both the LMC and SMC planetaries, gives an RMS velocity difference of 7.0 km s^{-1} between the observed and the fitted expansion velocities given by equation (3.1), where the distances to the LMC and SMC have been assumed to be 46 and 58 kpc respectively. This correlation is shown in Figure 1 ($a = 35 \pm 6$; $b = 3.1 \pm 0.7$; $c = 14 \pm 5$). The correlations for the LMC and the SMC, taken separately, are not significantly different, but that of the SMC is appreciably tighter, despite the possibility that the SMC is extended along the line of sight. For both Clouds, a significantly better correlation is obtained when both the parameters are included. For example, with $b = 0$, the best fit for the SMC planetaries gives an RMS velocity difference of 9.0 km s^{-1} ($a = 64$; $b = 0$; $c = 31$). With $c = 0$, the best fit RMS velocity difference is reduced to 7.8 km s^{-1} ($a = 10.5$; $b = 5$; $c = 0$). However when both parameters are included, the RMS velocity difference drops to 5.9 km s^{-1} ($a = 35 \pm 7$; $b = 3.4 \pm 0.8$; $c = 17 \pm 5$). In Figure 2, we show this best-fit V_{exp} surface projected onto the $\log F_{H\beta}$: excitation class plane. In the event that the PN are optically thick, this plane represents a transformed Hertzprung-Russell (H-R) diagram for the central stars, since excitation class is related to the Zanstra temperature and the Hβ flux counts the number of ionizing photons. Unfortunately, without a detailed nebular model, the relationship between the observed and true H-R diagrams remains uncertain.

Figure 1. The correlation between the observed expansion velocity and the fitted expansion velocity given from the excitation class / Hβ Flux combination of equation (3.1) with $a = 35$, $b = 3.1$ and $c = 14$. All objects for which these quantities have been adequately determined in the Large and Small Magellanic Clouds are plotted, with the SMC points normalized to the distance of the LMC. There are no corrections for reddening.

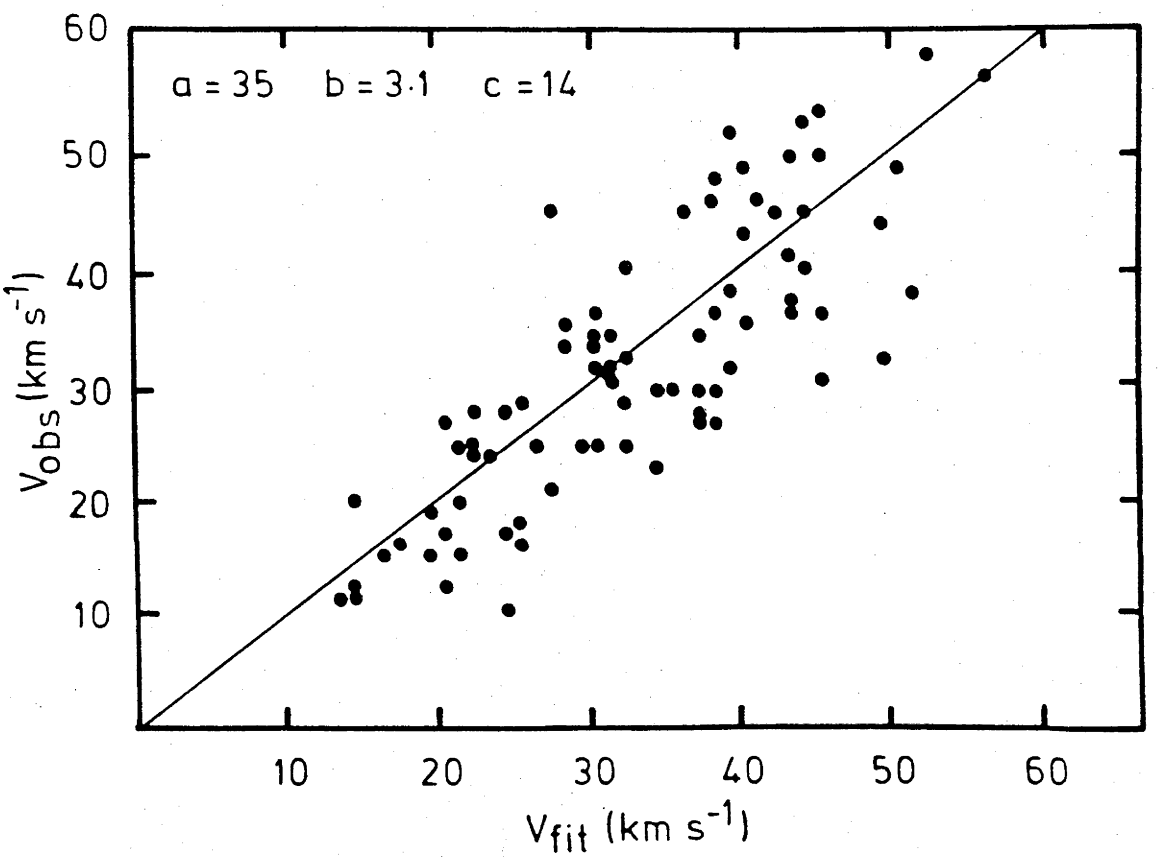
a = 35 b = 3·1 c = 14
60
50
40
30
20
10
10
20
30
40
50
60
V_{obs} (km s^{-1})
V_{fit} (km s^{-1})

Figure 2. The Hertzprung-Russell diagram for the planetary nebulae of the SMC transformed to the observable nebular parameters with lines of the least square expansion velocity fit and the measured expansion velocity for individual objects shown. The transformation is ill-defined, but this diagram demonstrates that the planetary nebulae are accelerated as the PNn fades, and that higher excitation class (high temperature, more massive PNn) expand more rapidly.

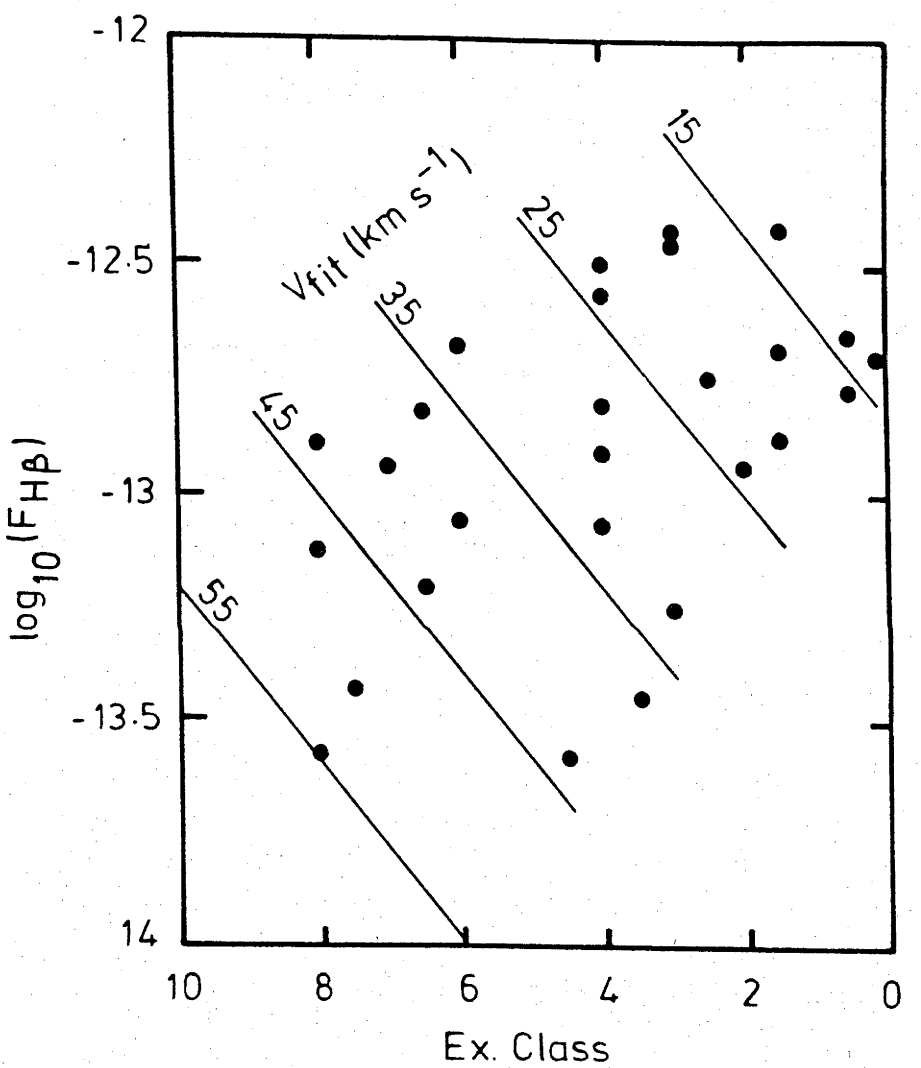
-12
-12.5
-13
-13.5
14
10
8
6
4
2
0
Ex. Class
log10(FHβ)
Vfit (km s-1)
55
45
35
25
15

b) A Dynamical Age / Mass / Expansion Velocity Relationship

A very direct evolutionary relationship is one that connects the dynamical age of the PN, $\tau_{dyn} = R_{neb}/V_{exp}$, to observable parameters such as nebular mass and/or the expansion velocity. The nebular mass and dynamical age is only known for those nebulae for which angular diameters have been measured, a total of nineteen objects of which four are in the SMC. A power-law relationship of the following form was adopted :

$$\log(\tau_{dyn}/\mathrm{yr}) = a + b\log(M_{neb}/\mathcal{M}_{\odot}) + c\log[(V_{exp} - d)/\mathrm{km\ s^{-1}}] \qquad (3.2)$$

where a, b, c and d are constants chosen to minimize the RMS difference between the dynamical ages calculated from equation (3.2) and those observed. The best fit was determined by progressive iteration, varying parameters in pairs. As different iterations converged from different starting points we conclude that an absolute minimum has been obtained. This fit is shown in Figure 3, with the constants determined as ($a = 2.95 \pm 0.25$; $b = 0.6 \pm 0.08$; $c = 0.6 \pm 0.1$; $d = 0.0 \pm 5.0$). The errors correspond to an increase in the least squares of 20% for each parameter. The RMS scatter is 0.175 dex. A correlation therefore exists between the *net momentum* and *dynamical age* of the ionized gas.

The objects in Figure 3 are well scattered along the correlation of Figure 1, so it is clear that the selection of objects for which angular diameters have been measured is in no way anomalous compared with the total population. There is, however, only a very poor correlation between the dynamical age and the expansion velocity. Thus the correlation of Figure 1 is independent of that of Figure 3, and the implication is that, for a given set of parameters characterizing the central star, the nebular mass may be quite widely variable.

Figure 3. The correlation between the observed dynamical age and the least squares fit dynamical age given by equation (3.2) with $a = 2.95$, $b = 0.6$ and $c = 0.6$. All objects in the LMC and SMC for which diameters have been directly measured are shown. This shows that momentum varies as $t^{5/3}$.

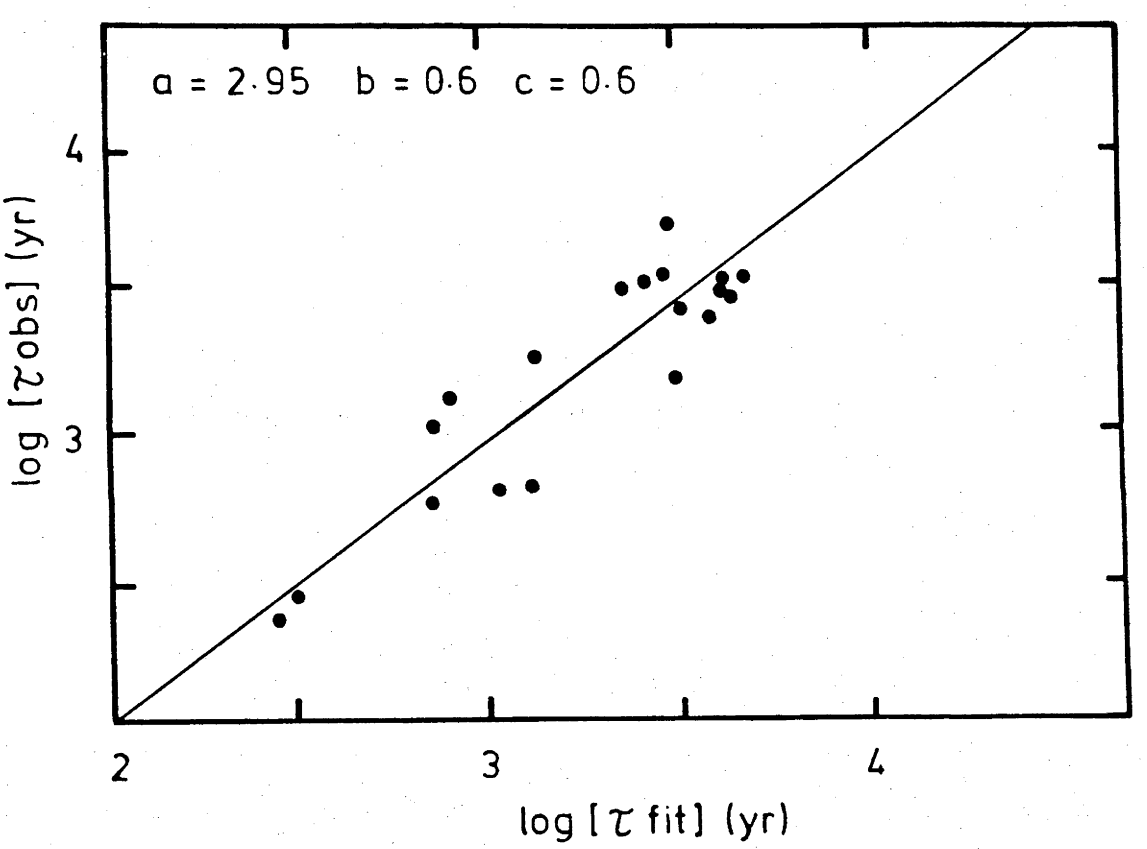
a = 2·95 b = 0·6 c = 0·6
log [τobs] (yr)
4
3
2
3
4
log [τ fit] (yr)

IV. DISCUSSION

A planetary nebula shell is believed to be expanding into, and ionizing, the wind produced during the Asymptotic Giant Branch phase of evolution. In the optically thick phase of evolution, the structure of the nebula around the planetary nebula nucleus (PNn) is composed of the following zones (in order, working in):

1. The undisturbed and un-ionized AGB wind (number density $n(r)$, temperature $T_{\rm I}$).
2. An isothermal shock.
3. A thin layer of shock-compressed isobaric un-ionized material (number density $n_{\rm I}$, temperature $T_{\rm I}$).
4. A weak D-type ionization front.
5. A shell of isobaric ionized gas, number density $n_{\rm II}$, temperature $T_{\rm II}$, which absorbs all the ionizing photons from the PNn.
6. A contact discontinuity between the ionized gas and shock-heated stellar wind gas.
7. A layer of shock-heated stellar wind gas.
8. A stellar wind shock.
9. A zone of undisturbed stellar wind gas about the PNn.

(See, for example, Dyson 1981; Kahn 1983; Kwok and Volk 1985; Volk and Kwok 1985). If the total energy content in the zones $3-7$ inclusive of

thermal energy, kinetic energy and trapped radiation is assumed to given by a power law:

$$E(t) = E_0 t^{\alpha} \tag{4.1}$$

and if the radial density distribution in the undisturbed AGB wind is given by:

$$\rho(r) = \rho_0 r^{\beta} \tag{4.2}$$

then, from dimensional considerations, the radius of the outer shock, R_{neb}, is

$$R_{neb} = A(E_0/\rho_0)^{1/(5+\beta)} t^{(2+\alpha)/(5+\beta)} \tag{4.3}$$

and the velocity of expansion V_{exp}, is given by

$$V_{exp} = B(E_0/\rho_0)^{1/(5+\beta)} t^{(\alpha-\beta-3)/(5+\beta)} \tag{4.4}$$

where A and B are dimensionless constants.

For a steady AGB wind, $\beta = -2$, and the mass swept up is therefore proportional to R_{neb}. However, the observable is the ionized mass, which does not necessarily show this dependence. From the work of Sabbadin (1986b) and Wood (1986), it appears that we can take $M_{ion} \approx C R_{neb}^{\gamma}$, where $1 < \gamma < 3/2$. The observed momentum content of the ionized shell, is therefore:

$$M_{ion} V_{exp} \approx (A^{\gamma} BC)(E_0/\rho_0)^{(1+\gamma)/(5+\beta)} t^{(\alpha-\beta+2\gamma-3+\alpha\gamma)/(5+\beta)} \tag{4.5}$$

However, our observed correlation between momentum and time is that $M_{ion} V_{exp} \approx D t^{5/3}$. For this to be consistent with (4.5) with $\beta = -2$ and $1 < \gamma < 3/2$ requires that $6/5 < \alpha < 2$, i.e., *that the energy content of the nebula rapidly increases with time.* This result puts limits on the possible dependence of the expansion velocity on radius, recalling that this

relationship is subject to considerable scatter (Sabbadin and Hamzaoglu 1984; Phillips 1984; Chu *et al.* 1984). Equations (4.3) and (4.4) imply, with $\beta = -2$ and $\alpha = 2$, that $V_{exp} \propto R_{neb}^{1/4}$. With $\alpha = 6/5$ we have $V_{exp} \propto R_{neb}^{1/16}$. This can be compared with the observational relationship found by Phillips (1984), $V_{exp} \propto R_{neb}^{0.22}$, suggesting that the $\gamma = 2$ solution is closer to the truth. In such an accelerating expansion, the contact discontinuity between the shocked stellar wind and the ionized nebular gas is Rayleigh-Taylor unstable, and radial mixing between these two phases is therefore expected.

Can the very steep increase in energy content with time be driven by a stellar wind from the central star? Certainly not on the Kahn (1983) or Kwok and Volk (1985) model, which have a thin photo-ionized nebular shell and which predict $\alpha = 1$ for a steady wind. Since pressure is energy content per unit volume, and since the photo-ionized gas at a temperature of $\sim 10^4$ K is in pressure balance with the shocked stellar wind, the ratio of the thermal energy content in these two zones is in the ratio of the volumes occupied by these zones. The fractional thickness of the ionized shell is typically of order 0.15 (Daub 1982, Phillips 1984) and the hot shocked stellar wind gas effectively fills the remainder of the volume (Kahn 1983), therefore the ratio of shocked stellar wind / photo-ionized nebula thermal energy is typically 1.5 : 1. For a nebular shell of mass M_{neb}, the total energy content is given by:

$$E(t) = M_{ion} c_{\rm II}^2/3 + M_{neb} V_{exp}^2/2 \qquad (4.6)$$

where $c_{\rm II}$ is the sound speed in the ionized gas. Since $M_{neb} \geq M_{ion}$ and $V_{exp} \geq c_{\rm II}$, the kinetic energy term is dominant. Thus $E(t) \approx 0.5 M_{neb} V_{exp}^2$. For the case of a time-invariant stellar wind running into a cloud with a radial density gradient, Kwok and Volk (1985) derive the efficiency of

conversion of wind energy into shell energy as $\epsilon = 3(5+\beta)/(2\beta+7)(\beta+11)$. For $\beta = -2$, $\epsilon = 1/3$. This is inconsistent with the ratio of 2/3 implied above, however, this difference may be the result of the breakdown of the thin-shell approximation used by Kwok and Volk, for the case where photo-ionization effects are negligible.

In effect, both the stellar wind parameters and the thickness of the photo-ionized layer are determined by the properties of the central star. If the stellar wind is radiation pressure driven, the energy input rate will vary as:

$$\begin{aligned} \partial\epsilon/\partial t &= 0.5mV_\infty^2 \\ &= \phi(L_*/c)V_{esc} \\ &= \phi c^{-1}(GM_*)^{1/2}(4\pi\sigma)^{1/4}L_*^{3/4}T_{eff} \end{aligned} \tag{4.7}$$

Where ϕ is a constant of order unity (with $V_\infty \approx 3V_{esc}$; Abbott 1978), c is the speed of light, σ is Stefan's constant and M_*, L_*, and T_{eff} are the mass, luminosity and effective temperature of the PNn, respectively. From Wood and Faulkner (1986), the typical lifetime of a $0.7\mathcal{M}_\odot$ PNn at high luminosity is about 1000 yr. Taking $\log L_*/\mathcal{L}_\odot = 4.1$, $\log T_{eff} = 4.9$, about 10^{45} ergs of mechanical energy can be deposited by the wind.

Provided that the ionization front is trapped in the swept-up matter, the pressure in the photo-ionized region and its extent are also determined by the properties of the central star. The pressure in the photo-ionized region is determined by the stellar wind, and the radial extent of photo-ionized region is fixed by this pressure and by the number of ionizing photons emitted by the central star. If the inner stellar wind shock occurs at $R = \theta R_{neb}$ the pressure in the photo-ionized gas, which is in pressure equilibrium with the

shocked stellar wind, is given by:

$$P = \phi(L_*/c)/4\pi\theta^2 R_{neb}^2 = \mu m_{\rm H} n_{\rm II} c_{\rm II}^2/3 \qquad (4.8)$$

where $\mu m_{\rm H}$ is the atomic weight, and $n_{\rm II}$ and $c_{\rm II}$ are the number density and sound speed, respectively, in the ionized gas. If the number of ionizing photons produced by the central star is S_* then setting the number of ionizations equal to the number of recombinations in a photo-ionized shell of thickness ΔR we have, from (4.8):

$$\Delta R/R_{neb} = [4\pi(c\mu m_{\rm H} c_{\rm II}^2)^2/(9\beta_{eff})][S_*/\phi^2 L_*^2]\theta^4 R_{neb} \qquad (4.9)$$

where β_{eff} is the effective recombination coefficient of hydrogen. Since T_{eff} is high, and varies only slowly through the fading epoch of the central star, we can take $S_* = const\, L_*$. The quantity $\Delta R/R_{neb}$ is observed to vary little with R_{neb} for Galactic PN, which implies that $L_* \propto 1/R_{neb}$, approximately. Notice that $\Delta R/R_{neb}$ is a sensitive function of θ. This emphasizes the the intimate relation between the position of the stellar wind shock and the observed properties of the photo-ionized shell. In view of this, the inconsistency between the observed conversion efficiency of stellar wind to shell energy and the Kwok and Volk value may not be severe.

Thus far our discussion has centered on the more readily interpretable momentum / age correlation. What of the expansion velocity / excitation class / Hβ flux correlation? As we have already pointed out, there is no correlation between the dynamical age and the position of a nebula on this correlation. However, despite this, we still believe that the correlation represents an evolutionary relationship. The definition of the excitation class (Morgan 1984) ensures that it is closely related to the Zanstra Temperature of the PNn. Furthermore, the Hβ flux should correlate well

with the luminosity of the PNn, at least for the optically thick nebulae. The position of a PN on the expansion velocity / excitation class / Hβ flux correlation should therefore depend principally on the properties of the PNn. Since T_{eff} changes rapidly only in the relatively short-lived high luminosity stage, and since the more massive stars achieve higher T_{eff}, the excitation class should reflect the mass of the PNn. More massive PNn fade more rapidly, therefore the lower Hβ fluxes associated with the higher excitation nebulae in Figure 2 is also consistent with the identification of high excitation nebulae with more massive PNn. The higher expansion velocities seen in this class of nebulae can therefore be interpreted as the consequence of the fact that these stars are more efficient at ionizing the surrounding AGB wind, and so delivering more energy to the nebula. The increase in velocity as Hβ luminosity decreases reflects the evolutionary trend towards higher expansion velocities in older nebulae.

If we accept that the expansion velocity is given by equation (4.4), then the fact that two nebulae at the similar stages of PNn evolution may have widely different dynamical ages implies on or both of two possibilities. Either the assumption of spherical symmetry has broken down, which is certainly the case in the bipolar nebulae, or else E_0/ρ_0 must differ strongly from one nebula to the next as a result of differing initial conditions in the ejected AGB star envelope. Such a variation would go a long way to explaining the considerable scatter in the V_{exp} : R_{neb} relation. The physical explanation of this is probably that the PNn leave the AGB at different phases of the helium flash cycle. Objects which do this following the peak of the helium flash are evolving into a dense shell driven off at low velocity near the peak luminosity, and therefore the initial ionized mass will be low, the acceleration slow, and a given expansion velocity will be reached

only at a relatively large radius and ionized mass. On the other hand, objects leaving the AGB between shell flashes will evolve into a low density wind, and rapidly accelerate to a high velocity. The low velocity sequence discussed by Phillips (1984) and apparent in the work of Chu *et al.* (1984) may be the result of evolution from the AGB near the peak luminosity of the helium shell flash cycle. Iben (1984) has shown that most bright PN should be powered by helium burning nuclei. Since this study is based on a luminosity limited sample, there is a selection effect with a bias towards hugh luminosity nebulae. This will tend to reinforce the population of PN along the low velocity sequence and should inhibit the scatter in the V_{exp} : R_{neb} relation. Thus there is some evidence that the scatter is real or spherical symmetry has broken down. The latter possibility is quite probable when one considers the difficulty in measuring accurate expansion velocities for PN without the advantage of spatial resolution (Chu *et al.* (1984))..

V. CONCLUSION

Two new evolutionary relationships have been found to apply to the Magellanic Cloud population of planetary nebulae. These, together with the previously known ionized mass : radius correlation put very strong observational restraints on the possible models to describe the PN evolution.

REFERENCES

Abbott, D.C. 1978, *Ap. J.*, **255**, 893.

Bohuski, T.J. and Smith, M.J. 1974, *Ap. J.*, **193**, 197.

Chu Y-H, Kwitter, K.B., Kaler, J.B, and Jacoby, G.H. 1984, *Pub. A.S.P.*, **96**, 598.

Daub, C.J. 1982, *Ap. J.*, **260**, 612.

Dopita, M.A., Ford, H.C., Lawrence, C.J. and Webster, B.L. 1985, *Ap. J.*, **296**, 390.

Dopita, M.A., Meatheringham, S.J., Webster, B.L. and Ford, H.C. 1988, *Ap. J.*, April 15.

Dyson, J.E. 1981, in *Investigating the Universe*, ed. F.D. Kahn, (Dordrecht : Reidel), p. 125.

Henize, K.G. and Westerlund, B.E. 1963, *Ap. J.*, **137**, 747.

Iben, I. 1984, *Ap. J.*, **277**, 333.

Jacoby, G.H. 1980, *Ap. J. Suppl.*, **42**, 1.

Kahn, F.D. 1983, in *IAU Symposium 103, Planetary Nebulae*, ed. D.R. Flower, (Dordrecht : Reidel), p. 305.

Kwok, S. and Volk, K. 1985, *Ap. J.*, **299**, 191.

Meatheringham, S.J., Dopita, M.A., Ford, H.C. and Webster, B.L., 1988a, *Ap. J.*, April 15.

Meatheringham, S.J., Dopita, M.A., and Morgan, D.H., 1988b, *Ap. J.*, June 1.

Morgan, D.H. 1984, *M.N.R.A.S.*, **209**, 241.

Morgan, D.H., and Good, A.R. 1985, *M.N.R.A.S.*, **213**, 491.

Phillips, J.P. 1984, *Astr. Ap.*, **137**, 92.

Robinson, G.J., Reay, N.K. and Atherton, P.D. 1982, *M.N.R.A.S.*, **199**, 649.

Sabbadin, F. 1986a, *Astr. Ap.*, **160**, 31.

Sabbadin, F. 1986b *Astr. Ap. Suppl.*, **64**, 579.

Sabbadin, F., Bianchini, A. and Hamzaoglu, E. 1984, *Astr. Ap.*, **136**, 200.

Sabbadin, F., Gratton, R.G., Bianchini, A., and Ortolani, S. 1984, *Astr. Ap.*, **136**, 181.

Sabbadin, F. and Hamzaoglu, E. 1982, *Astr. Ap.*, **110**, 105.

Sanduleak, N., McConnell, D.J. and Philip, A.G.D. 1978, *Pub. A.S.P.*, **90**, 621.

Smith, H.C. 1969, M.A. Thesis, University of Virginia.

Stapinski, T.E., Rodgers, A.W. and Ellis, M.J. 1981, *Pub. A.S.P.*, **93**, 242.

Volk, K. and Kwok, S. 1985, *Astr. Ap.*, **153**, 79.

Wood, P.R. 1986, workshop on *The Late Stages of Stellar Evolution*, (in press).

Wood, P.R., Bessell, M.S. and Dopita, M.A. 1985, Proc. Astr. Soc. Aust., **6**, 54.

Wood, P.R. and Faulkner, D.J. 1986, *Ap. J.*, **307**, 659.

Wood, P.R., Meatheringham, S.J., Dopita, M.A. and Morgan, D.H. 1987, *Ap. J.*, **320**, 178.

THE INTERNAL DYNAMICS OF THE PLANETARY NEBULAE IN THE LARGE MAGELLANIC CLOUD

Michael A. Dopita, Stephen J. Meatheringham

Mount Stromlo and Siding Spring Observatories,

Australian National University

B. Louise Webster

School of Physics,

University of New South Wales.

Holland C. Ford

Space Telescope Science Institute,

Johns Hopkins University

Received: 1987 January 28

Accepted: 1987 October 10

To appear in *Astrophysical Journal*, 1988, April 15.

ABSTRACT

The radial velocity and expansion velocity in the [O III] λ5007 line have been determined for a sample of 94 planetary nebulae (PN) in the Large Magellanic Cloud. In addition, densities and expansion velocities have been determined for a subset of 44 objects in both the Large and Small Magellanic Clouds using the [O II] $\lambda\lambda$3727, 3729 doublet. With a few notable exceptions, the [O II] expansion velocities are well correlated with, but are systematically higher than, the [O III] expansion velocities. For a given excitation class, there appears to be an upper limit to the density, in the sense that very high density objects are always of low excitation, but low density objects can occur at any excitation. The population of PN in the Magellanic Clouds appears to form a sheet in dynamical age / excitation class / nebular density space, and therefore represents a two parameter family. The implication of this is that the nebular parameters are entirely determined by the properties of the central star. This fact could represent the basis of a solution to the distance scale problem for Galactic PN.

Subject Headings: galaxies : Magellanic Clouds
nebulae : planetary
stars : evolution, white dwarfs

I. INTRODUCTION

There exists a substantial body of literature on the planetary nebula stage of stellar evolution. However, from an observational viewpoint much remains to be learnt about the relationship between the expanding nebular shell and the planetary nebula nuclear star (PNn) during the evolution from an asymptotic giant branch (AGB) star to a hot, dense white dwarf. The major reason for this is that dynamical studies have, in the past, been exclusively concerned with the study of the Galactic PNs, with all of the concomitant problems of uncertain distance scale, population type and reddening. For example, no clear consensus has emerged on what is the evolutionary trend of expansion velocity. Robinson, Reay and Atherton (1982) have suggested that the high- and low-mass PNs have different expansion velocity / radius relationships. Phillips (1984) finds a monotonic relationship, with a small subset of large-diameter, slowly expanding nebulae. Some authors have suggested that a maximum in expansion velocity is reached at a radius of about 0.2 pc, with a slow decline to larger sizes (Smith 1969; Bohuski and Smith 1974; Sabbadin and Hamzaoglu 1982). The recent series of papers by Sabbadin and his collaborators has provided a great detail of knowledge on the evolution of the nebular properties of galactic PN with age (Sabbadin, Bianchini and Hamzaoglu 1984; Sabbadin *et al.* 1984; Sabbadin 1986a, b).

The sample of planetary nebulae in the Magellanic Clouds offers notable advantages in evolutionary studies by furnishing us with a luminosity-limited sample at a known distance and with low line-of-sight reddening. This paper extends the results of our (almost) complete survey of the kinematics and internal dynamics of the PN in the Small Magellanic Cloud

(Dopita *et al.* 1985), hereafter DFLW, to the population of Large Magellanic Cloud (LMC) planetary nebulae. The radial velocities are given in this paper, but the kinematical results are of sufficient interest in their own right to be the subject of a separate paper (Meatheringham *et al.* 1988a).

The results of this paper add to the homogeneous data set that is being accumulated on the Magellanic Cloud PN in order to provide an understanding of the post-Asymptotic Giant Branch evolution. This data set includes Hβ photometry (Meatheringham *et al.* 1988b), sizes from speckle interferometry and direct imaging (Wood, Bessell and Dopita 1985, Wood, Dopita and Bessell 1986; Wood *et al.* 1987), and spectrophotometric studies (Dopita *et al.* 1988).

II. OBSERVATIONS AND DATA REDUCTION

a) Selection of Objects

The majority of the objects we have observed come from the list of Sanduleak, McConnell and Philip (SMP) (1978), which includes many objects previously known as planetary nebulae (Henize and Westerlund 1963). This list was supplemented by a few objects from the Jacoby (J) (1980) list, many of which are exceedingly faint and difficult to observe. Some of these objects appear to show no trace of [O III] emission, but rather a faint structured continuum. Since these objects were selected on the basis of their apparent [O III] emission in narrow band images, they are unlikely to be low excitation PN. Indeed, they may not be PN at all, but this conclusion needs to be confirmed with low-dispersion spectroscopy. Recently, Morgan and Good (1985) (MG) have undertaken a deep search of high-dispersion

UK Schmidt Telescope objective prism material with the aim of extending the sample of objects to a wider search region and to lower luminosities. A few of the brightest of these have also been observed. All appear to be bona fide PN, frequently in an advanced evolutionary state. The excitation classifications were made by Morgan (1984) on the basis of UK Schmidt objective prism material. Morgan adapted the classification scheme of Feast (1968) which was in turn based on the classification originally proposed by Aller (1956). On average the excitation classification should be good to about one class, although errors may be larger than this in the case of faint objects.

b) The Observations

We have used three telescopes, two spectrographs and two photon-counting systems in this study. Observations in the [O III] λ5007 line were made in October and November 1983 and October 1984 on the 1.0-metre telescope at Siding Spring Observatory, and observations in January 1985 used the 2.3-metre Advanced Technology Telescope also at Siding Spring. Both these telescopes are operated by the Australian National University, and the Perkin-Elmer échelle spectrograph was used on both telescopes as the dispersing element, with the Photon Counting Array as detector. Supplementary [O III] observations of the fainter objects were made in December 1983 on the 3.9-metre Anglo-Australian Telescope using its RGO Spectrograph and the Image Photon Counting System as the detector.

The instrumental parameters and the reduction procedures for the [O III] data are identical to those described in DFLW, and will not be described again here. The resolution of both systems are very similar, 11.5 km s^{-1} FWHM for the échelle spectrograph, and 11.75 km s^{-1} for the RGO spectrograph. The estimated errors in determination of the radial velocity are ± 1.5 km s^{-1} for the 1.0-metre observations, ± 0.6 km s^{-1} for the 2.3-metre data, and ± 0.3 km s^{-1} in the case of the AAT data.

The observations in the [O II] $\lambda\lambda 3727, 3729$ doublet were made on the 3.9-metre Anglo-Australian Telescope in January 1985. The RGO spectrograph was used with its 82cm camera a with a grating of 1200 lines mm^{-1} blazed at J and operating in second order. The slit width of 80μ gave a system resolution (FWHM) of 11.4 km s^{-1}. As for the [O III] data the spectral line profiles were fitted using the multiple gaussian fitting routines of the SPECTRE code (Pelat, Alloin and Fosbury 1981). Up to four gaussian components were used for each line, but the widths and spacings of the two doublet components were kept fixed, relative to each other. Figure 1 shows the result of this fitting process on a representative PN, both for the [O III] line and the [O II] doublet.

III. RESULTS

a) The [O III] $\lambda 5007$ *Data*

In Tables 1 and 2 we present the excitation class and Hβ flux (where known) for the LMC PN that we observed. Also given are the measured [O III] $\lambda 5007$ radial velocities with respect to the Local Standard of Rest, and the measured expansion velocities in this spectral line. Here we follow

Figure 1. Observed line profiles in [O III] λ5007 (a) and the [O II] $\lambda\lambda$3727,3729 doublet (b) for a representative LMC planetary nebula, SMP#6 . Also shown is the multiple gaussian line fits to these profiles. The bars represent the instrumental full width at half maximum.

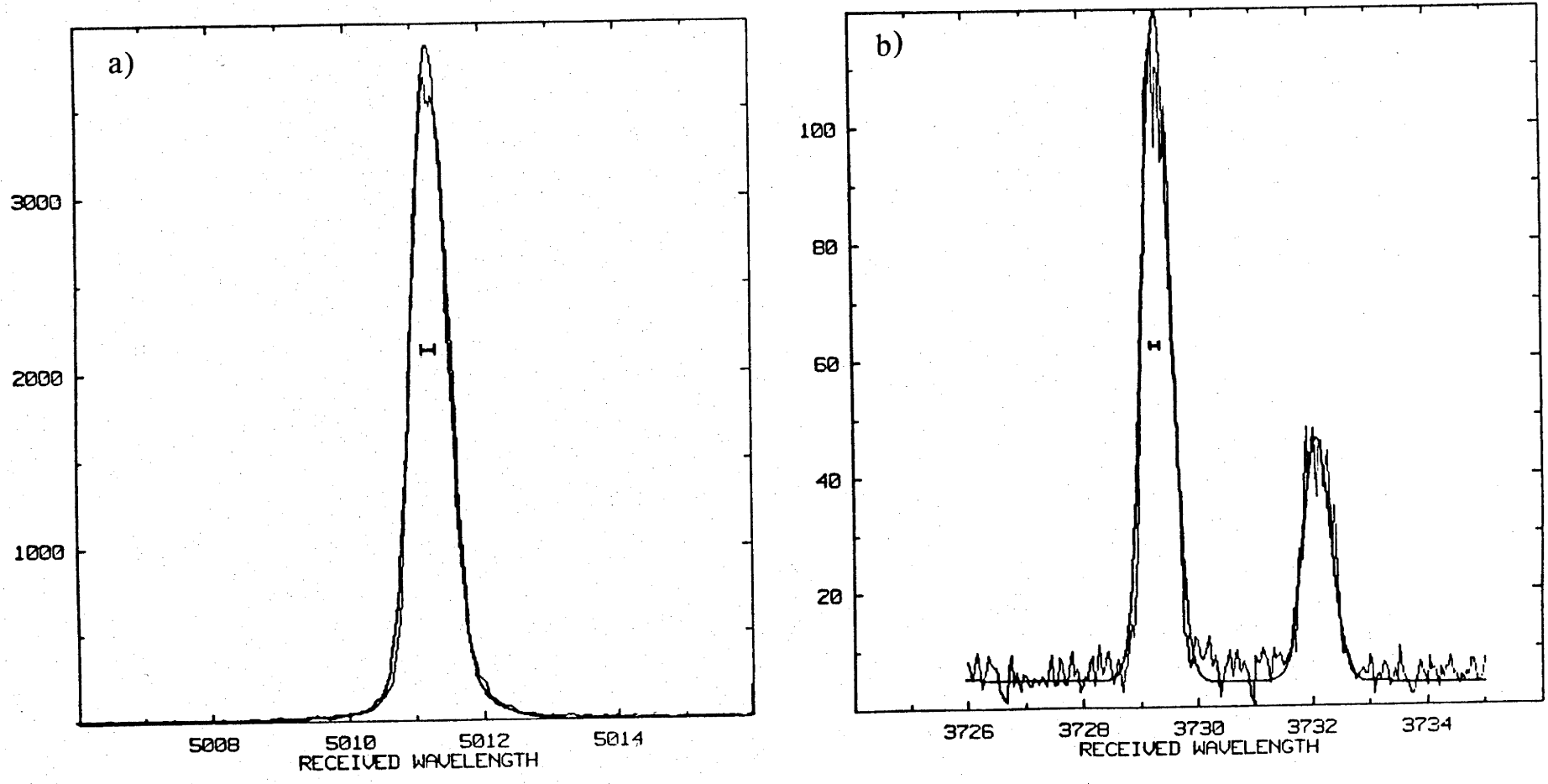
a)
3000
2000
1000
I
5008
5010
5012
5014
RECEIVED WAVELENGTH
b)
100
80
60
40
20
I
3726
3728
3730
3732
3734
RECEIVED WAVELENGTH

TABLE 1

VELOCITY AND FLUX DATA FOR LMC PLANETARY NEBULAE FITTED BY A SINGLE GAUSSIAN COMPONENT

Object Name[a]	Excitation[b] Class	$\log F_{H\beta}$[c] (erg cm^{-2} s^{-1})	V_{lsr} (km s^{-1})	V_{exp} (km s^{-1})
SMP 1	4	−12.46	209.1	17.2
SMP 2	...	−13.18	248.2	9.9
SMP 3	...	−12.48	172.0	20.0
SMP 4	...	−13.52	282.9	37.9
SMP 6	7	−12.67	249.0	28.6
SMP 7	6	−13.12	204.8	44.7
SMP 8	2	−12.74	277.1	25.2
SMP 9	6 − 7	−13.38	270.7	22.9
SMP 13	6	−12.82	212.3	46.1
SMP 14	3 − 7	−13.69	236.9	51.5
SMP 15	5 − 6	−12.66	188.0	41.2
SMP 16	8	−13.30	237.5	33.0
SMP 18	2 − 6	−13.36	228.7	27.4
SMP 19	7	−12.73	220.2	28.6
SMP 20	2	−13.37	273.1	25.8
SMP 23	4	−12.68	267.1	21.6
SMP 24	...	−13.77	254.7	56.4
SMP 27	3 − 6	−13.40	258.2	33.3
SMP 28	6 − 7	−13.35	233.7	55.0
SMP 29	7	−12.71	228.2	35.9
SMP 31	0	−12.91	248.1	5.1
SMP 32	8 − 9	−12.80	240.2	42.3
SMP 33	6 − 7	−12.81	253.9	30.8
SMP 36	5 − 6	−12.72	247.6	34.6
SMP 37	7	−12.85	255.2	39.2
SMP 38	5	−12.62	225.4	34.5
SMP 42	5 − 6	−13.11	273.4	37.9
SMP 45	6	−13.17	275.0	36.8
SMP 46	6	−13.60	258.0	26.1

TABLE 1 (continued)

VELOCITY AND FLUX DATA FOR LMC PLANETARY NEBULAE FITTED BY A SINGLE GAUSSIAN COMPONENT

Object Name[a]	Excitation[b] Class	$\log F_{H\beta}$[c] (erg cm^{-2} s^{-1})	V_{lsr} (km s^{-1})	V_{exp} (km s^{-1})
SMP 48	3 – 4	−12.43	240.8	15.8
SMP 50	5	−12.71	284.1	35.0
SMP 51	3 – 9	...	256.4	23.3
SMP 52	5	−12.52	256.9	36.3
SMP 53	5	−12.62	261.8	25.0
SMP 55	0.5	−12.66	194.7	6.0
SMP 56	1	−13.13	276.1	10.3
SMP 57	3 – 6	−13.41	297.6	32.5
SMP 58	4	−12.48	264.2	18.8
SMP 60	9.5	−13.50	207.0	58.3
SMP 61	4	−12.48	178.4	29.3
SMP 62	6	−12.31	223.6	34.6
SMP 63	4 – 5	−12.48	248.8	16.7
SMP 65	2 – 5	−13.31	195.7	17.8
SMP 66	5 – 6	−12.95	289.2	23.1
SMP 67	1	−12.81	274.1	27.9
SMP 69	8 – 9	−13.17	289.9	44.3
SMP 71	6 – 7	−12.86	201.2	28.0
SMP 73	6	−12.54	225.6	25.9
SMP 74	6	−12.66	253.6	35.1
SMP 77	1	−12.78	328.2	12.9
SMP 78	6	−12.58	240.7	33.4
SMP 79	5	−12.63	215.1	37.2
SMP 81	5	−12.61	242.2	32.6
SMP 84	4	−12.63	235.0	46.2
SMP 85	1	−12.42	217.0	11.3
SMP 87	8 – 9	−12.91	264.6	37.4
SMP 88	9	−13.26	211.0	24.7
SMP 89	5	−12.61	261.2	25.2
SMP 91	7	−13.55	295.3	45.3

TABLE 1 (continued)

VELOCITY AND FLUX DATA FOR LMC PLANETARY NEBULAE

FITTED BY A SINGLE GAUSSIAN COMPONENT

Object Name[a]	Excitation[b] Class	$\log F_{H\beta}$[c] (erg cm^{-2} s^{-1})	V_{lsr} (km s^{-1})	V_{exp} (km s^{-1})
SMP 92	6	−12.54	256.4	29.3
SMP 95	5 − 7	−13.47	290.9	31.2
SMP 96	9	−13.34	239.4	60.9
SMP 99	5	−12.54	248.8	25.3
SMP 100	6	−12.86	270.1	46.4
SMP 102	7	−13.22	286.5	41.2
J 5	1	−13.25	262.9	25.4
J 33	...	...	231.2	43.2
A 0	...	...	288.5	34.3
A 3	...	...	272.9	20.3
A 22	...	...	236.6	22.1
A 24	...	...	267.2	34.6
A 54	...	...	282.8	33.3

[a] For nomenclature, see section II (a).
[b] Excitation class from Morgan (1984).
[c] Flux from Meatheringham *et al.* (1988b).

TABLE 2

VELOCITY AND FLUX DATA FOR LMC PLANETARY NEBULAE

FITTED BY MULTIPLE GAUSSIAN COMPONENTS

Object Name[a]	Excitation Class[b]	$\log F_{H\beta}$[c] (erg cm^{-2} s^{-1})	$< V_{lsr} >$ (km s^{-1})	V_{exp} (km s^{-1})	V_{lsr} (km s^{-1})	ΔV (km s^{-1})	A^d_{rel}
SMP 5	1	−12.85	271.0	20.8	270.7	7.5	1.000
					271.7	35.6	0.545
				(76.6)	271.2	83.2	0.190
SMP 10	6 – 7	−13.15	207.0	47.0	189.7	33.1	1.000
					224.5	31.8	0.901
SMP 11	7[e]	−13.15	249.4	122.0	237.0	54.5	1.000
					204.5	96.7	0.694
					296.6	56.3	0.583
					354.7	84.5	0.153
SMP 21	7	−12.76	244.8	49.1	249.8	37.4	1.000
					209.4	25.8	0.272
				(128.0)	237.9	141.0	0.476
SMP 30	8	−13.45	264.9	40.9	270.1	58.2	1.000
					258.5	18.9	0.831
SMP 35	5	−12.81	295.0	41.3	281.6	31.5	1.000
					314.0	23.6	0.673

TABLE 2 (continued)

VELOCITY AND FLUX DATA FOR LMC PLANETARY NEBULAE

FITTED BY MULTIPLE GAUSSIAN COMPONENTS

Object Name[a]	Excitation Class[b]	$\log F_{H\beta}$[c] (erg cm^{-2} s^{-1})	$< V_{lsr} >$ (km s^{-1})	V_{exp} (km s^{-1})	V_{lsr} (km s^{-1})	ΔV (km s^{-1})	A^d_{rel}
SMP 40	7	−13.25	238.9	54.5	238.7	29.9	1.000
					261.8	64.3	0.623
					210.4	118.0	0.491
SMP 41	6	−13.33	244.2	51.7	240.3	48.0	1.000
					278.7	23.4	0.207
				(155.0)	205.9	136.0	0.133
					335.4	61.6	0.058
SMP 47	6 – 7	−12.52	258.3	50.1	254.9	55.0	1.000
				(148.0)	195.7	115.0	0.089
					297.8	99.3	0.361
SMP 49	6	−13.35	232.2	38.1	222.8	33.3	1.000
					248.6	22.0	0.116
SMP 54	8	−13.51	264.3	42.3	250.4	31.1	1.000
					279.8	29.7	0.837
				(96.2)	214.4	56.3	0.123
					299.3	61.7	0.198

TABLE 2 (continued)

VELOCITY AND FLUX DATA FOR LMC PLANETARY NEBULAE

FITTED BY MULTIPLE GAUSSIAN COMPONENTS

Object Name[a]	Excitation Class[b]	$\log F_{H\beta}$[c] (erg cm^{-2} s^{-1})	$< V_{lsr} >$ (km s^{-1})	V_{exp} (km s^{-1})	V_{lsr} (km s^{-1})	ΔV (km s^{-1})	A^d_{rel}
SMP 76	3	−12.54	262.8	29.0	264.0	22.8	1.000
					273.7	30.2	0.554
SMP 82	3 – 4	...	239.6	38.4	238.9	66.4	1.000
					240.9	15.9	0.513
SMP 83	8 – 9[e]	−12.65	274.5	82.9	232.5	57.7	1.000
					323.9	41.8	0.839
				(142.0)	212.3	104.0	0.118
					348.9	57.6	0.193
SMP 94	7[e]	−12.99	259.4	40.7	(Symbiotic Star)		
SMP 97	8 – 9	−12.85	271.8	46.1	287.8	31.5	1.000
					255.3	32.9	0.976
SMP 101	7 – 8	−12.81	266.0	47.3	250.2	40.0	1.000
					284.5	26.3	0.699
J 26	...	...	230.3	61.7	243.9	60.2	1.000
					228.1	58.0	0.970

TABLE 2 (continued)

VELOCITY AND FLUX DATA FOR LMC PLANETARY NEBULAE

FITTED BY MULTIPLE GAUSSIAN COMPONENTS

Object Name[a]	Excitation Class[b]	$\log F_{H\beta}$[c] (erg cm^{-2} s^{-1})	$< V_{lsr} >$ (km s^{-1})	V_{exp} (km s^{-1})	V_{lsr} (km s^{-1})	ΔV (km s^{-1})	A^d_{rel}
J 38	...	...	265.6	36.9	265.1	40.5	1.000
				(74.1)	245.1	52.0	0.208
					306.6	43.3	0.111
J 41	...	...	240.0	29.3	232.1	29.7	1.000
					247.7	61.5	0.833
A 4	...	...	254.2	68.8	268.2	54.0	1.000
					218.5	42.7	0.393
A 46	...	...	243.4	52.5	232.3	39.0	1.000
					285.8	37.7	0.464

[a] For nomenclature, see section II (a).
[b] Excitation Class from Morgan (1984).
[c] Flux from Meatheringham *et al.* (1988b).
[d] Area under Gaussian, relative to main component.
[e] See discussion in Dopita, Ford and Webster (1985).

the definitions given in DFLW, and we refer the reader to that paper for a full discussion. Briefly, the expansion velocity is defined to be half the full width at 10% maximum. This figure was found from models to give an answer which is largely independent of brightness distribution within the nebula. If the more usual FWHM definition had been used, then, for example, nebulae with two bright ansae would have apparently different expansion velocities depending on whether these ansae lie in the plane of the sky or along the line of sight. The 10% figure adopted ensures that the expansion velocity of these unresolved objects is determined by the fastest gas in the outer ionized shell. This figure should rather closely related to the maximum line splitting observed in resolved objects. The velocity dispersion (ΔV) of each component has been corrected for the instrumental half-width, assuming that it adds in quadrature. For those objects fitted by a single gaussian (in Table 1), the relationship between the expansion velocity, V_{exp}, and full width at half maximum (FWHM), ΔV, is given by $V_{exp} = 0.911\Delta V$. In the case of those objects showing double and multi-component profiles, which are most likely to show a bipolar structure when resolved, our definition of expansion velocity measures half the velocity difference between the (low velocity) 10% maximum point on the low velocity component with radial velocity $V_{lsr}(1)$ and FWHM width $\Delta V(1)$, and the corresponding high velocity point on the high velocity component with radial velocity $V_{lsr}(2)$ and width $\Delta V(2)$, $V_{exp} = 0.455[\Delta V(1) + \Delta V(2)] + 0.5|V_{lsr}(1) - V_{lsr}(2)|$. In Table 2 we give the mean radial velocity and the expansion velocity for the objects observed. Two or more radial velocities are given for those objects which required more than one gaussian component for a fit. Two expansion velocities are given for those objects fitted by three or four components (double shell

objects), but in the analysis below, the expansion velocity used is that measured by the principal components of the fit. Also given in Table 2 are the parameters which characterize the individual gaussians of the fit, radial velocity, width and integrated intensity with respect to the principal component. Without spatial information it is not possible to determine accurately the true internal kinematics of the nebulae.

The existence of PN in the LMC which show extremely high velocity motions has already been reported (Dopita, Ford and Webster 1985). However, Table 2 suggests that the existence of a high velocity outer shell or bipolar flow is not very unusual amongst the fainter (optically thin?) PN. Several examples are shown in Figure 2, which serves to emphasize how the faint tails of the profiles are difficult to observe, even though they may contribute a substantial fraction of the total flux.

The agreement between the radial velocities given here and those found in earlier studies is very good. For a discussion, see Meatheringham *et al.* 1988a.

b) The [O II] $\lambda\lambda 3727, 3729$ *Data*

The [O II] data were collected on a sub-sample of objects in both the Large and Small Magellanic Clouds, chosen to cover as wide a range of excitation class and flux as possible. Size estimates based on preliminary density and flux estimates were used to select objects for subsequent speckle interferometry observations (Wood, Bessell and Dopita 1985; Wood, Dopita and Bessell 1986).

Figure 2. Observed [O III] line profiles for those objects showing evidence for a high-velocity outer shell of matter. These are: A) SMP#41, B) SMP#47, C) SMP#54, D) SMP#83. Although the faint wings of the profile contain an appreciable fraction of the total flux, they are nevertheless difficult to observe.

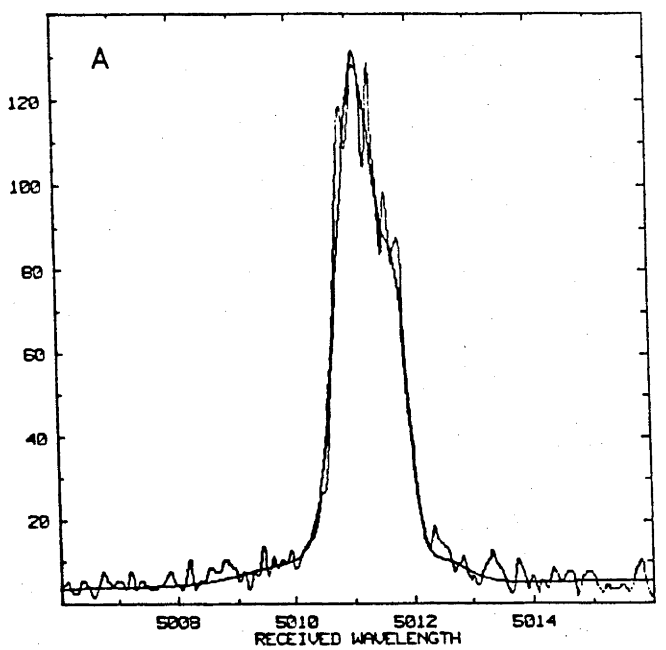
A
120
100
80
60
40
20
5008
5010
5012
5014
RECEIVED WAVELENGTH

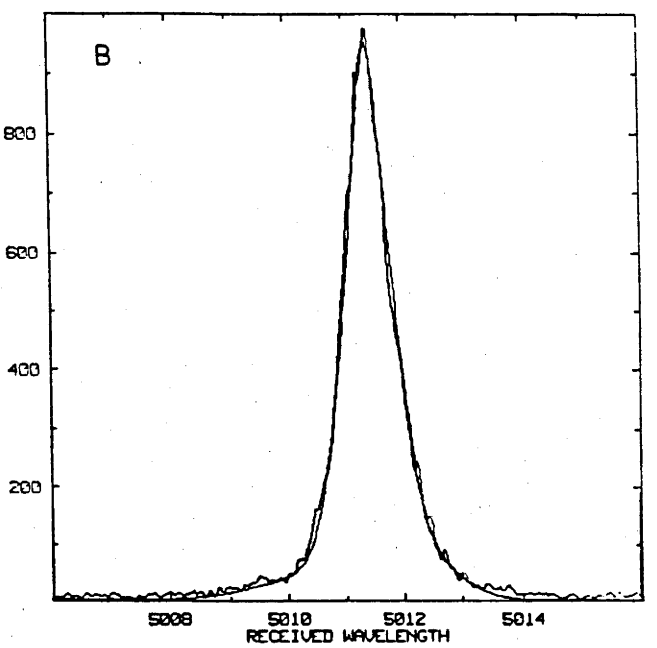
B
800
600
400
200
5008
5010
5012
5014
RECEIVED WAVELENGTH

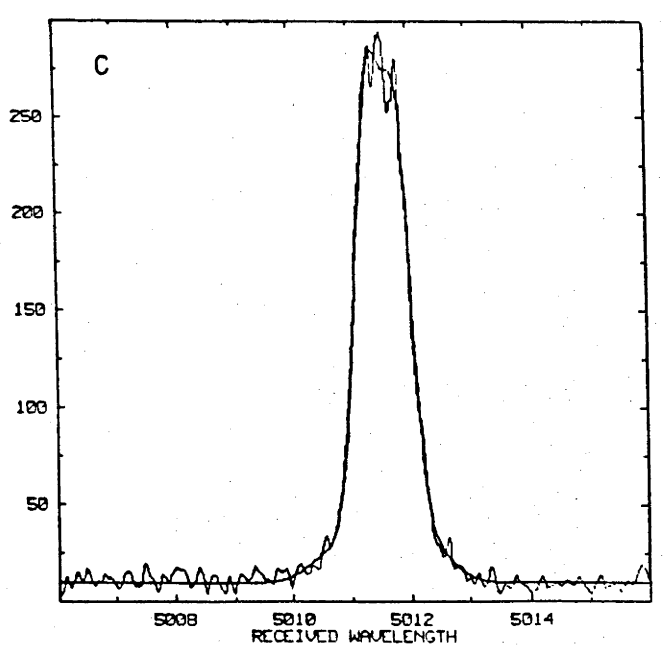
C
250
200
150
100
50
5008
5010
5012
5014
RECEIVED WAVELENGTH

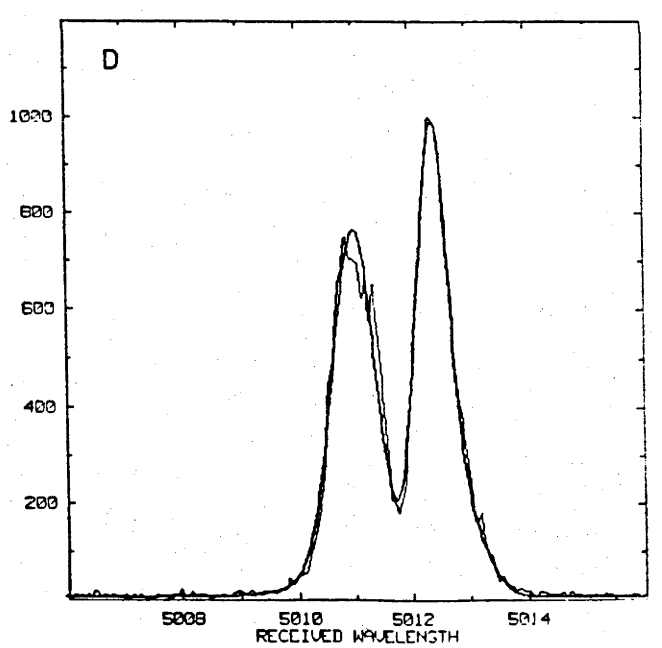
D
1000
800
600
400
200
5008
5010
5012
5014
RECEIVED WAVELENGTH

The electron densities determined from the observed $\lambda 3727/\lambda 3729$ line ratio with the aid of five level model atom calculations using collisions strengths of Pradhan (1976) and the transition probabilities of Zeippen (1982). The densities given are for an assumed electron temperature of 10000 K. The derived expansion velocities and densities are summarized in Tables 3 and 4. Most of the line profiles obtained were adequately fitted by a single gaussian component, but for the rest, two components were required. For these cases, expansion velocities were determined in the same manner as for the [O III] data. It is also possible to determine the electron densities for each of the components of the fit, and these are given separately in Tables 3 and 4. Such cases probably correspond physically to a bipolar morphology, since integration over a spherical expanding shell can, at best, produce only a marginal resolution into two components.

The [O II] doublet ratios and densities of 32 Magellanic Cloud PN have recently been measured by Barlow (1987), but at a resolution which did not permit a measurement of internal motions. These are also given in the Tables. In general, the agreement is good, but there are one or two discrepant results. For those objects observed in common, we believe that our results, with higher resolution, exposure time and total counts, should be more reliable. Exceptions to this are SMC SMP#13, 14 and 27 and LMC SMP#47 and 50 where the signal is low in our observations.

TABLE 3

EXPANSION VELOCITIES AND DENSITIES IN THE SMC PLANETARY NEBULAE DERIVED FROM THE [O II] DOUBLET

Object Name[a]	Excitation Class[b]	V_{exp}[O III] (km s^{-1})	V_{exp}[O II] (km s^{-1})	$\frac{\text{I(3729)}}{\text{I(3727)}}$	n_e (cm^{-3})
SMP 1	0.5	15.4	16.1	0.42	10500
SMP 2	6	32.2	...	0.59[d]	2900
SMP 3	4	32.9	...	0.68[d]	1800
SMP 5	6 – 7	29.2	43.6	0.56	3500
				0.54[d]	3900
SMP 6	4	21.9	...	0.38[d]	26000
SMP 9	7 – 8	37.9	...	1.19[d]	270
SMP 13	4	28.1	29.8	0.69	1800
				0.45[d]	7200
SMP 14	6	48.9	62.7	0.54	3900
				0.58[c]	3000
				0.56[d]	3300
SMP 15	2 – 4	15.2	20.8	0.35	65000
				0.43[d]	8800
SMP 16	0	11.7	8.8	0.40	15500
SMP 17	3 – 5	24.2	31.5	0.50	5100
				0.50[d]	4600
SMP 18	0.5	12.7	19.2	0.46	7300
SMP 19	7	30.1	...	0.53[d]	3920
SMP 20	1 – 2	20.2	30.3	0.37	35000
				0.34	70000
SMP 21	3	35.2	...	0.35[d]	40000

TABLE 3 (continued)

EXPANSION VELOCITIES AND DENSITIES IN THE SMC

PLANETARY NEBULAE DERIVED FROM THE [O II] DOUBLET

Object Name[a]	Excitation Class[b]	V_{exp}[O III] (km s^{-1})	V_{exp}[O II] (km s^{-1})	I(3729)/I(3727)	n_e (cm^{-3})
SMP 22	8	50.9	51.2	0.56	3500
				0.48[c]	5100
				0.52[d]	4200
SMP 24	1 – 2	16.6	35.6	0.46	6800
				0.42[d]	9800
SMP 26	8	50.6	41.0	0.79	1300
SMP 27	3	31.3	36.3	0.49	5400
				0.46[d]	6400
SMP 28	8	54.4	...	0.70	1900

NOTES (to this Table and to Table 4):

[a] For nomenclature, see section II (a).
[b] Excitation class from Morgan (1984).
[c] Where two values are given, the second refers to the higher velocity component.
[d] From Barlow (1986).

TABLE 4

EXPANSION VELOCITIES AND DENSITIES IN THE LMC PLANETARY NEBULAE DERIVED FROM THE [O II] DOUBLET

Object Name[a]	Excitation Class[b]	V_{exp}[O III] (km s^{-1})	V_{exp}[O II] (km s^{-1})	I(3729)/I(3727)	n_e (cm^{-3})
SMP 1	4	17.2	23.1	0.55	3600
SMP 5	1	20.8	20.9	0.67	2000
SMP 6	7	28.6	39.3	0.40	14000
				0.54[d]	3850
SMP 8	2	25.2	27.1	0.48	6300
SMP 15	5 – 6	41.2	51.0	0.49	5400
SMP 20	2	25.8	36.3	0.78	1300
SMP 21	7	49.1	55.4	0.45	7800
				0.62[d]	2400
SMP 23	4	21.6	38.5	0.48	5900
SMP 29	7	35.9	49.3	0.50	4900
				0.44	8200
SMP 31	0	5.1	14.4	0.44	8800
SMP 32	8 – 9	42.3	51.4	0.60	2800
SMP 37	7	39.2	...	0.45[d]	7300
SMP 38	5	34.5	...	0.35[d]	13000
SMP 40	6	51.7	39.1	0.81	1200
SMP 44		...	57.4	0.78	1300
				0.81[c]	1100
SMP 45	6	36.8	47.2	0.76	1400
				0.76[c]	1400
SMP 46	6	26.1	42.6	0.54	4000
SMP 47		50.1	58.4	0.50	5100
				0.62[d]	2500
SMP 50	5	35.0	55.7	0.50	5000
SMP 52	5	36.3	42.8	0.59	2900

TABLE 4 (continued)

EXPANSION VELOCITIES AND DENSITIES IN THE LMC

PLANETARY NEBULAE DERIVED FROM THE [O II] DOUBLET

Object Name[a]	Excitation Class[b]	V_{exp}[O III] (km s^{-1})	V_{exp}[O II] (km s^{-1})	I(3729)/I(3727)	n_e (cm^{-3})
SMP 55	0.5	6.0	18.2	0.37	40000
SMP 58	4	18.8	...	0.35	66000
SMP 61	4	29.3	33.3	0.36	40000
				0.37[d]	30000
SMP 62	6	34.6	47.5	0.48	6200
				0.49[d]	4800
SMP 63	4 – 5	16.7	48.1	0.43	9800
				0.44[d]	7700
SMP 67	1	27.9	42.7	0.55	3700
SMP 76	3	29.0	32.9	0.40	14500
SMP 77	1	12.0	17.4	0.56	3500
SMP 78	6	33.4	36.7	0.52	4300
				0.51[d]	4500
SMP 83	8 – 9	82.9	80.9	0.64	2300
				0.84[c]	1100
				0.59[d]	2600
SMP 85	1	11.3	11.2	0.34	High
SMP 87	8 – 9	37.4	39.8	0.70	1800
SMP 89	5	25.2	36.8	0.50	4900
				0.53[d]	3900
SMP 92	6	29.3	37.4	0.43	10000
SMP 96	9	60.9	37.0	0.61	2700
J 5	1	25.4	25.6	0.84	1100

Figure 3. The correlation between the measured [O II] and [O III] expansion velocities for PN in both the LMC and SMC. The [O II] expansion velocity is well correlated with, but systematically larger than, the [O III] expansion velocity.

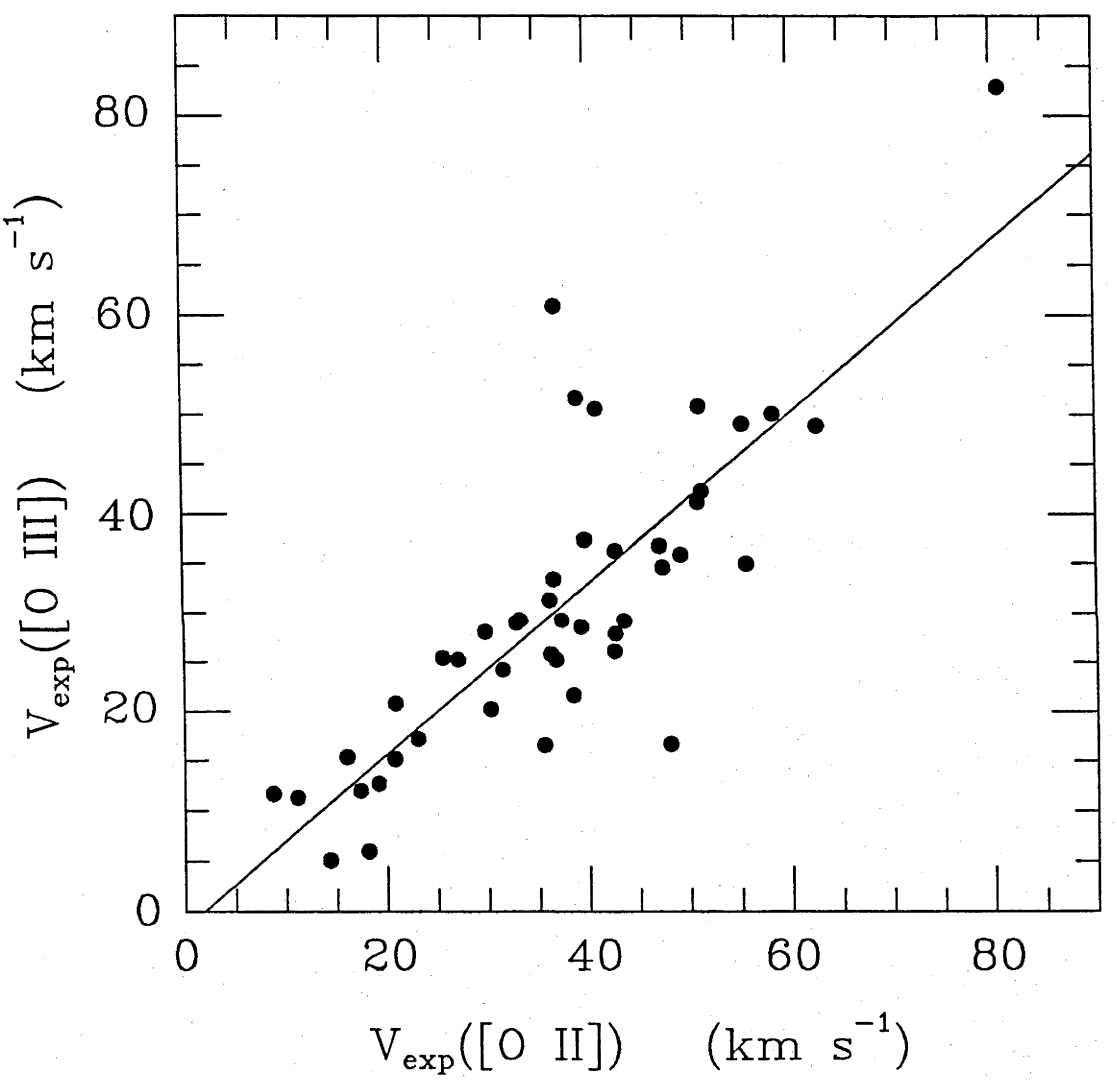
80
60
40
20
0
0
20
40
60
80
V_{exp}([O III]) (km s^{-1})
V_{exp}([O II]) (km s^{-1})

c) A Comparison of the [O III] *and* [O II] *Expansion Velocities*

The [O II] and [O III] expansion velocities are, in general, well correlated (see Figure 3). However, notable exceptions to the correlation are SMP 26 in the SMC, and SMP 40, 83 and 96 in the LMC. These are all low density nebulae of high excitation, and show anomalously high [O III] expansion velocities. These are likely to be nebulae which are optically thin in some directions. In such nebulae the low excitation lines would originate near ionization fronts close to a central reservoir of H I, whereas the [O III] emission is found in strongly accelerated flows towards the outer optically thin portions of the nebula. The LMC nebula, SMP 63 is anomalous in the other sense, but is not otherwise remarkable.

It might have been expected that this data would show evidence for ionization stratification effects, particularly for the low-excitation nebulae below class 3, where, according to photo-ionization models, the O^{++} zone becomes confined to the inner region of the nebula. One would therefore expect the [O III] expansion velocities to lie well below the [O II] expansion velocities. In fact, no evidence of this effect is found. However, there is some evidence for a stratification effect at all excitation classes, because the [O II] expansion is systematically higher than that found for the [O III] line. The slope of the correlation in Figure 3 is 0.818 ± 0.095. Since the [O II] emission always arises near the outer boundary of the ionized region, this indicates that the nebula reaches its maximum velocity of expansion in the outer regions. Since O^{++} is usually the dominant ionization stage, then the ratio of measured expansion velocities gives, in effect, an estimate for the thickness of the ionized shell, provided that there exists an outwardly increasing velocity gradient, $V_{exp} \propto R$, such as observed by Wilson (1950).

Figure 4. The correlation between excitation class and [O III] expansion velocity for those LMC planetaries fitted by a single gaussian component.

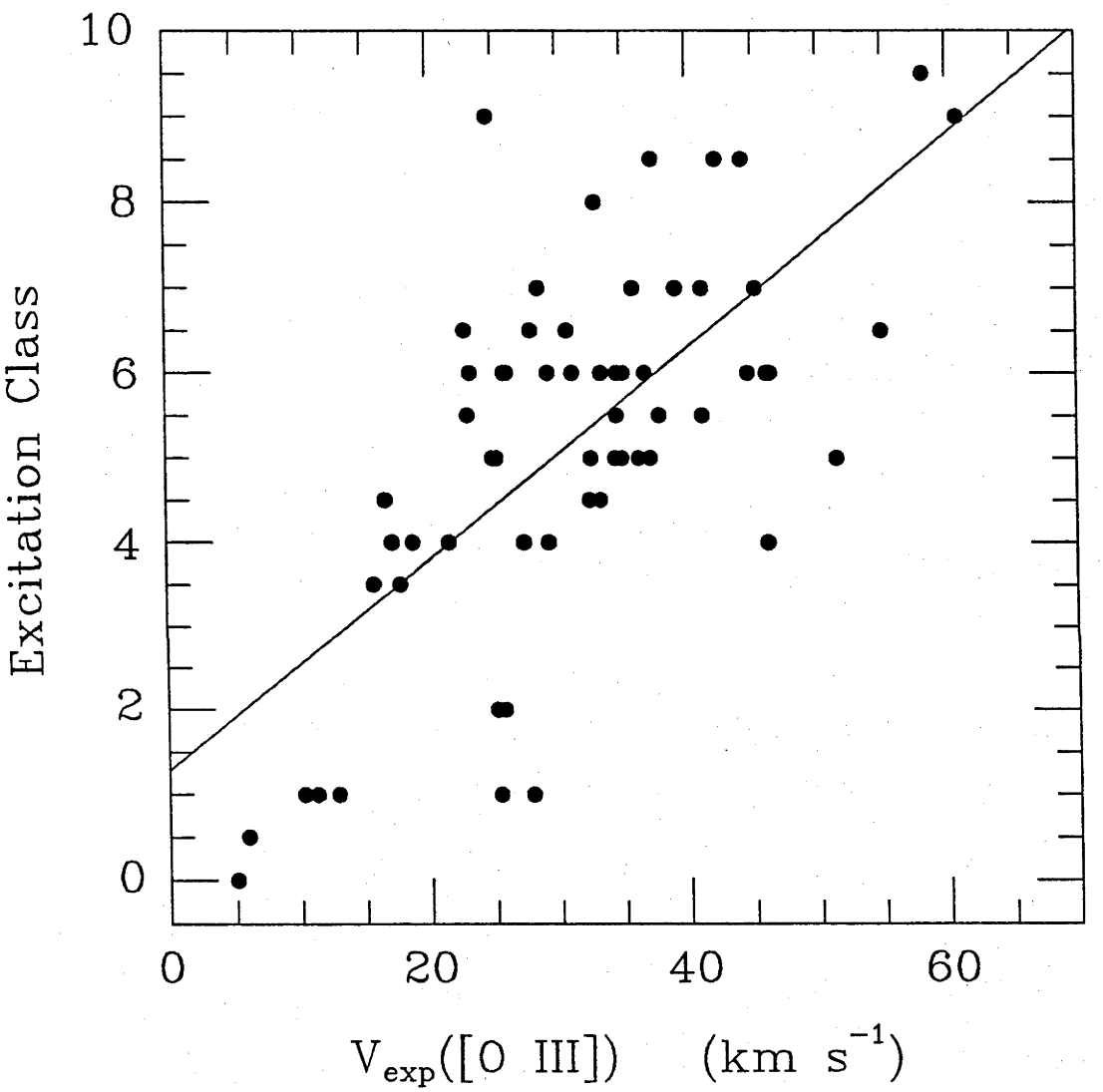
10
8
6
4
2
0
Excitation Class
0
20
40
60
V_{exp}([O III]) (km s^{-1})

Thus the fractional thickness of the ionized shell, $\Delta R/R_{neb}$, is of order 0.18. This should be compared with the mean value of about 0.15 found for Galactic PN (Daub 1982, Phillips 1984).

IV. OBSERVATIONAL CORRELATIONS

a) Correlations Between Expansion Velocity, Excitation Class and Flux

In DFLW it was shown that a good correlation exists between the expansion velocity and the excitation class for SMC planetary nebulae. Such a correlation also applies to the LMC population (see Figure 4). However, it is apparent from the Hβ Flux determinations (Meatheringham *et al.* 1988b), that some correlation also exists between this quantity and the expansion velocity. Although this is best for the SMC planetaries (Dopita *et al.* 1987), it is still apparent in the LMC population where the correlation coefficient is 0.34. The best-fit correlation between the expansion velocity, V_{exp}, and a combination of both of the excitation class and Hβ flux of the form:

$$V_{exp} = a + b\,E + c\,\log F_{\mathrm{H}\beta} \tag{4.1}$$

where E refers to the excitation class and a, b and c are constants, has the parameters $a = -58$, $b = 3.53$ and $c = -5.56$. With these values an RMS velocity difference of 8.3 km s^{-1} between the observed and the fitted expansion velocities is found (see Figure 5).

Figure 5. The expansion velocity given by equation (4.1) compared with the observed [O III] expansion velocity. The fit is much less good than for the SMC planetaries, indicating that the latter group of objects may be drawn from a more homogeneous population.

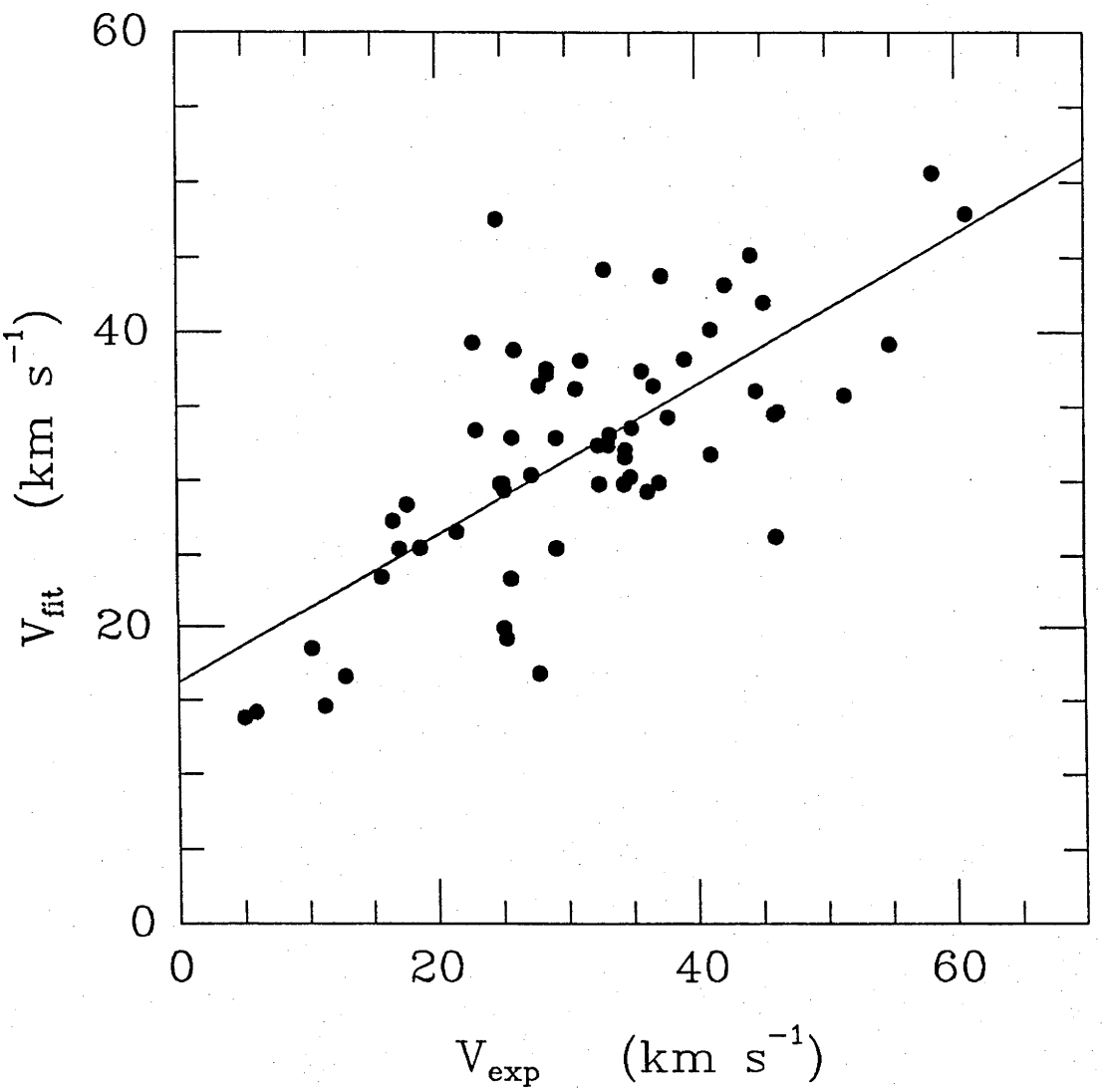
60
40
20
0
0
20
40
60
V_{fit} (km s^{-1})
V_{exp} (km s^{-1})

Figure 6. The excitation class / electron density plane for LMC and SMC planetaries. Planetaries known to be of Type I are marked with larger symbols. Note the forbidden region at high density and excitation. It is argued in the discussion section that, at a given mass of the PNn, the evolutionary track proceeds from lower right to upper left in a direction somewhat parallel to the upper envelope of observed points in this diagram.

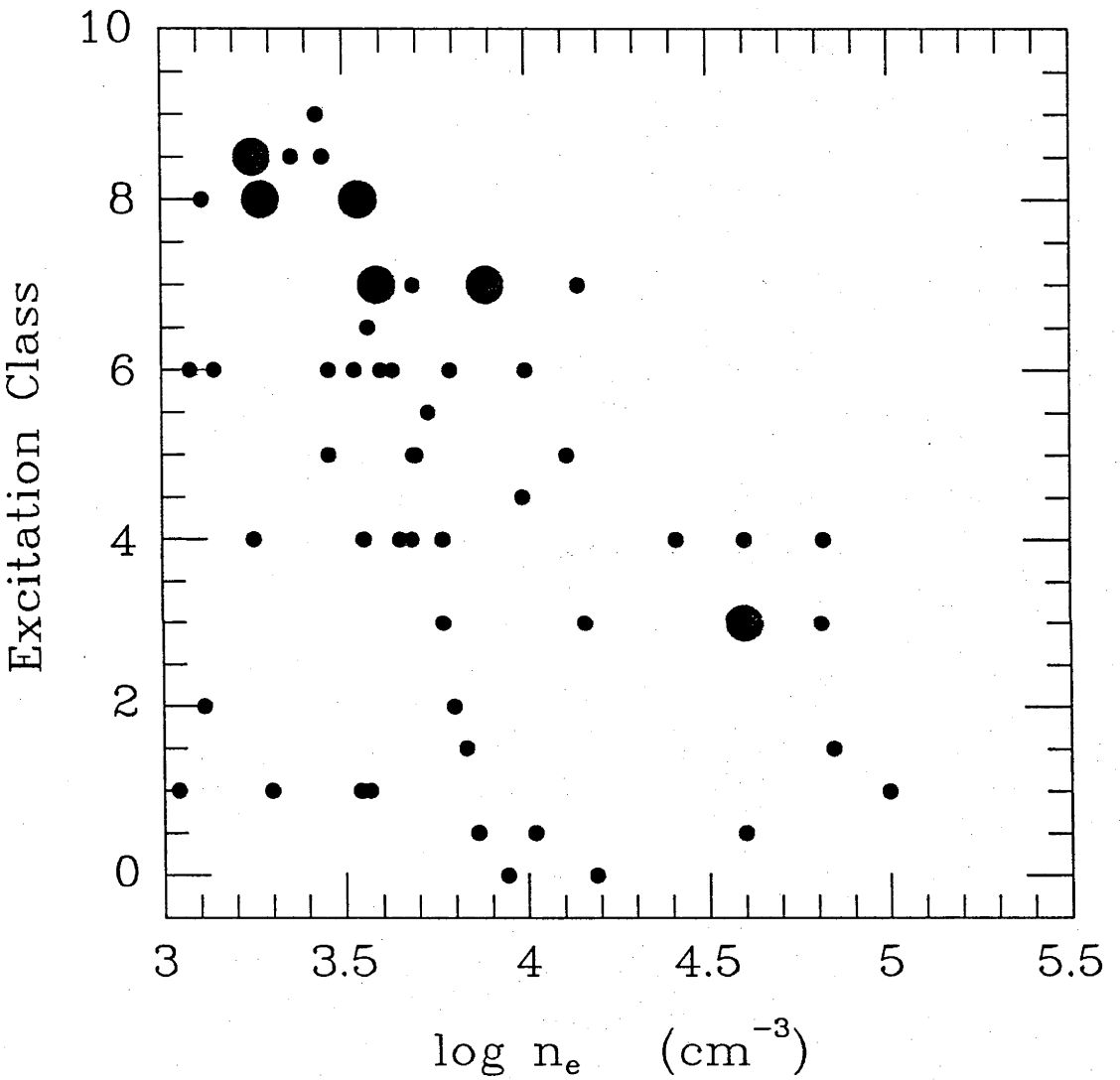
10
8
6
4
2
0
Excitation Class
3
3.5
4
4.5
5
5.5
log n_e (cm^{-3})

b) The Density / Excitation Correlation

Excitation class and density are not well correlated in the sample of nebulae of Tables 3 and 4 (see Figure 6). However, there is a clear upper limit to the permissible density at a given excitation class. No high density, high excitation nebulae are observed. Excitation class depends to some extent on the ionization parameter, but it is, of course, more affected by the stellar effective temperature. The absence of high density, high excitation objects appears therefore to point to a real lack of high temperature PNn in compact nebulae.

c) The Mass / Density Correlation

In the limit of low reddening, the observed flux, $F_{\mathrm{H}\beta}$, and the mean electron density, n_e, can be used to derive the ionized mass of the PN, from the formula:

$$M_{neb} = 4\pi D^2 F_{\mathrm{H}\beta}(1+4y)m_{\mathrm{H}}/\alpha_{eff}h\nu n_e \qquad (4.2)$$

where D is the distance, y = N(He)/N(H) and α_{eff} is the effective recombination coefficient of hydrogen for the emission of Hβ photons of energy $h\nu$. However, the mean electron density is not directly determined, only its emission weighted mean from the [O II] forbidden line ratio. These are related through $n_e(\mathrm{forbid}) = n_e\epsilon^{1/2}$, where ϵ is the volume filling factor of matter. For galactic PN, the filling factor appears to depend very little, if at all, on density, and lies between $0.3 < \epsilon < 1.0$. Indeed the best correlation between densities derived from flux measurements and those derived from the [O II] forbidden line is found for $\epsilon = 1.0$ (Seaton 1966; Pottasch 1980). In what follows we derive the mass on the assumption of $\epsilon = 1.0$, recognizing

that this could cause the masses to be systematically overestimated. On the other hand, our Hβ fluxes are uncorrected for reddening, and this will tend to lead to an underestimate in the mass.

Substituting numerical values in equation (4.2) yields:

$$\log M_{neb} = 15.5 + \log F_{\mathrm{H}\beta} - \log n_e \qquad (4.3)$$

We have used the figures given in Tables 3 and 4 to derive the nebular mass directly from this equation.

The correlation between the density and the ionized mass so derived is shown on Figure 7. The linear regression relation is:

$$\log M_{neb} = (1.36 \pm 0.30) - (0.626 \pm 0.079) \log n_e \qquad (4.4)$$

and the correlation coefficient is 0.774. The discrepant point in the lower left is LMC; SMP#46. Measurement of density from the [O II] lines becomes more uncertain at higher densities, and those above about 30000 cm^{-1} can be quite inaccurate. Even if those points are excluded from the figure the overall change is only slight as the shape of the correlation is well fixed.

d) Dynamical Age / Momentum Correlation

This relationship, and its physical basis, has been discussed elsewhere (Dopita *et al.* 1987), and this discussion will not be further developed here. In that paper, on the basis of sizes derived from speckle interferometry (Wood, Bessell and Dopita 1985) and on high speed direct imaging (Wood *et al.* 1987), it was found that the Magellanic Cloud PN conform to a relationship of the form:

Figure 7. The correlation between ionized mass and density for LMC and SMC planetaries.

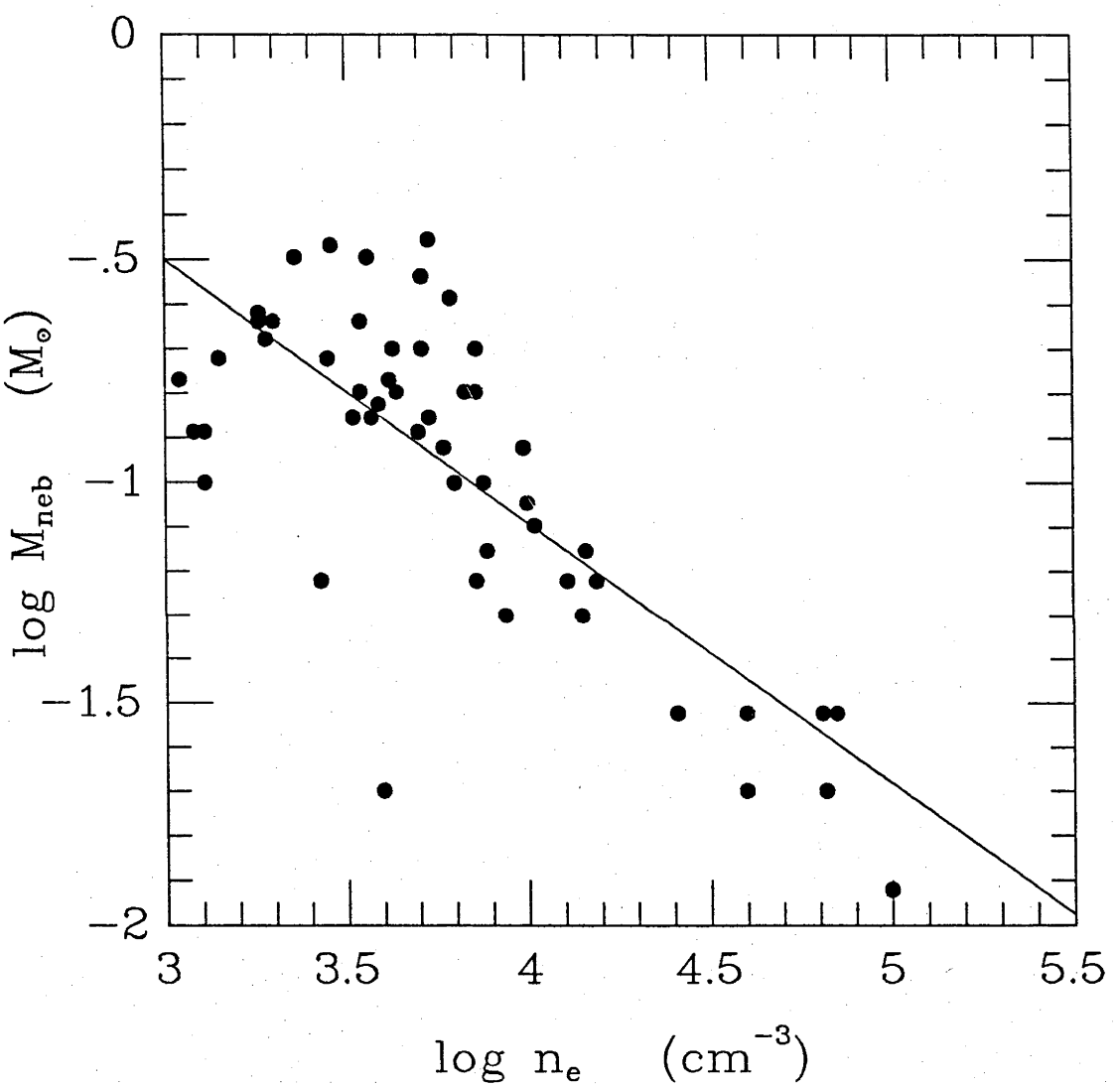
0
−.5
−1
−1.5
−2
log M_{neb} ($M_\odot$)
3
3.5
4
4.5
5
5.5
log n_e (cm^{-3})

$$\tau_{dyn} = 890(M_{neb}V_{exp})^{0.6} \text{ years} \quad (4.5)$$

where M_{neb} is the mass in solar units and V_{exp} is the [O III] expansion velocity in km s^{-1}.

The dynamical age has been directly established for very few of the objects in Tables 3 and 4. However, the age is such a vital parameter in understanding the evolution, that here we adopt equation (4.5) as being established, and use the derived mass and observed expansion velocity to determine the dynamical age.

e) The Age / Density / Excitation Plane

The dynamical age as derived above is strongly correlated with either the excitation class, E, (correlation coefficient 0.575) or with the logarithm of the electron density (correlation coefficient -0.811). We were therefore encouraged to find whether the PN are, in fact, a two parameter family in these variables. In fact, this turns out to be the case. Figure 8 shows that the observed points fall in a plane in the dynamical age / density / excitation class space defined by:

$$\log \tau_{dyn} = (4.70 \pm 0.23) + (0.0375 \pm 0.0106)\, E - (0.441 \pm 0.055) \log n_e \quad (4.6)$$

The fit between the dynamical age computed using (4.6) and the observed value is shown in Figure 9.

Figure 8. The evolutionary plane in terms of the density and excitation class. The observed points, are shown in black with their projections onto the (X,Y) plane as open squares. The observed points define a tilted plane shown in outline.

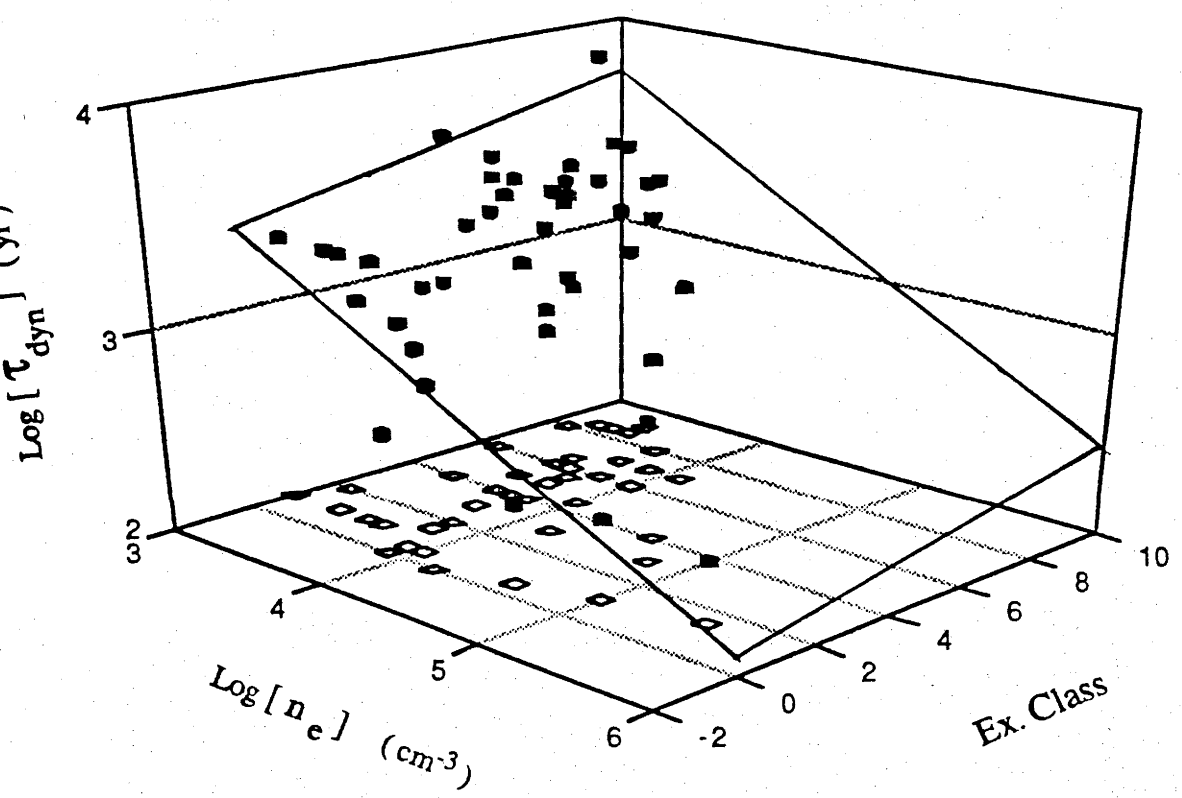
4
3
2
Log [τ dyn] (yr)
3
4
5
6
Log [n e] (cm-3)
-2
0
2
4
6
8
10
Ex. Class

Figure 9. The dynamical age given by equation (4.6) compared with the "observed" dynamical age. The scatter is sufficiently small that this could be used as a new method for determining the distances of Galactic PN.

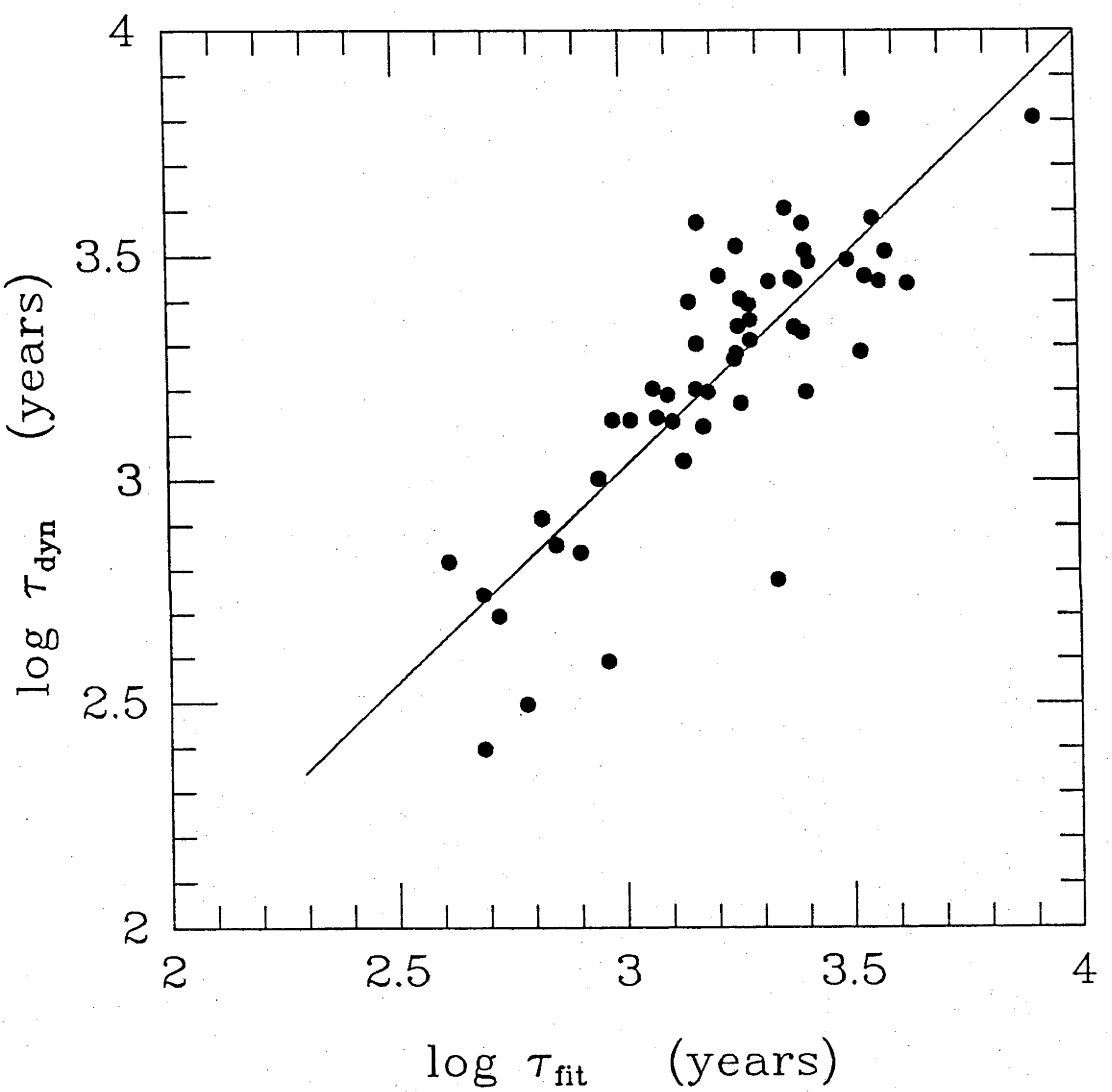
4
3.5
3
2.5
2
2
2.5
3
3.5
4
log τ_{dyn} (years)
log τ_{fit} (years)

V. DISCUSSION

The observed correlations discovered in this paper, in Dopita *et al.* 1987 and in Wood *et al.* 1987, put very powerful restraints on the possible models of the evolution of planetary nebulae and their central stars. Although fairly good correlations have been found connecting individual nebular quantities such as nebular mass and radius or density, or between excitation class and velocity of expansion, when the all important variable of nebular age is considered, two nebular parameters are required to give a good correlation. In the two particular cases we have discussed here, the topology of the observed surface appears to be a flat sheet.

These are dynamical age versus mass and velocity of expansion and dynamical age versus density and excitation class. However, dynamical age versus excitation class and Hβ flux also produces a sheet-like correlation, albeit distorted.

What is the physical meaning of such dual correlations? Firstly, the Hβ flux should correlate well with the luminosity of the PNn, at least for the optically thick nebulae. Second, the definition of the excitation class as adopted by Morgan (1984) ensures that this is closely related to the Zanstra temperature of the PNn, provided that the ionization parameter of the nebula is high enough. Nebulae in which the fading of the central star is sufficient to allow the excitation to drop will have been strongly discriminated against in our effectively flux-limited sample. The mass, radius and density of the ionized region are closely correlated, and are clearly related in some way with age. The position of a PN on such dual correlations should therefore depend principally on the properties of the

PNn.

The low excitation / high density PN appear to be genuinely young objects. Not only do they have the smallest dynamical ages observed, on the order of 100 years (see Figure 8), but they also tend to be the most luminous Hβ objects. The definition of excitation class ensures that with increasing excitation class the [O III] to Hβ ratio increases also. Spectrophotometry confirms that the higher excitation class nebulae are the more luminous objects in the [O III] lines, a finding that is in agreement with Jacoby and Ford (1986) for M31. Since Figure 8, and equation (4.6) imply that high density, high excitation class objects should have greater dynamical ages than the low excitation class objects the diagram cannot be ascribed to selection effects. If these objects existed, we would see them. We must therefore conclude that the upper boundary observed on the excitation class / density plane is determined by the evolutionary track of the most massive PNn in this diagram. This supposition is confirmed by the fact that the low excitation / high density objects are also the most luminous, as would be expected to be the case with massive PNn. Conversely, the fainter, low density, low excitation objects have long dynamical timescales, and therefore probably originate from low mass PNn, which only evolve slowly in the HR Diagram. We therefore postulate that, at a given mass for the PNn, the evolutionary tracks of constant PNn mass in the excitation class / density plane (Figure 6), are from lower right to upper left, approximately parallel to the upper envelope of points. If this is the case, then the Type I planetaries (Greig 1971; Peimbert 1978) might be expected to occur preferentially close to this upper envelope, since these are thought to come from massive precursors. This certainly appears to be the case. Objects

known to be of Type I on the basis of their spectra (in particular, the strength of nitrogen lines or the abundance derived for this element) are marked as larger symbols in Figure 6. These include LMC SMP#83 (see Dopita, Ford and Webster 1985), SMC SMP#21, 22, 28 and LMC SMP#21 and 29, all classified as Type I by Barlow (1987).

The implication of Figure 8, that the population of PN in the Magellanic Clouds are a two-parameter family with little intrinsic scatter, could be of great value in the solution of the thorny question of the Galactic Distance Scale for PN. Most past studies have used the Shklovsky method, which relies on the assumption of constant nebular mass, and a measurement of angular radius and Hβ flux to obtain distance (e.g. O'Dell 1962; Seaton 1968; Cahn and Kaler 1971). In its original formulation this method is now largely discredited since it has been recognized that, for optically thick objects, the ionized mass is a widely variable quantity (see, for example, Figure 7), and the more recent statistical distance scales are based on empirical relationships between ionized mass and nebular radius (Daub 1982; Maciel and Pottasch 1980; Maciel 1981, 1984; Amnuel *et al.* 1984). However, even assuming that this relation is properly calibrated, the statistical uncertainty is fairly large, of order 0.25 in the logarithm for nebular sizes smaller than 0.1 pc, and increasing rapidly for larger nebulae (Wood *et al.* 1987). However, figures 8 and 9 imply that we could derive a distance simply from a knowledge of excitation class, electron density in the [O II] zone, and a determination of the expansion velocity. Since none of these quantities is affected by reddening, the technique should be more reliable. It should also be somewhat more accurate. The mean scatter of points in Figure 9 is only 0.17 in the logarithm. Since the expansion velocity

can be measured with very little error, except in the case of the bipolar nebulae, the mean error in the derived distance will also be of this order, about 40%. This promising new distance indicator will be investigated in a future paper.

VI. CONCLUSIONS

Expansion velocities in both the [O III] and [O II] lines, and electron densities in the [O II] lines have been determined for many nebulae in the Large Magellanic Cloud. Correlations have been found between quantities determined largely by the central star (luminosity, excitation), and the nebular parameters (expansion velocity, nebular momentum and dynamical age). These give clear observational evidence that the planetary nebular shell parameters are determined only by the parameters of the central star, a fact which will much simplify the construction of theoretical models. This fact also suggests a new method for determining the distances of Galactic PN.

REFERENCES

Aller, L. H. 1956, *"Gaseous Nebulae"*, John Wiley & Sons, Inc., New York.

Amnuel, P.R., Guseinov, O.H., Novruzova, H.I. and Rustamov, Yu. S. 1984, *Ap. Space Sci.*, **107**, 19.

Barlow, M.J. 1987, *M.N.R.A.S.*, **227**, 161.

Bohuski, T.J. and Smith, M.J. 1974, *Ap. J.*, **193**, 197.

Cahn, J.H. and Kaler, J.B. 1971, *Ap. J. Suppl.*, **22**, 319.

Daub, C.T. 1982, *Ap. J.*, **260**, 612.

Dopita, M.A., Ford, H.C., Lawrence, C.J. and Webster, B.L. 1985, *Ap. J.*, **296**, 390.

Dopita, M.A., Ford, H.C. and Webster, B.L. 1985, *Ap. J.*, **297**, 593.

Dopita, M.A., Meatheringham, S.J., Wood, P.R., Webster, B.L., Morgan, D.H. and Ford, H.C. 1987, *Ap. J. (Letters)*, **315**, L107.

Dopita, M.A., Meatheringham, S.J., Morgan, D.H, Webster, B.L. and Ford, H.C. 1988b, in preparation.

Feast, M.W. 1968, *M.N.R.A.S.*, **140**, 345.

Grieg, W.E. 1971, *Astr. Ap.*, **10**, 161.

Henize, K.G. and Westerlund, B.E. 1963, *Ap. J.*, **137**, 747.

Jacoby, G.H. 1980, *Ap. J. Suppl.*, **42**, 1.

Jacoby, G.H. & Ford, H.C., 1986, *Ap. J.*, **304**, 490.

Maciel, W.J. 1981, *Astr. Ap. Suppl.*, **44**, 123.

Maciel, W.J. 1984, *Astr. Ap. Suppl.*, **55**, 253.

Maciel, W.J. and Pottasch, S.R. 1980 *Astr. Ap.*, **88**, 1.

Meatheringham, S.J., Dopita, M.A., Ford, H.C. and Webster, B.L. 1988a, *Ap. J.*, (April 15).

Meatheringham, S.J., Dopita, M.A., and Morgan, D.H. 1988b, *Ap. J.*,

(April 15).

Morgan, D.H. 1984, *M.N.R.A.S.*, **208**, 633.

Morgan, D.H., and Good, A.R. 1985, *M.N.R.A.S.*, **213**, 491.

O'Dell, C.R. 1962, *Ap. J.*, **135**, 371.

Peimbert, M. 1978, *in IAU Symposium 76, "Planetary Nebulae"*, ed. Y. Terzian, (Reidel : Dordrecht).

Pelat, D., Alloin, D. and Fosbury, R.A.E. 1981, *M.N.R.A.S.*, **195**, 787.

Pottasch, S.R. 1980, *Astr. Ap.*, **89**, 336.

Pradhan, A.K. 1976, *M.N.R.A.S.*, **177**, 31.

Phillips, J.P. 1984, *Astr. Ap.*, **137**, 92.

Robinson, G.J., Reay, N.K. and Atherton, P.D. 1982, *M.N.R.A.S.*, **199**, 649.

Sabbadin,F. 1986a, *Astr. Ap.*, **160**, 31.

Sabbadin, F. 1986b *Astr. Ap. Suppl.*, **64**, 579.

Sabbadin, F., Bianchini, A. and Hamzaoglu, E. 1984, *Astr. Ap.*, **136**, 200.

Sabbadin, F., Gratton, R.G., Bianchini, A., and Ortolani, S. 1984, *Astr. Ap.*, **136**, 181.

Sabbadin, F. and Hamzaoglu, E. 1982, *Astr. Ap.*, **110**, 105.

Sanduleak,N., McConnell, D.J. and Philip, A.G.D. 1978, *Pub. A.S.P.*, **90**, 621.

Seaton, M.J. 1966, *M.N.R.A.S.*, **132**, 113.

Seaton, M.J. 1968, *Astrophys. Lett.*, **2**, 55.

Smith, H.C. 1969, M.A. Thesis, University of Virginia.

Wilson, O.C. 1950, *Ap. J.*, **111**, 279.

Wood, P.R., Bessell, M.S. and Dopita, M.A. 1985, *Proc. Astr. Soc. Aust.*, **6**, 54.

Wood, P.R, Dopita, M.A., and Bessell, M.S. 1986, *Ap. J.*, **311**, 632.

Wood, P.R. and Faulkner, D.J. 1986, *Ap. J.*, **307**, 659.

Wood, P.R., Meatheringham, S.J., Dopita, M.A. and Morgan, D.H. 1987, *Ap. J.*, **320**, 178.

Zeippen, C.J. 1982, *M.N.R.A.S.*, **198**, 111.

FLUXES AND IONIZED MASSES OF MAGELLANIC CLOUD PLANETARY NEBULAE

Stephen J. Meatheringham, Michael A. Dopita

Mount Stromlo and Siding Spring Observatories,

Australian National University,

David H. Morgan

Royal Observatory,

Edinburgh

Received: 1987 August 17

Accepted: 1987 December 1

To appear in *Astrophysical Journal*, 1988, June 1.

ABSTRACT

Absolute Hβ nebular fluxes are presented for a total of 97 planetary nebulae (PN) in the Magellanic Clouds. These new fluxes are compared with all previously published data. Nebular masses are derived for 54 objects, and found to lie in the range $0.01 - 0.35\mathcal{M}_{\odot}$. A relationship between density and ionized mass ($M_{neb} \propto 1/n_e$) for a subset of the nebulae, is used to show that these objects are optically thick. Another relationship between Hβ flux and nebular density is examined. The point at which the nebulae become optically thin is seen as a change in the slope of this curve. From these relationships a nebular mass — radius relation of the form $M_{neb} \propto R^{3/2}$ is found to apply to optically thick nebulae, while optically thin nebulae evolve at constant M_{neb}.

Subject Headings: galaxies : Magellanic Clouds
nebulae : planetary

I. INTRODUCTION

The planetary nebular phase of stellar evolution is one which despite a considerable amount of effort, both theoretical and observational, over the past twenty years, still contains many contentious issues. For example, the evolutionary paths of planetary nebulae nuclei (PNn) have been subject to a large amount of debate. The empirical Harman–Seaton sequence (Harman and Seaton 1964) was generally accepted as being a single evolutionary track. However, this changed after temperatures and luminosities were re-derived, and it became interpreted as a superposition of different mass tracks in the range $0.6-1.2\mathcal{M}_{\odot}$ (Paczyński 1971; O'Dell 1974). Schonberner (1981) studied the evolution from the AGB phase and concluded it was possible to assign only a very small mass range around $0.58\mathcal{M}_{\odot}$ for PNn masses. Wood and Faulkner (1986) carried out a more extensive set of evolutionary sequence calculations for PNn of varying masses (0.6, 0.7, 0.76 and 0.89 $\mathcal{M}_{\odot}$) and conclude there is a large range in possible nuclei masses. They have also found evidence that recent luminosity determinations may have underestimated the stellar luminosities by a factor of up to 3. However, calculation of the absolute luminosity of the PNn relies on a knowledge of its distance, and distance is not a well known quantity for many Galactic planetary nebulae. Various authors quote distances to individual nebulae that may differ by factors of up to $2-3$ (Cahn and Kaler 1971; Maciel and Pottasch 1980; Daub 1982; Amnuel *et al.* 1984; Phillips and Pottasch 1984). This can be attributed to, amongst other things, uncertain amounts of extinction within our Galaxy, uncertainty in the optical thickness / thinness of nebulae, and the fact only a small number of nebulae are close enough for independent distance measurements not relying on physical nebular parameters. We believe the Magellanic Clouds hold the solution to many

of the unanswered questions relating to planetary nebulae, by furnishing us with a luminosity limited sample at a common, known distance, and with a low line of sight reddening. As a result of this we have been systematically investigating both the kinematics and dynamics of the planetary nebulae populations in the Large and Small Magellanic Clouds over the past few years (Dopita *et al.* 1985; Dopita *et al.* 1987, 1988; Meatheringham *et al.* 1988; Wood, Bessell and Dopita 1985; Wood *et al.* 1987).

In this paper we present absolute Hβ fluxes for a total of 23 planetary nebulae in the Small Magellanic Cloud and 74 in the Large Cloud. Together with Wood *et al.* (1987) (hereafter WMDM), who obtained Hβ and also [O III] λ5007 flux information for 80 planetary nebulae we have now covered the majority of known planetary nebulae in the Magellanic Clouds. These fluxes are being used in conjunction with line intensities measured from spectrophotometry to produce absolute nebular line fluxes for all important emission lines from λ3400 to λ7200. This information will be used further in modelling codes to derive abundances, and physical parameters for a large sample of Magellanic Cloud planetary nebulae (Meatheringham and Dopita 1988).

The only previously published flux information for Magellanic Cloud PN is from Webster (1969, 1976, 1983) who made photoelectric measurements of absolute emission line fluxes for 25 planetary nebulae. Osmer (1976) used a spectrophotometric scanner to derive fluxes for selected nebular emission lines from λ3700 to λ6600 for 6 planetary nebulae, and Aller (1983) derived Hβ fluxes for 8 LMC planetary nebulae from spectrophotometry.

The flux information together with nebular electronic densities (n_e) from the [O II] $\lambda\lambda$3727,3729 doublet (Dopita *et al.* 1988; Barlow 1987) allows a

determination of the ionized nebular mass. In section III(b) masses are derived for a subset of 54 nebulae in this paper. The density can also be used in conjunction with the flux information and masses to determine at what point a nebula becomes optically thin to Hydrogen ionizing radiation, as well as a nebular mass — radius relationship.

II. OBSERVATIONS AND DATA REDUCTION

a) Selection Of Objects

The majority of objects observed in this study come from Sanduleak, McConnell and Philip (SMP) (1978) who presented a list of 102 planetary nebulae in the LMC and 28 in the SMC. Many of these had been catalogued as emission nebulae in the Henize (1956) catalogue, had also been listed by Lindsay and Mullen (1963), and had been positively identified as planetary nebulae by Henize and Westerlund (1963). Throughout this paper we have adopted the numbering system as given by Sanduleak *et al.* (1978), this being the most comprehensive single listing to date.

The Jacoby (J) (1980) objects present a more difficult group. Many of these are very faint, and only one object (J5) was observed in this study.

b) The Observations

Observations were made in December 1982, January 1983, December 1984, and November and December 1985 using the 1-metre telescope operated by the Australian National University at Siding Spring Observatory. A narrow band two cycle interference filter manufactured by Spectrofilm Inc. was used to isolate the Hβ nebular line. This filter had a full-width at half maximum (FWHM) of 16Å centered at the Hβ rest

wavelength.

The detector system used was the two dimensional Photon Counting Array (PCA) (Stapinski, Rodgers, and Ellis 1981). This uses a 25 mm ITT microchannel plate proximity focus intensifier tube with an S20 photocathode coupled to a single-stage electrostatic image tube. The photon events on the output phosphor are read out using an uncooled Fairchild CCD221 lens coupled to the image tube assembly. After frame subtraction to remove fixed pattern noise in the chip and afterglow from previous photon events, the data are digitized and the centroid of each photon event found to give a resolution (pixel size) in the 512K pixel external memory of $15 \times 36\mu$m. Calculation to within 1/2 a pixel of where the photon landed in one spatial direction (double binning) is the final step. At the f/8 focus of the 1-metre telescope this gave an image resolution of $\sim 0.5 \times 1$ arcseconds on the sky.

Exposure times were varied to give a peak signal in the range $30 - 100$ photons per pixel, giving total counts per exposure approximately in the range $900 - 3000$ photons.

c) Reduction Procedure

In order to remove small-scale variations of sensitivity across the CCD, each observation was divided by a normalized flat field obtained by summing two exposures of the morning and evening twilight sky. The data were then rebinned to give pixels square on the sky.

The Starlink applications program PATCH was used to remove any stars or image defects near the planetary nebula that would cause problems later

in the reduction, and lead to errors in sky measurements for the photometry. The Starlink aperture photometry program APERASP was then used to derive a magnitude for each object. A circular aperture was centered on the planetary nebula to give the total number of counts for object plus sky. Four separate sky apertures were selected around the planetary nebula to find an average sky value. The sky contribution was removed to leave an instrumental magnitude for the planetary nebula. In choosing suitable aperture sizes it had to be ensured that the aperture was large enough to cover the largest planetary nebulae image for the night, as changes in seeing were frequently encountered throughout a night. As well, due to different seeing conditions on various nights appropriately sized apertures were chosen separately for each night.

The instrumental magnitude was corrected for the effect of differential atmospheric extinction, and the final step in the reduction was conversion to absolute Hβ fluxes. Standard fluxes were taken from those objects which had well agreed upon fluxes as determined previously by various authors (Webster 1969, 1976, 1983; Osmer 1976; Aller 1983). Those planetary nebulae adopted as standards are marked with a (*) in column 1, after the object name in Tables 2 and 3. Standards were measured as every third or fourth object throughout the nights to ensure sufficient coverage.

d) Accuracy

There are two main sources of error in our measurements. The first, is simply a statistical error due to the finite number of photons detected from each planetary nebula. Table 1 shows the error as a function of $\log F_{\mathrm{H}\beta}$ as determined by repeated measurements of planetary nebulae of various

fluxes.

The second source of error is more difficult to quantify, and arises from the fact that we have attempted flux measurements in fields that are frequently extremely crowded. This is especially so in the LMC near the region of the bar. In the most crowded fields it proved difficult to find sky regions not contaminated by faint stars, however, by interactively assigning sky apertures this uncertainty has been minimized. This is borne out by comparing the fluxes determined in this paper with those obtained by WMDM (section III(a)).

e) Continuum Contributions

It should be mentioned that the observations will also include contributions from the nebular and central star continuums. The primary source of the nebular continuum involves interactions between electrons and Hydrogen ions (free–bound, free–free, and two quantum processes). Pottasch (1984, p. 75) gives the nebular continuum emission as a function of wavelength for a typical high excitation planetary nebula. At Hβ (λ4861Å) the nebular emission is 0.1% of Hβ, and so through our interference filter (FWHM $\sim$ 16Å) we receive a contribution of $\sim$ 1.6% due to the nebular continuum. As the continuum flux is proportional to Hβ flux at a given nebular temperature, and since nebular temperature varies little from nebula to nebula, this contribution will be effectively the same for all nebulae. When standards are used the fluxes are renormalized and this contribution is removed.

The other continuum source is the central star, and to determine its contribution we make use of the Zanstra Hydrogen temperature method as

given by Pottasch (1984, pp. 169–172). The ratio of Hβ nebular line flux to central star continuum flux is given by :

$$F(\mathrm{H}\beta)/F_\lambda(vis) = 3.95 \times 10^{-11}\, T^3\, G_1(T)\, (\mathrm{e}^{2.665\times10^4/T} - 1)\ \text{Å} \qquad (2.1)$$

where

$$G_1(T) = \int_{h\nu/kT}^{\infty} x^2(\mathrm{e}^x - 1)^{-1}\, dx \qquad (2.2)$$

where ν is the frequency of the Hydrogen Lyman limit.

Multiplying the result of equation 2.1 by the FWHM of the filter gives the expected ratio of Hβ nebular line flux to central star flux for a given stellar temperature (T). This ratio varies from 20 for a temperature $T = 3\times 10^4$ K, rising to $\sim$ 1300 at $T = 10^5$ K. Hence, the contribution is a maximum of approximately 5% for a very cool central star, and rapidly decreases with increasing stellar temperatures. And for all nebulae with excitation class greater than 2 (corresponding to $T > 45000$ K the contribution is less than 1% of the Hβ flux.

Hence we may conclude that the overall continuum contributions to the observed nebular line fluxes are very small, and in most cases negligible.

III. RESULTS

a) Comparison With Previous Flux Measurements

Tables 2 and 3 present fluxes for the 97 planetary nebulae we observed. Column 1 is the SMP designation, column 2 our flux measurement, while column 3 gives any previously published fluxes.

TABLE 1

FLUX ERRORS DUE TO FLUCTUATIONS

IN PHOTON STATISTICS

$\log F_{H\beta}$	Error
-12.45	±0.01
-12.65	±0.02
-12.85	±0.03
-13.15	±0.04
-13.40	±0.07

TABLE 2

FLUX DATA FOR SMC PLANETARY NEBULAE

Object Name	This Study	Previous
SMP1	-12.77	-12.76 (1)
SMP2	-12.67	-12.76 (1) ; -12.72 (2) ; -12.78 (3) -12.67 (4)
SMP3	-13.06	-13.07 (1)
SMP4	-12.90	
SMP5*	-12.81	-12.78 (1) ; -12.86 (2) ; -12.81 (4)
SMP6	-12.80	-12.79 (2)
SMP8	-12.74	
SMP10	-12.93	
SMP11	-12.87	-12.99 (1)
SMP13	-12.56	-12.56 (1) ; -12.49 (2)
SMP14	-13.05	-13.02 (1) ; -12.86 (2)
SMP15	-12.43	-12.44 (2) ; -12.40 (4)
SMP16	-12.70	-12.72 (1) ; -12.75 (2)
SMP17	-12.49	-12.61 (1) ; -12.54 (2) ; -12.50 (4)
SMP19	-12.93	
SMP20*	-12.42	-12.47 (1) ; -12.42 (3) ; -12.42 (4)
SMP21	-13.25	-13.23 (1)
SMP22*	-12.88	-12.83 (1) ; -12.88 (3)
SMP23	-13.06	
SMP24	-12.68	-12.69 (1) ; -12.72 (2) ; -12.67 (4)
SMP25	-13.20	
SMP27	-12.44	-12.44 (1) ; -12.48 (2) ; -12.43 (4)
SMP28	-13.12	

(1) Wood, Meatheringham, Dopita and Morgan (1987).
(2) Webster (1969, 1976, 1983).
(3) Osmer (1976).
(4) Aller (1981).

TABLE 3

FLUX DATA FOR LMC PLANETARY NEBULAE

Object Name	This Study	Previous
SMP1	-12.46	-12.47 (2)
SMP2	-13.18	
SMP3	-13.48	
SMP5	-12.85	
SMP6	-12.67	-12.67 (4)
SMP7	-13.12	
SMP8	-13.74	
SMP9	-13.38	-13.30 (1)
SMP10	-13.15	-13.14 (1)
SMP11	-13.15	-13.15 (1)
SMP13	-12.82	
SMP14	-13.69	-13.68 (1)
SMP15	-12.66	-12.65 (1)
SMP16	-13.30	-13.29 (1)
SMP18	-13.36	-13.30 (1)
SMP19	-12.73	
SMP20	-13.37	-13.42 (1)
SMP21*	-12.76	-12.81 (1) ; -12.69 (2) ; -12.78 (3) -12.78 (4)
SMP23	-12.68	
SMP27	-13.40	
SMP29	-12.71	-12.70 (2) ; -12.74 (4)
SMP30	-13.45	-13.43 (1)
SMP31	-12.91	-12.90 (1)
SMP32	-12.80	-12.80 (1)
SMP33	-12.81	
SMP35	-12.81	-12.79 (1)

TABLE 3 (Continued)

FLUX DATA FOR LMC PLANETARY NEBULAE

Object Name	This Study	Previous
SMP36	-12.72	
SMP37*	-12.85	
SMP38	-12.62	
SMP40	-13.25	-13.44 (1)
SMP42	-13.11	
SMP48	-12.43	-12.47 (2)
SMP50	-12.71	-12.68 (1) ; -12.70 (2)
SMP52	-12.52	-12.53 (1)
SMP53	-12.62	
SMP55	-12.66	
SMP56	-13.13	
SMP57	-13.41	
SMP58	-12.48	
SMP60	-13.50	-13.63 (1)
SMP61	-12.48	-12.41 (2)
SMP62*	-12.31	-12.32 (1) ; -12.30 (2) ; -12.32 (4)
SMP63	-12.48	-12.45 (2)
SMP64	-12.70	
SMP65	-13.31	
SMP66	-12.95	
SMP67	-12.81	
SMP69	-13.17	
SMP71	-12.86	
SMP73	-12.54	-12.52 (2)
SMP74	-12.66	
SMP76	-12.54	-12.53 (2)
SMP77	-12.78	

TABLE 3 (Continued)

FLUX DATA FOR LMC PLANETARY NEBULAE

Object Name	This Study	Previous
SMP78*	-12.58	-12.57 (1) ; -12.60 (2) ; -12.58 (4)
SMP79	-12.63	
SMP81	-12.61	
SMP83	-12.65	-12.65 (2)
SMP84	-12.63	
SMP85	-12.42	
SMP86	-13.68	
SMP87	-12.91	-12.90 (1)
SMP88	-13.26	
SMP89	-12.61	-12.65 (2) ; -12.63 (4)
SMP91	-13.55	
SMP92	-12.54	-12.55 (2)
SMP93	-13.36	
SMP94	-12.99	
SMP95	-13.47	-13.39 (1)
SMP97	-12.85	-12.80 (2) ; -12.79 (3) ; -12.84 (4)
SMP100	-12.86	
SMP101	-12.89	
SMP102	-13.22	
SMP103	-13.53	
J5	-13.25	

(1) Wood, Meatheringham, Dopita and Morgan (1987).
(2) Webster (1969, 1976).
(3) Osmer (1976).
(4) Aller (1983).

It is instructive to compare our fluxes with those obtained in previous studies. Figure 1 is a plot of our fluxes as compared with those obtained by previous authors (excluding the measurements from WMDM). The line is of slope unity. Where more than one value had been published we have adopted the mean. In general the agreement is better than 0.03 dex, the only object which differs significantly from previous work is SMC SMP14 (0.19 dex). Our value compares favourably with that from WMDM (0.03 dex difference) and hence we conclude that Webster's measurement is probably incorrect.

WMDM used high time resolution imaging (1/60 sec) on the 3.9-metre Anglo-Australian Telescope to obtain the sharpest possible images under the prevailing observing conditions by removing the translational component of seeing. Narrow band filters centered on Hβ and [O III] λ5007 were used to isolate the nebular lines. This work yielded fluxes for some 80 Magellanic Cloud planetary nebulae. A comparison of the fluxes obtained in the two studies is shown in Figure 2. The agreement between the two studies for the objects in common is excellent (average of 0.04 difference in the dex), there being only a few objects (SMC SMP2, SMP11, SMP17; LMC SMP40, and SMP60) that differ significantly. The fact that the discrepant WMDM fluxes are always lower than the values found in this paper, and that the difference seems independent of brightness probably indicates a slight error. This is most likely to be in the WMDM measurements, for two reasons. Firstly, there is no such difference between our fluxes and those excluding the WMDM measurements. And secondly, the WMDM fluxes were derived by summing all observation frames except those that may have had cloud contamination. If, however, some cloudy

Figure 1. Fluxes measured in this study compared with those previously published (excluding the Wood *et al.* (1987) data). Where more than one value was available the mean was adopted.

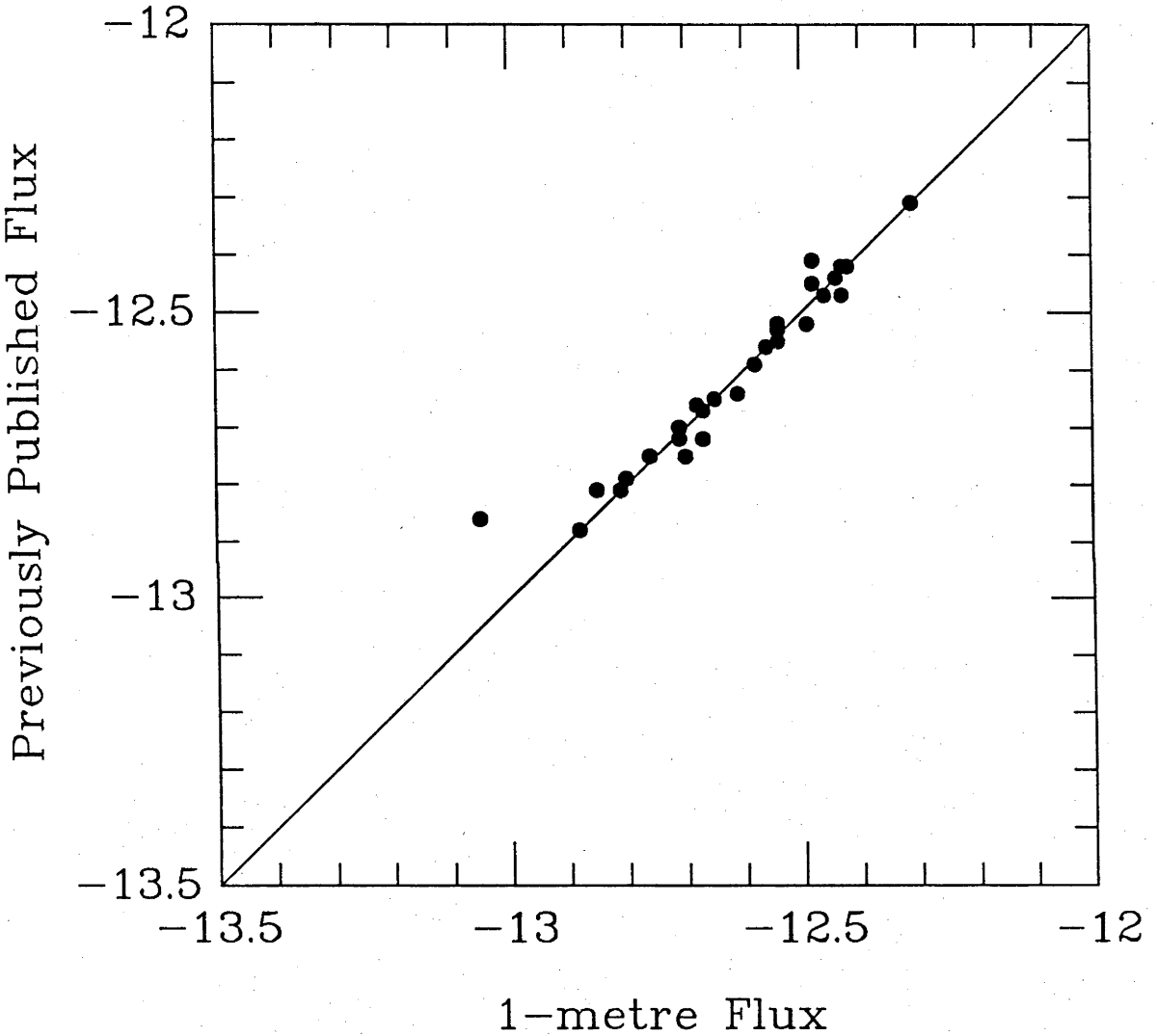
−12
−12.5
−13
−13.5
−13.5
−13
−12.5
−12
Previously Published Flux
1−metre Flux

Figure 2. Fluxes measured in this paper compared with those in common from Wood *et al.* (1987).

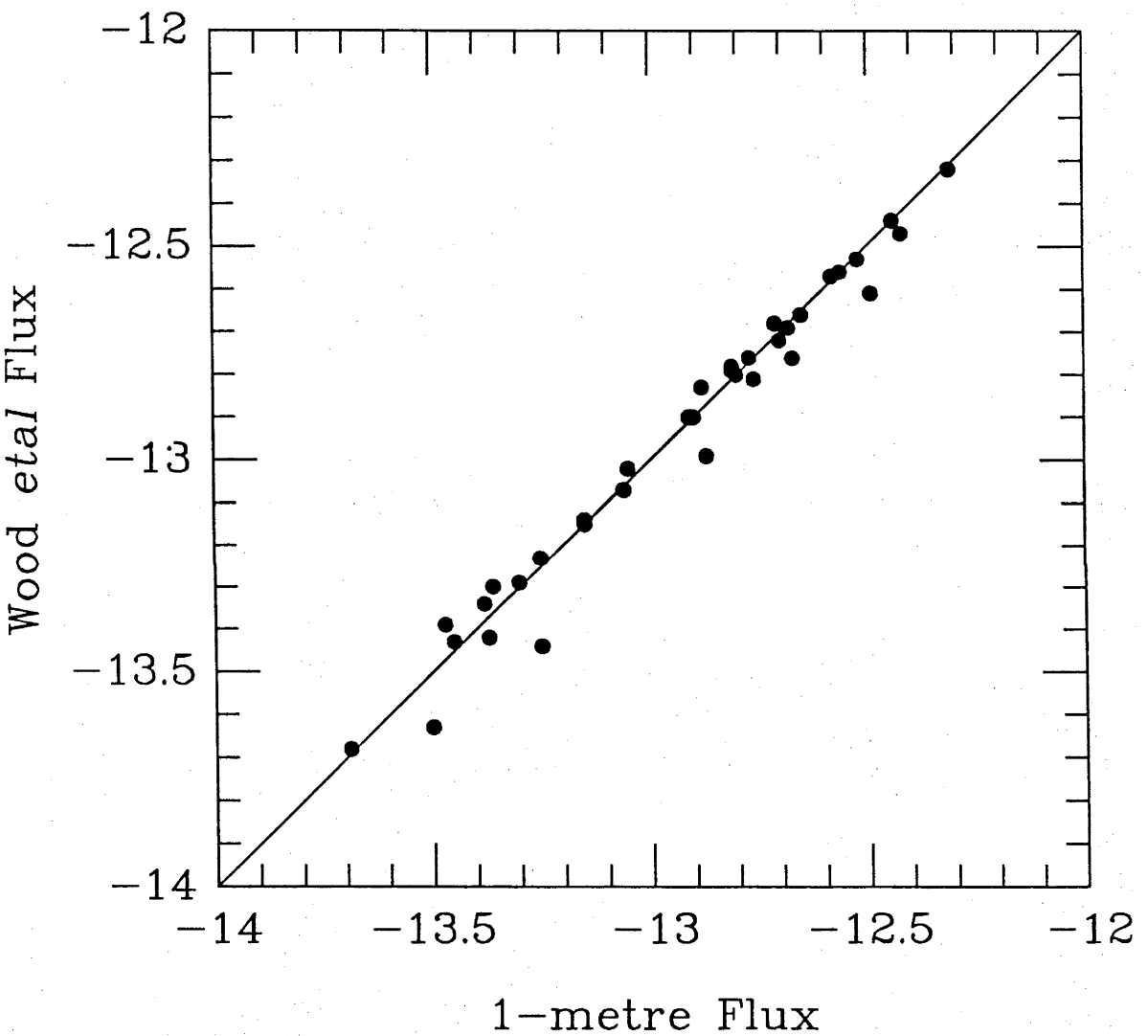
−12
−12.5
−13
−13.5
−14
−14
−13.5
−13
−12.5
−12
Wood *etal* Flux
1−metre Flux

frames did remain then this would give an effect such as we see. Another possibility is that WMDM may have had some faint field stars in their concentric sky aperture, the effect of which would be to lower the flux measured for that nebula.

A total of 39 PN in the SMC and 99 in the LMC have now had their fluxes measured, out of a total known of 62 in the Small Cloud and 170 in the Large Cloud. Those that are still to be measured are the fainter Morgan (1984), Morgan and Good (1985) and Jacoby (1980) objects, or SMP nebulae that could not be found. Those SMP objects that could not be found were assumed to be either too faint for the 1 metre telescope or erroneously identified from our objective prism plates.

b) Nebular Masses

We may calculate the approximate ionized mass contained in the nebular shell using the following formula:

$$M_{neb} = 4\pi D^2 F_{\mathrm{H}\beta}(1+4y)m_{\mathrm{H}}/(\alpha_{eff}h\nu n_e) \qquad (3.1)$$

where D is the distance (which we have taken as 53 kpc for the LMC and 66 kpc for the SMC), y = N(He)/N(H) = 0.11 and α_{eff} is the effective recombination coefficient of hydrogen for the emission of Hβ photons of energy $h\nu$ ($\alpha_{eff}h\nu = 1.24 \times 10^{-25}$ erg cm^3 s^{-1} at $T = 10^4$ K and $n_e = 10^4$ cm^{-3}).

Substituting numerical values into equation (3.1) and taking logarithms gives:

$$\log M_{neb} = \log F_{\mathrm{H}\beta} - \log n_e \begin{array}{ll} +\,15.52 & (\mathrm{LMC}) \\ +\,15.71 & (\mathrm{SMC}) \end{array} \qquad (3.2)$$

Equation (3.2) has been used to derive nebular masses for 20 PN in the SMC and 34 in the LMC. The Hβ fluxes used are a mean of all measurements from Tables 2 and 3 (excluding those thought to be erroneous). The densities are from Dopita *et al.* (1988) and Barlow (1987). The masses are given in Tables 4 and 5 for the SMC and LMC PN respectively. Figure 3 shows a histogram of the distribution of nebular masses, additional masses coming from WMDM (Table 1 therein). The distribution is strongly peaked around a mass of $0.17\mathcal{M}_{\odot}$ but has a wide range from $0.35\mathcal{M}_{\odot}$ with a tail extending down to $0.01\mathcal{M}_{\odot}$. This may be compared with the results of Maciel and Pottasch (1980) who derived ionized masses for a total of 121 Galactic PN. Their results have a mean mass of $0.14\mathcal{M}_{\odot}$, with a range of ionized masses very similar to what we have calculated. This apparent large range in ionized mass has been noted by various authors (Pottasch 1980, 1983; Maciel and Pottasch 1980; Daub 1982; Wood and Faulkner 1986), and must cast serious doubts on the use of the Shklovsky method in its original form (Shklovsky 1956) for determining PN distances.

Barlow (1987) derived masses for 32 Magellanic Cloud planetary nebulae. On the whole the two mass estimates are quite similar, a mean difference of only $0.02\mathcal{M}_{\odot}$ existing between the majority of the objects in common. However, a few of the nebular masses are quite different between the two studies, due to differences in adopted density and Hβ flux. For two nebulae in the SMC (SMP9 and SMP28) the masses are different as Barlow has used flux measurements which appear to be in error. For those other objects where large variations are found (SMC SMP15 and SMP22; LMC SMP6, SMP21 and SMP47) we believe our density measurements to be

TABLE 4

NEBULAR MASSES OF SMC PLANETARY NEBULAE

Object Name	$\log F_{\mathrm{H}\beta}$	$\log n_e$ (cm^{-3})	M_{neb} ($\mathcal{M}_\odot$)
SMP 1	-12.76	4.02	0.08
SMP 2	-12.72	3.46	0.34
SMP 3	-13.06	3.26	0.24
SMP 5	-12.80	3.54	0.23
SMP 6	-12.79	4.41	0.03
SMP 9	-13.43	2.43	0.71
SMP 13	-12.56	3.86	0.20
SMP 14	-13.03	3.52	0.14
SMP 15	-12.42	4.81	0.03
SMP 16	-12.72	4.19	0.06
SMP 17	-12.53	3.71	0.29
SMP 18	-12.64	3.86	0.16
SMP 19	-12.93	3.59	0.15
SMP 20	-12.43	4.85	0.03
SMP 21	-13.24	3.60	0.01
SMP 22	-12.86	3.62	0.17
SMP 24	-12.67	3.83	0.16
SMP 26	-13.50	3.11	0.13
SMP 27	-12.44	3.73	0.35
SMP 28	-13.12	3.28	0.21

TABLE 5

NEBULAR MASSES OF LMC PLANETARY NEBULAE

Object Name	$\log F_{H\beta}$	$\log n_e$ (cm^{-3})	M_{neb} ($\mathcal{M}_\odot$)
SMP 1	-12.47	3.56	0.32
SMP 5	-12.85	3.30	0.23
SMP 6	-12.67	4.15	0.05
SMP 8	-13.74	3.80	0.10
SMP 15	-12.66	3.73	0.14
SMP 20	-13.40	3.11	0.10
SMP 21	-12.76	3.89	0.07
SMP 23	-12.68	3.77	0.12
SMP 29	-12.72	3.88	0.10
SMP 31	-12.91	3.94	0.05
SMP 32	-12.80	3.45	0.19
SMP 37	-12.85	3.86	0.06
SMP 38	-12.62	4.11	0.06
SMP 40	-13.34	3.08	0.13
SMP 45	-13.10	3.15	0.19
SMP 46	-13.60	3.60	0.02
SMP 47	-12.52	3.71	0.20
SMP 50	-12.70	3.70	0.13
SMP 52	-12.52	3.46	0.34
SMP 55	-12.66	4.60	0.02
SMP 58	-12.48	4.82	0.02
SMP 61	-12.45	4.60	0.03
SMP 62	-12.31	3.79	0.26
SMP 63	-12.47	3.99	0.12
SMP 67	-12.81	3.57	0.14
SMP 76	-12.53	4.16	0.07
SMP 77	-12.78	3.54	0.16
SMP 78	-12.58	3.63	0.20
SMP 83	-12.65	3.36	0.32
SMP 87	-12.91	3.26	0.23
SMP 89	-12.63	3.64	0.16
SMP 92	-12.54	4.00	0.09
SMP 96	-13.34	3.43	0.06
J 5	-13.25	3.04	0.17

Figure 3. Histogram of the relative numbers of nebulae of different masses derived is this paper. The distribution is quite strongly peaked around $M_{neb} \approx 0.17$ $M_{\odot}$.

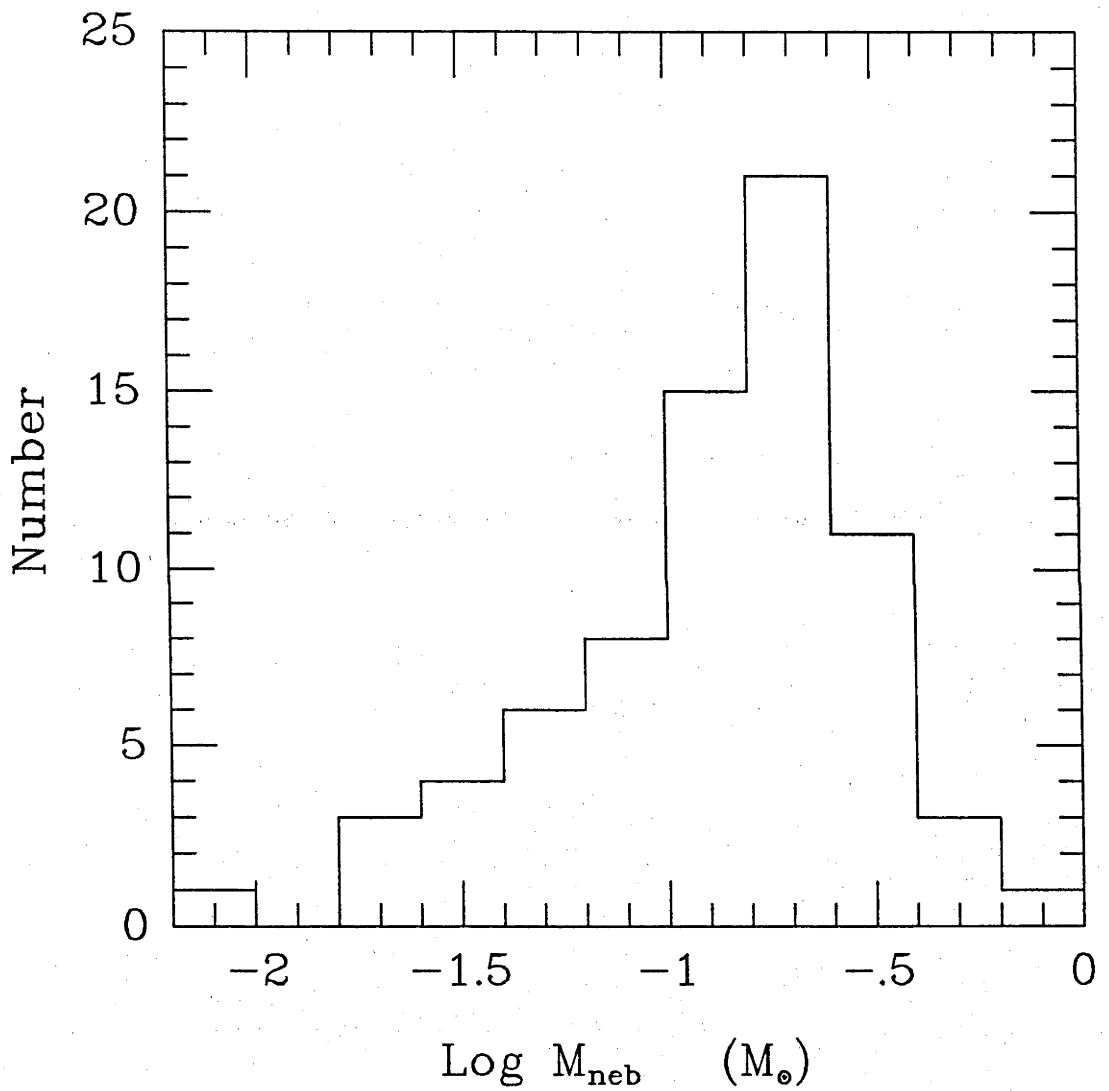
25
20
15
10
5
0
Number
−2
−1.5
−1
−.5
0
Log M_{neb} $(M_\odot)$

more accurate (see Dopita *et al.* (1988)) and hence our masses more appropriate.

It must be noted that there may be two possible criticisms of our masses. Firstly, the Hβ fluxes are uncorrected for reddening, and hence, our masses will tend to underestimate a actual nebular mass if the reddening should be high. Barlow (1987) gives C(Hβ) estimates for a number of Magellanic Cloud PN most of which are found to be of the same order C(Hβ)$<$ 0.2. Secondly, the density as measured from the [O II] $\lambda\lambda$3727, 3729 doublet may not necessarily be representative of the mean density throughout the nebula, and as the objects are not spatially resolved we are unable to determine whether this is the case. However, good agreement is generally found for those Galactic objects with known [O II] densities and densities derived from other means (Aller and Czyzak 1979; Pottasch 1980), which leads us to believe we are justified in using the [O II] densities.

IV. DISCUSSION

Dopita *et al.* (1987, 1988) have found a number of tight correlations between various nebular parameters (Hβ flux, expansion velocity, density, excitation class, mass and dynamical age) leading to tight constraints on models of the pre- and post-nebular ejection phase of evolution. In this paper we consider two more possible relationships. The first, between nebular electronic density (n_e) and ionized mass, and the second being between density and Hβ flux.

Figure 4 is a diagram of nebular density versus ionized mass. The density information is taken from [O II] $\lambda\lambda$3727, 3729 profiles (Dopita *et al.*

1988, Barlow 1987), while the masses are those derived in this paper (section III(b)). Much of the scatter at nebular densities greater than $\log n_e = 4.4$ is simply due to increased error in the electronic densities from [O II] line ratios. Measurement of the ratio becomes less accurate at high densities and very low densities as the ratio I(3729)/I(3727) tends to finite limits (Osterbrock 1974). For instance, at a nebular temperature of 10000°K and an electronic density of 30000 cm^{-3} an uncertainty of ± 0.01 in the ratio introduces a difference of ± 6000 cm^{-3} in the density. However, this reduces to only ± 1000 cm^{-3} at a density of 10000 cm^{-3}. From the Dopita *et al.* study, the errors associated with densities less than 10^4 cm^{-3} is typically 10%.

The diagram shows that $M_{neb} \propto 1/n_e$, at least for those objects with $\log n_e > 3.6$. This is expected, as from Figure 5 those objects have only a very small range in $\log F_{H\beta}$, and in conjunction with equation 2, this implies the proportionality. However, we may show that this is what we would expect if these nebulae were optically thick. For an optically thick nebula the number of recombinations is equal to the number of ionizations, ie. $n_e^2 R^3 = const\ F_{ion}$. Where F_{ion} is the flux of ionizing photons from the central star. The ionizing flux is proportional to the stellar luminosity, and is a function of effective temperature. Wood *et al.* (1987) showed that the number of ionizing photons per unit stellar luminosity does not vary by more than about 30% over a large range in PN central star temperatures. Hence, given that the evolutionary tracks of PN nuclei are essentially at constant luminosity early on ($\approx$ 10000 years for a $0.6\mathcal{M}_\odot$ star, Wood and Faulkner (1987)), we may take $F_{ion} = const$ over this part of the evolution. As the permissible mass range is also probably small this gives

Figure 4. Nebular ionized mass plotted against the electronic density (n_e). The objects for which $\log n_e > 3.6$ are optically thick, while those with lower densities are optically thin. There is an upper limit to the observed mass of about $0.4\mathcal{M}_\odot$.

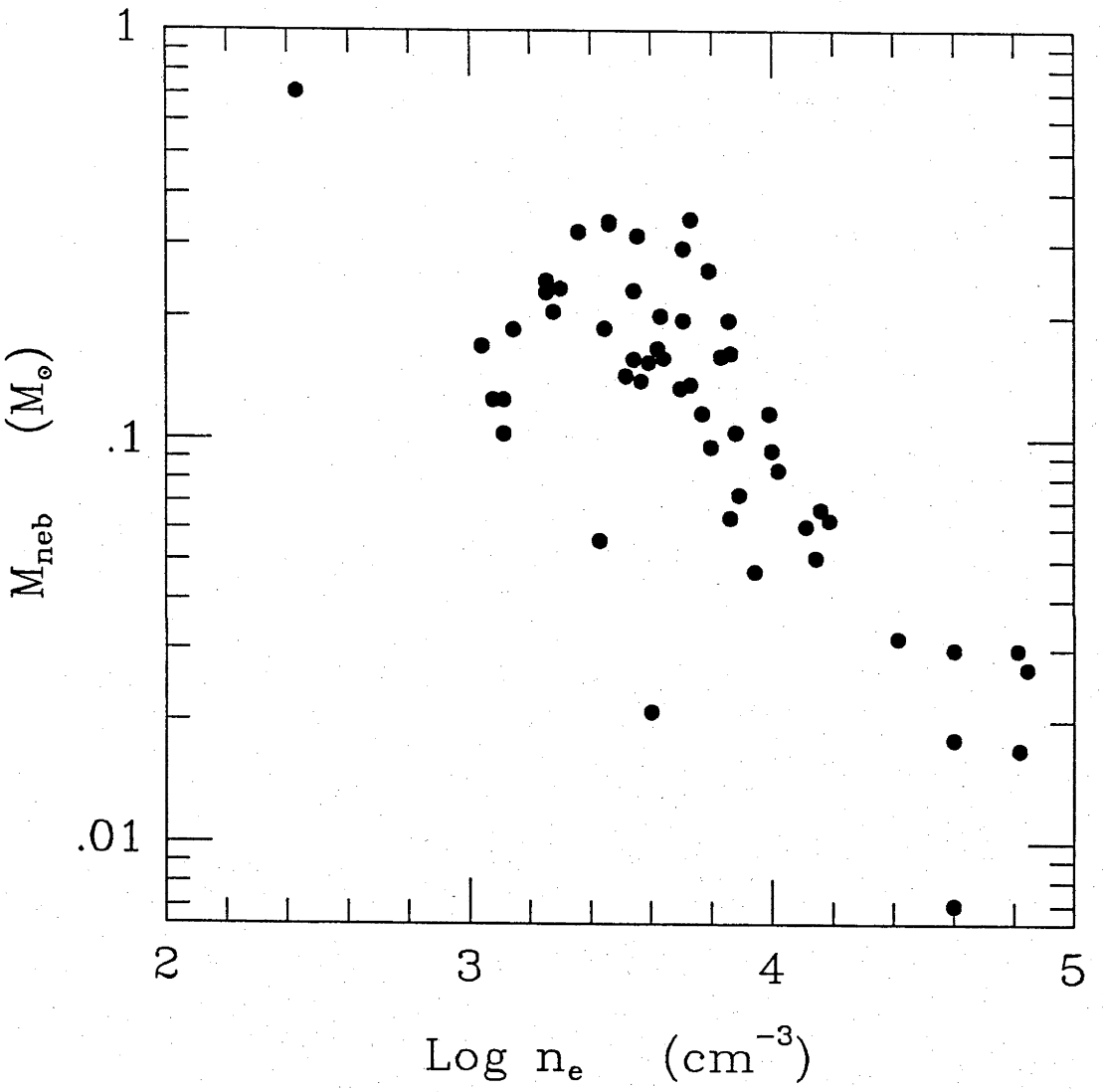
1
.1
.01
M_{neb} $(M_\odot)$
2
3
4
5
Log n_e (cm^{-3})

Figure 5. Nebular electronic density (n_e) as derived from [O II] line ratios versus Hβ flux. Those fluxes for SMC PN have been corrected to the distance of the LMC. Those nebulae with $\log n_e > 3.6$ are evolving at constant luminosity and are optically thick, while those with $\log n_e < 3.6$ are evolving at a constant nebular mass and will be becoming progressively optically thinner.

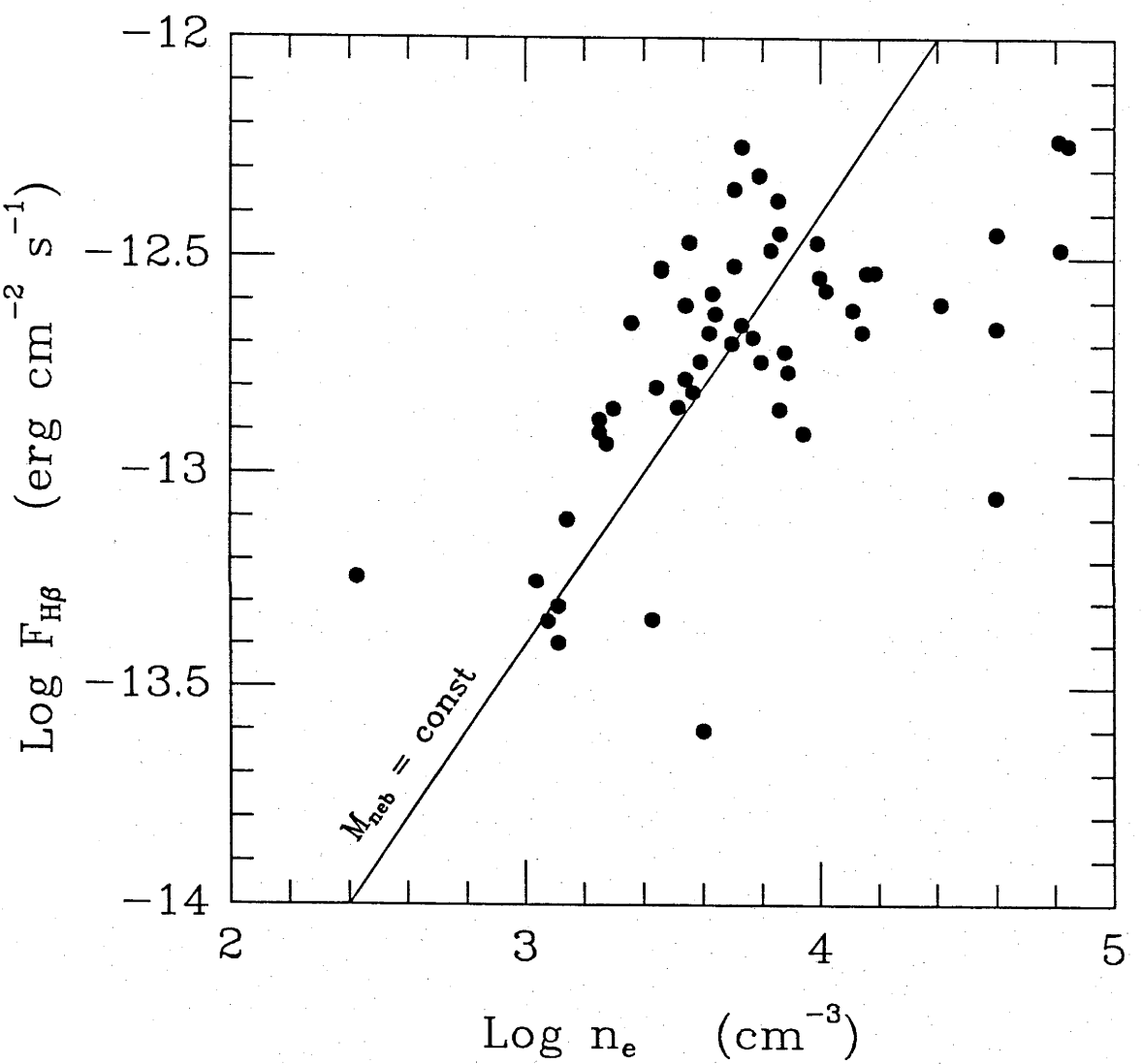
−12
−12.5
−13
−13.5
−14
2
3
4
5
Log $F_{H\beta}$ (erg cm^{-2} s^{-1})
Log n_e (cm^{-3})
M_{neb} = const

$n_e^2 R^3 = const.$ A planetary nebula is essentially a Strömgren sphere absorbing a constant flux of ionizing photons (F_{ion}) pumped out from the central star. Hence, as the nebula expands the ionized radius must increase in order to dissipate F_{ion}, and so the nebular density decreases if we assume an homologous expansion. But as the ionized radius increases so does the ionized mass. The ionized nebular mass is then $M_{neb} \propto n_e R^3 = const/n_e$. This is the relation we see in Figure 4, and is as found for Galactic PN (Pottasch 1980). A change in the slope will come about as the nebula begins to become optically thin. There is some indication of this in Figure 4 for those nebulae with densities $n_e < 3.6$, however, as we shall show this is more convincingly seen in Figure 5. The fact that there appears to be an upper limit to the ionized mass also supports the hypothesis that the nebulae in this region are becoming optically thin. Although there is another possible explanation which allows the nebulae to remain optically thick. If the ionizing flux F_{ion} decreases due to the luminosity of the central star dropping, then $M_{neb} \propto F_{ion}/n_e$ will also drop. This could give rise to an apparent upper limit to nebular masses. The limit seems to occur at a maximum ionized mass, $M_{neb} \approx 0.4\mathcal{M}_\odot$, with only one point ($M_{neb} = 0.7\mathcal{M}_\odot$) being an exception to this. This upper limit is once again supported by the observations of Pottasch (1980), who finds a similar cut-off in ionized mass for Galactic objects, and Wood *et al.* (1987) who find an upper limit of $\approx 0.5\mathcal{M}_\odot$ for Magellanic Cloud PN.

We have also constructed a plot of Hβ flux versus nebular density (Figure 5). The Hβ fluxes of the SMC planetary nebulae have been corrected to the distance of the LMC (53 kpc) for this study (a correction of 0.19 in log flux). One possible objection that may be raised is that the

observed fluxes have had no reddening corrections applied and so the actual shape of the diagram may be altered slightly.

This figure is similar to Figure 4, and it shows more clearly a change in slope at the point at which the nebulae begin to become optically thin to Hydrogen ionizing radiation. The fact that the slope is greater than a line of constant nebular mass indicates that the ionized mass may be dropping slightly due to the reasons mentioned earlier. Nebulae with densities $\log n_e > 3.6$ form a band ≈ 0.4 dex wide in $\log F_{\mathrm{H}\beta}$. The nebulae in this part of the diagram are those that we have shown to be optically thick, and to be evolving at approximately constant Hβ luminosity. This implies that $M_{neb} \propto R^{3/2}$, as a nebular mass — radius relation, in agreement with Wood, Bessell and Dopita (1986) and Daub (1982). Sabbadin *et al.* (1984) find $\log n_e \propto -\beta \log R$, where $\beta = -1$. Although from their diagram 6 it appears more that $\beta \approx -3/2$, which is in agreement with what we find. The width of the constant luminosity band is proportional to the permitted range in central star luminosities, and closely related to the range in masses.

As the nebulae become optically thin they evolve at constant nebular mass. From this we have $n_e \propto R^{-3}$ which is in agreement with Sabbadin *et al.* (1984) who found the same relationship for for optically thin nebulae. A representative line of slope unity shows a line of constant nebular mass. We would expect the nebulae to evolve parallel to this line, however, it appears that some of the older and fainter objects fade faster and tend to fall below lines of constant nebular mass. This is supported by the dynamical ages of the group of four nebulae in Figure 5 clustered between $-13.4 < \log F_{\mathrm{H}\beta} < -13.2$ and lying near the line of constant mass. We may calculate a dynamical age using the observational relationship presented by

Dopita *et al.* (1988). The ages are found to be between 3500 and 5000 years, whereas those clustered around $\log F_{\mathrm{H}\beta} = -12.5$ have ages closer to 2000 years.

The results shown in Figure 5 are consistent with such an evolutionary scheme. The one discrepant point, with $\log n_e = 2.4$, is SMC SMP9. It is probable that this nebula has evolved from a massive progenitor. However, Barlow (1987) gives a flux measurement fainter than our adopted flux by 0.4 dex. If the value given by Barlow is taken to be correct then this would bring the ionized mass down to $0.27\mathcal{M}_{\odot}$. The absence of many nebulae from the optically thin area near SMC SMP9 is most probably a selection effect, due to the short fading timescale for massive PN nuclei. Hence, Figure 5 shows the nebulae evolving from being optically thick to optically thin as in Figure 4, as well as allowing us to derive a nebular mass — radius relation.

While the density at which the transition from being optically thick to optically thin may appear difficult to tie down accurately from Figure 5, it is worth noting that Barlow (1987) concluded independently to us that the transition occurs at densities between 5000 and 6000 cm^{-1}, which is almost exactly the value we derive. Barlow also classifies his sample of nebulae as optically thick or thin on the basis of central star analyses and the presence or absence of nebular He II λ4686 emission. With the exception of one object (LMC SMP6) his classification agrees exactly with that obtained from our Figure 5 using density as the discriminant.

V. SUMMARY

A large sample of planetary nebulae in the Magellanic Clouds have now had Hβ fluxes measured. These fluxes together with [O II] $\lambda\lambda 3727, 3729$ electron densities allow a determination of ionized masses within the nebular shells. A subset of 54 nebulae have had masses derived in this way. These masses together with densities have been used to show at what density the nebulae begin to become optically thin. The Hβ fluxes have been used with the densities to derive a nebular mass — radius relation of the form $M_{neb} \propto R^{3/2}$ for those nebulae that are optically thick, and shown that optically thin nebulae evolve at a constant nebular mass.

Acknowledgement. It is a pleasure to thank Dr P. Wood for his helpful discussions and comments on this paper, which have led to its considerable improvement.

REFERENCES

Aller, L.H. 1983, *Ap. J.*, **273**, 590.

Aller, L.H., and Czyzak, S.J., 1979, *Ap. Space Sci.*, **62**, 397.

Amnuel, P.R., Guseinov, O.H., Novruzova, H.I., and Rustamov, Yu.S. 1984, *Ap. Space Sci.*, **107**, 19.

Barlow, M.J. 1987, *M.N.R.A.S.*, **227**, 161.

Cahn, J.H., and Kaler, J.B. 1971, *Ap. J. Suppl.*, **22**, 319.

Daub, C.T. 1982, *Ap. J.*, **260**, 612.

Dopita, M.A., Ford, H.C., Lawrence, C.J., and Webster, B.L. 1985, *Ap. J.*, **296**, 390.

Dopita, M.A., Meatheringham, S.J., Wood, P.R., Ford, H.C., Webster, B.L., and Morgan D.H. 1987, *Ap. J. (Letters)*, **315**, L107.

Dopita, M.A., Meatheringham, S.J., Webster, B.L., and Ford, H.C. 1988, *Ap. J.*, in press (April 15).

Harman, R.J. and Seaton, M.J. 1964, *Ap. J.*, **140**, 824.

Henize, K.G. 1956, *Ap. J. Suppl.*, **2**, 315.

Henize, K.G., and Westerlund, B.E. 1963, *Ap. J.*, **137**, 747.

Jacoby, G.H. 1980, *Ap. J. Suppl.*, **42**, 1.

Lindsay, E.M., and Mullen, D.J. 1963, *Irish Astr. J.*, **6**, 51.

Maciel, W.J., and Pottasch, S.R. 1980, *Astr. Ap.*, **88**, 1.

Meatheringham, S.J., Dopita, M.A., Ford, H.C., and Webster, B.L. 1988, *Ap. J.*, in press (April 15).

Meatheringham, S.J., and Dopita, M.A., 1988, *in preparation.*

Morgan, D.H. 1984, *private communication.*

Morgan, D.H. and Good, A.R. 1985, *M.N.R.A.S.*, **213**, 491.

O'Dell, C.R. 1974, *in IAU Symposium 66, "Late Stages Of Stellar*

Evolution", ed. R.J. Tayler, (Reidel : Dordrecht), 213.

Osmer, P.S. 1976, *Ap. J.*, **203**, 352.

Osterbrock, D.E., 1974, *"Astrophysics of Gaseous Nebulae"*, (W.H. Freeman and Co.), 112.

Paczyński, B. 1971, *Acta. Astr.*, **21**, 417.

Phillips, J.P. and Pottasch, S.R., 1984, *Astr. Ap.*, **130**, 91.

Pottasch, S.R. 1980, *Astr. Ap.*, **89**, 336.

Pottasch, S.R. 1983, *in IAU Symposium 103, "Planetary Nebulae"*, ed. D.R. Flower, (Reidel : Dordrecht), 391.

Pottasch, S.R. 1984, *Astrophys. & Space Sci. Libr.*, **107**, *"Planetary Nebulae"*, (Reidel : Dordrecht).

Sabbadin, F., Gratton, R.G., Bianchini, A., and Ortolani, S., *Astr. Ap.*, **136**, 181.

Sanduleak, N., McConnell, D.J., and Philip, A.G.D. 1978, *Pub. A.S.P.*, **90**, 621.

Schonberner, D. 1981, *Astr. Ap.*, **103**, 119.

Shklovsky, I.S., 1956, *Astron. Zh.*, **33**, 222, 315.

Stapinski, T.E., Rodgers, A.W., and Ellis, M.J. 1981, *Pub. A.S.P.*, **93**, 242.

Webster, B.L., 1969, *M.N.R.A.S.*, **143**, 79.

Webster, B.L., 1976, *M.N.R.A.S.*, **174**, 513.

Webster, B.L., 1983, *Pub. A.S.P.*, **95**, 610.

Wood, P.R., Bessell, M.S., and Dopita, M.A., 1986, *Proc. Astr. Soc. Aust.*, **6**, 54.

Wood, P.R., and Faulkner, D.J. 1986, *Ap. J.*, **307**, 659.

Wood, P.R., Meatheringham, S.J., Dopita, M.A., and Morgan, D.H., *Ap. J.*, **320**, 178.

A STUDY OF SOME SOUTHERN PLANETARY NEBULAE

Stephen J. Meatheringham, P.R. Wood, D.J. Faulkner

Mount Stromlo and Siding Spring Observatories,

Institute of Advanced Studies,

Australian National University

Received:

Accepted:

Submitted to *Astrophysical Journal.*

ABSTRACT

Radial velocities and expansion velocities ([O III], [O II], and He II) have been measured for a sample of 64 Southern Galactic planetary nebulae. Nebular electronic densities have been derived from the [O II] $\lambda\lambda 3727, 3729$ doublet for 23 of these objects. These data are compared with previously published values. The Dopita *et al.* (1987) distance scale for Magellanic Cloud planetary nebulae based on a correlation between observable nebular parameters is used to derive distances to 33 Galactic nebulae. These distances are compared with published values and lead to the conclusion that the Dopita *et al.*, Daub (1982) and Maciel (1984) distance scales agree well for the objects in common. Nebular ionized masses are calculated for these objects and exhibit a large range from $\sim 10^{-3}\mathcal{M}_{\odot}$ to $\sim 0.6\mathcal{M}_{\odot}$. The nebulae are found to lie in the same area of the mass–radius diagram occupied by the Magellanic Cloud and Galactic Centre objects. The nebulae become optically thin at densities $n_e < 5000$ cm^{-3}.

Subject Headings: nebulae : planetary

I. INTRODUCTION

The concept that planetary nebulae (PN) are differentially expanding goes back to Perrine, and separately Zanstra, in 1928. Over the years the idea that the nebulae are approximately spherical, expanding shells has been built up by many authors (eg. Wilson 1950; Osterbrock *et al.* 1966; Weedman 1968), both due to observational data as well as theoretical modelling. The basic result found is that PN are expanding gaseous envelopes, with expansion velocities from a few km s^{-1} to a maximum of approximately 80 km s^{-1}, with a mean value of order 20 km s^{-1}. Sabbadin (1984) published a catalogue of 165 expansion velocities for galactic planetaries containing all the data published to the end of 1983. We have enlarged the number of published expansion velocities by 43, as well as remeasuring another 21.

The measurement of planetary nebular radial velocities has a number of uses. Most importantly it allows an investigation of the kinematics of the galactic PN population. The concentration towards the galactic centre is obvious in plots of their distribution in galactic coordinates. Schneider *et al.* (1983) collected all known radial velocities for 524 galactic planetaries, and also provide a detailed error analysis. We present radial velocity measurements for 64 southern nebulae, of which 17 are new to Schneider's paper.

One of the most difficult problems associated with planetary nebulae has proved to be that of assigning a distance. The main method used in the past assumed all planetary nebulae to have the same mass (Shklovsky 1956; Cahn and Kaler 1971; Milne and Aller 1975). For the Shklovsky

method to be applicable, the nebulae should be optically thin so that the ionized mass is equal to the total nebular mass. However, recent observations (Pottasch 1980; Maciel and Pottasch 1980; Daub 1982; Wood *et al.* 1987; Meatheringham *et al.* 1988b) indicate that nebular masses vary by factors of up to $\sim 10^3$, and hence the Shklovsky method may not be applicable. In order to try to overcome the difficulties of application of the Shklovsky method to optically thick nebulae Daub (1982) determined a relation between the ionized mass and a particular function of observable quantities, and determined distances from this relation. While the distances to the majority of objects which are common to Cahn and Kaler (1971) and Daub (1982) agree quite well for optically thin objects, there are some optically thick nebulae which have distances differing by factors of $2-3$.

The sample of planetary nebulae in the Magellanic Clouds offers notable advantages in evolutionary studies by providing us with a luminosity-limited sample at a known distance and with low line-of-sight reddening. While we gain with the immense advantage of knowing the distance we do lose spatial resolution, as practically all the Magellanic Cloud planetary nebulae are unresolved. Over the past four years a substantial amount of work, both observational and theoretical, has gone into the study of the Magellanic Cloud planetary nebulae (Dopita *et al.* 1985, 1987, 1988; Meatheringham *et al.* 1988a, b; Wood *et al.* 1986, 1987). This work has yielded amongst other things, an empirical relationship between the excitation class of the nebula, electronic density, and [O III] expansion velocity, which leads to a determination of the distance to the nebula (Dopita *et al.* 1987). In this paper we examine the applicability of this relation to Galactic planetary nebulae.

II. OBSERVATIONS AND DATA REDUCTION

a) Observations

The observations were made during the period from March to July 1984 on the 1-metre telescope operated by the Australian National University at Siding Spring Observatory. The Perkin Elmer échelle spectrograph was used with a 79 line mm^{-1} échelle grating and a 316 line mm^{-1} cross disperser. This gave a dispersion of 5.08 Å mm^{-1} at the [O III] λ5007 line. The 2-dimensional Photon Counting Array (2D PCA) developed at the Mount Stromlo Observatory (Stapinski, Rodgers & Ellis 1981) was used as the detector. The PCA has a 745 by 244 element pixel array giving a spectral range per échelle order of approximately 63Å. The telescope and échelle system combined with a 25mm Quantex television camera gave a 315 arcsec field of view on the sky. Using a slit width of 150 microns a resolution of 11.5 km s^{-1} at λ5007 was obtained. Two settings of the cross disperser were used; one to record the [O III] λ5007 and He II λ4686 lines, and the other for the [O II] $\lambda\lambda$3727, 3729 doublet. Exposure times varied between 300 and 1800 seconds. Some of the nebulae were very faint and the resulting spectra had a low signal to noise ratio. As a result of this a statistical error is present simply due to the finite number of photons counted, and may amount to as much as 10% in the measurement of the full width at half maximum (FWHM).

b) Reduction

To reduce the data it was first necessary to extract and straighten the spectral orders containing the nebular images. The straightened

spectra were then rebinned in the wavelength direction to give a constant wavelength increment per pixel. This was done by identifying known lines in a Th-Ar arc lamp exposure, and calculating a full 2-dimensional quadratic fit of wavelength to pixel position across the order. The quadratic wavelength fits were then applied to the nebular images. To minimize any instrumental drifts that occurred during the night each planetary nebula exposure was bracketed by arc exposures, and the appropriate arcs added to give a mean arc for use in the rebinning procedure. With the individualized arc fitting the standard deviation (σ) was less than 0.10 pixels, corresponding to a velocity error of 0.5 km s^{-1}.

III. RESULTS

After wavelength rebinning it was possible to examine sections of the images and extract profiles, which were found to fall into two main classes. Firstly, a single peak, which may correspond to either an unresolved double peak (implying an expansion velocity of somewhat less than the resolution of the instrument), or to a filled shell (with all velocities out to the maximum being present). The latter possibility is generally seen as a broad feature, whereas the unresolved case is only a few pixels ($\leq 12 - 15$ km s^{-1}) across. And secondly, a double peak, which corresponds to emission from two separate areas of gas moving with different velocities relative to us. There are a number of possible configurations which may give rise to such a profile, the most common being either shell or "bi-polar" structures. Examples of the different types of profiles can be seen in Figure 1.

Figure 1. Representative profiles of nebulae obtained in this study. The bars indicate the instrumental full width half maximum (FWHM). The third spectrum shows an [O II] doublet profile.

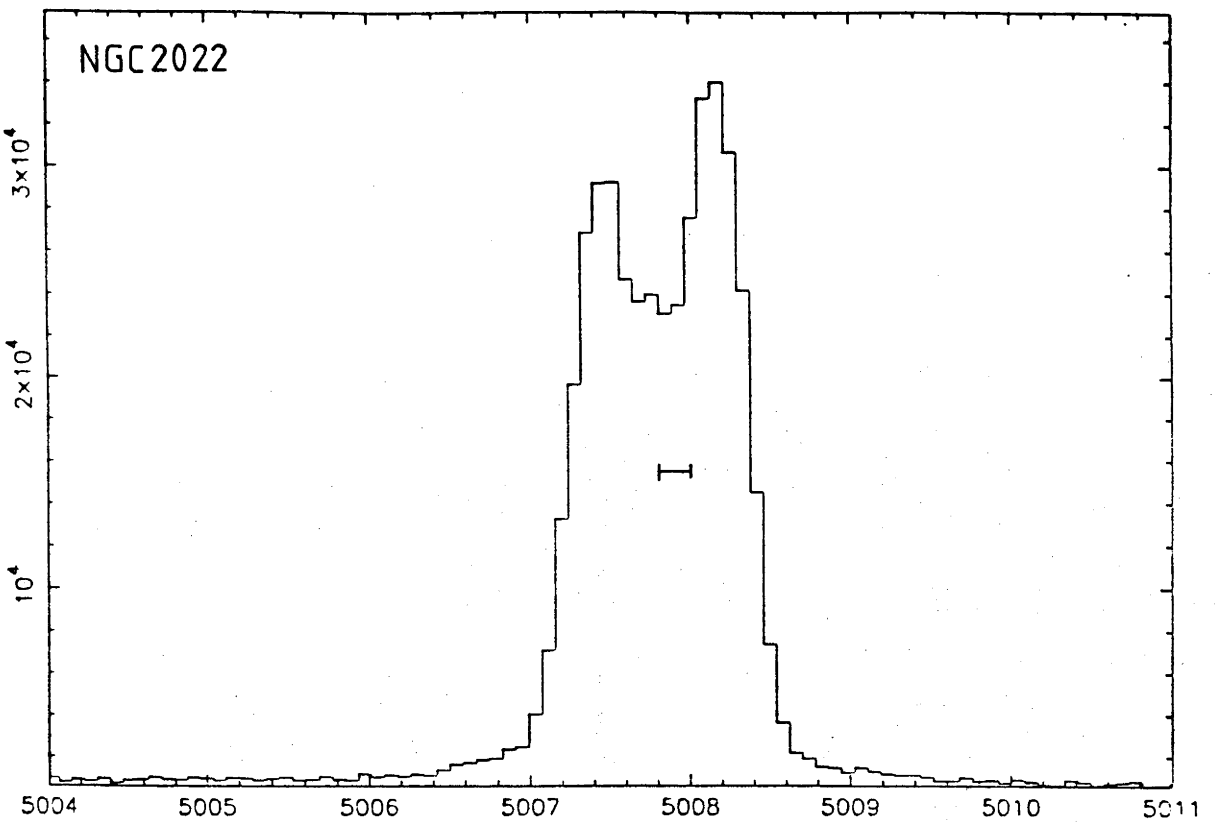
NGC2022
3×10⁴
2×10⁴
10⁴
5004
5005
5006
5007
5008
5009
5010
5011

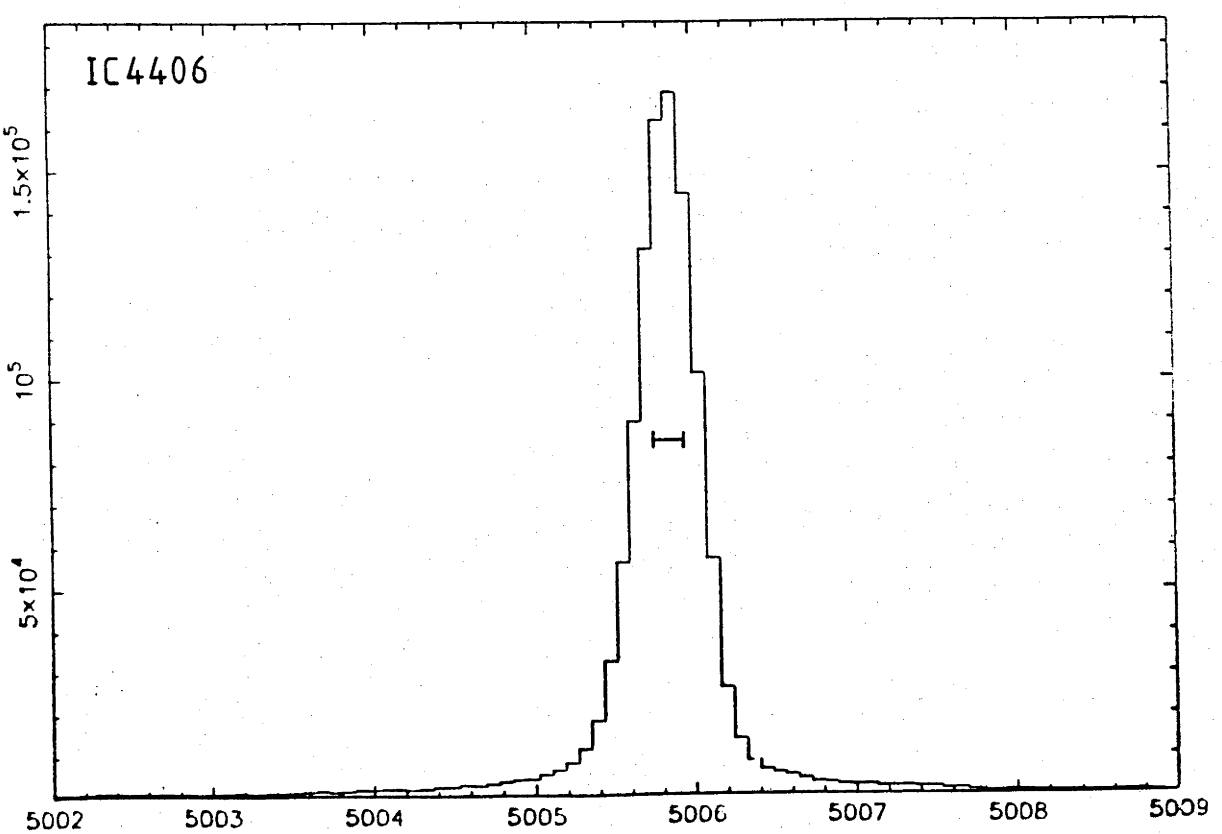
IC4406
1.5×10⁵
10⁵
5×10⁴
5002
5003
5004
5005
5006
5007
5008
5009

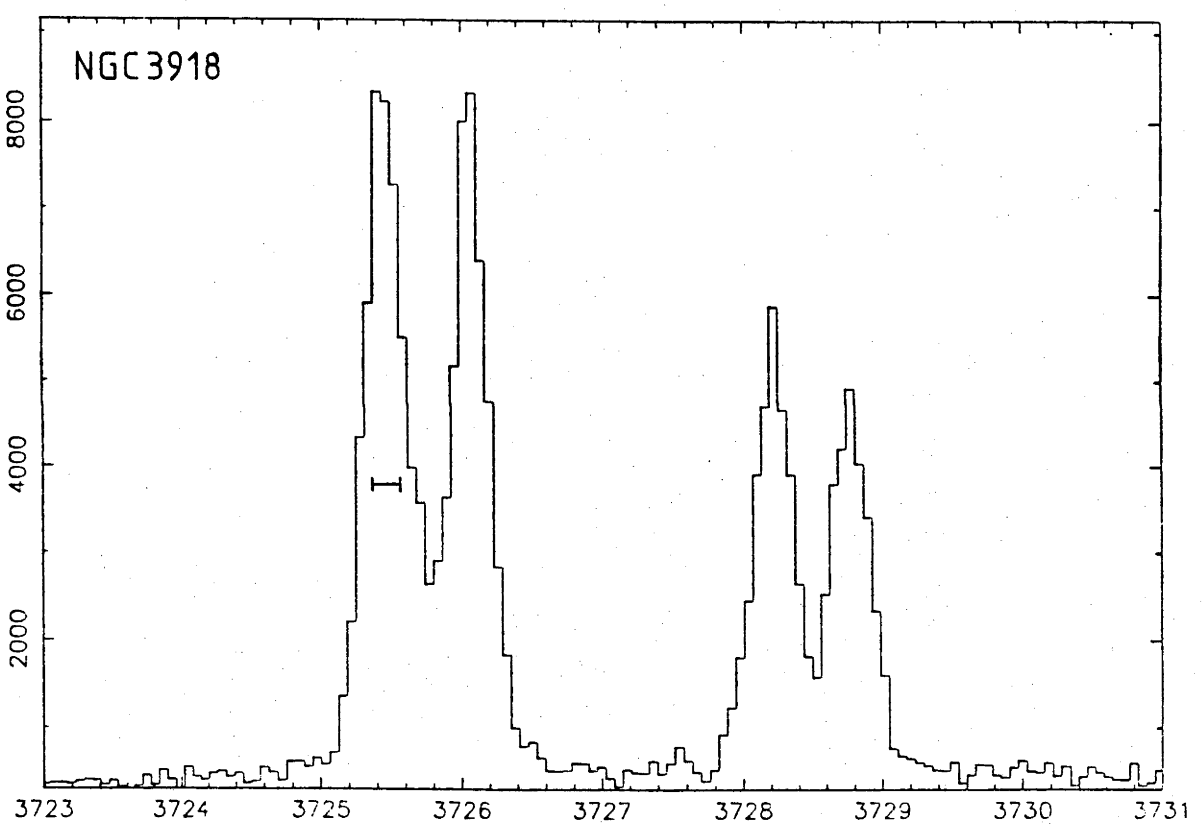
NGC3918
8000
6000
4000
2000
3723
3724
3725
3726
3727
3728
3729
3730
3731

a) Radial Velocities

We have determined radial velocities for 64 nebulae in this study, of which 17 are new to the compilation of Schneider *et al.* (1983). The multiple gaussian fitting program SPECTRE (Pelat, Alloin and Fosbury 1981) was used to determine the central wavelengths of the profiles. Depending on the type of profile, one of two methods was chosen to calculate the radial velocity. In the case where the profile was a single peak we simply adopted the velocity corresponding to the central wavelength. When there was a split double profile the central velocity, as found from the two peaks, was used. The radial velocities so obtained were then corrected for the Earth's motion around the Sun (Heliocentric velocities). These velocities are listed in Table 1. The values given are a weighted mean of those obtained from the [O III], [O II], and He II profiles.

The mean difference between the radial velocities as given in Schneider *et al.* (1983) and our values is less than 0.1 km s^{-1}. Our values have smaller errors than those given by Schneider *et al.* for many of the objects, and hence these new velocity measurements represent a considerable improvement in accuracy. These objects are : NGC2452, 2610, 2792, 2818, 2899, 3195, 3699, 6026, 6072, 6537, 6772, Fg1, He2–103, 2–111, 2–114, 2–120, 2–146, 2–165, IC4406, 4673, M1–42, 3–39, Mz1, Sp1. The errors associated with each velocity determination are also listed in Table 1 and were derived from the uncertainty in defining a central wavelength for the profiles. These errors are close to what we derive using $\pm\sigma/N^{1/2}$ (Bevington, 1969), where σ is the e-folding width of a gaussian fit, and N the number of photons in the profile.

TABLE 1

RADIAL VELOCITY DATA

Object Name	V_{HEL} (km s^{-1})	Object Name	V_{HEL} (km s^{-1})
NGC2022	14 ± 2	A 51	23 ± 10
NGC2346	20 ± 3	A 65	13 ± 4
NGC2438	74 ± 4	A 70	−79 ± 18
NGC2440	63 ± 3	ESO 259–10 ..	49 ± 3
NGC2452	65 ± 3	Fg 1	29 ± 3
NGC2610	89 ± 3	He 2–7	88 ± 4
NGC2792	14 ± 3	He 2–29	25 ± 6
NGC2818	−1 ± 3	He 2–37	12 ± 5
NGC2867	12 ± 4	He 2–51	8 ± 3
NGC2899	3 ± 4	He 2–82	−10 ± 12
NGC3132	−10 ± 3	He 2–103	−30 ± 2
NGC3195	−7 ± 3	He 2–111	−11 ± 4
NGC3211	−22 ± 2	He 2–114	−37 ± 2
NGC3699	−22 ± 4	He 2–120	−20 ± 6
NGC3918	−17 ± 3	He 2–146	62 ± 4
NGC4071	11 ± 3	He 2–165	−18 ± 2
NGC4361	9 ± 2	He 2–198	−1 ± 3
NGC5307	40 ± 4	Hf 4	22 ± 12
NGC6026	−103 ± 5	Hf 38	64 ± 4
NGC6072	7 ± 2	IC418	61 ± 2
NGC6153	37 ± 3	IC4406	−41 ± 2
NGC6326	9 ± 4	IC4642	44 ± 3
NGC6337	−71 ± 4	IC4673	−15 ± 2
NGC6369	−101 ± 2	IC5148–50	−23 ± 6
NGC6537	−16 ± 3	M 1–42	−92 ± 3
NGC6565	−2 ± 4	M 1–46	30 ± 3
NGC6629	14 ± 3	M 3–39	4 ± 3
NGC6772	0 ± 4	Mz 1	−33 ± 4
NGC6818	−13 ± 3	Mz 2	−30 ± 3
NGC6852	−11 ± 5	Skwl 3–2	66 ± 12
NGC7009	−44 ± 3	Sp 1	−31 ± 3
A 44	44 ± 6	Th 2–A	−45 ± 18

b) Expansion Velocities

The velocity with which a planetary nebula is expanding is one of its most important properties, yet it is something which is difficult to measure accurately. To find the maximum outflow velocity it is necessary to use an ion found in the outer regions of the nebula, this being where the expansion velocity is greatest (except for very large nebulae where the velocity is found to drop off at the outer edges); or alternatively to measure an ion such as O^{++} down to very low levels of surface brightness. Ideally, we wish to measure the half width at zero intensity, however, this introduces large errors due to the low number of photons found in the wings, and the presence of a faint stellar continuum. Previous authors (eg. Osterbrock 1974; Robinson *et al.* 1982) have instead preferred to measure the velocity separation of the two peaks. Another problem that exists in defining an expansion velocity is that many planetary nebulae show non-spherical structure, an example being those objects with "bi-polar" outflows. This means that depending on slit orientation a wide range in expansion velocities may be obtained. In this study, objects with obvious non-spherical structure were observed with the spectrograph slit laid along the longest axis, in an effort to measure the maximum velocity splitting.

In this paper we have elected to calculate a number of different expansion velocities, and compare the results obtained. Firstly, we have taken the velocity separation of the two peaks ($2V_{exp,pp}$) (in the cases where there was only a single maximum a velocity $2V_{exp,pp} \leq 12$ km s^{-1} was assumed). Secondly, we measured the full width at 20% maximum ($2V_{exp,20}$) corrected for instrumental broadening, assuming that it adds in quadrature. We find a good correlation between these two definitions of expansion

velocity (Figure 2), and hence, provided that a consistent definition is used between authors equivalent results should be obtained.

Our expansion velocities, as measured from peak to peak, are shown in Table 2. Gaps in columns indicate that [O II] was not of sufficient intensity in the spectrum to allow a determination of V_{exp}, or in the case of He II that it may not have been present. Of the 64 nebulae measured, only a few have [O III] expansion velocities determined by other authors. However, most of these agree well, the mean difference being only 1 km s^{-1}. An exception is NGC2610, Sabbadin *et al.* (1986) quote $2V_{exp} = 67$ km s^{-1} where we find only 18 km s^{-1}.

We find a good correlation between the [O III] and [O II] expansion velocities (Figure 3), with the [O II] velocities being systematically higher. The slope of the correlation is 1.13. Using the same argument as Dopita *et al.* (1988), in that since the [O II] emission always occurs near the outer boundary of the ionized shell, this indicates that the maximum expansion velocity occurs in the outer regions. Since O^{++} is the dominant ionization stage and provided there is an outward increase in velocity through the nebulae (ie. $V_{exp} \propto R$), then the ratio of the [O III] to [O II] expansion velocities gives an estimate of the thickness of the ionized shell. This yields a fractional thickness $\Delta R/R_{neb} \approx 0.13$, compared with a value of 0.15 derived for Galactic PN by Phillips (1984), and 0.18 for Magellanic Cloud nebulae (Dopita *et al.* 1988).

Figure 2. Relationship between the [O III] expansion velocities as measured from peak to peak and at the 1/20th maximum intensity. The line of best fit is at a slope of 0.9. If the actual expansion velocities of those objects for which we have only $2V_{exp} < 12$ km s^{-1} were determined this would make the slope even closer to unity.

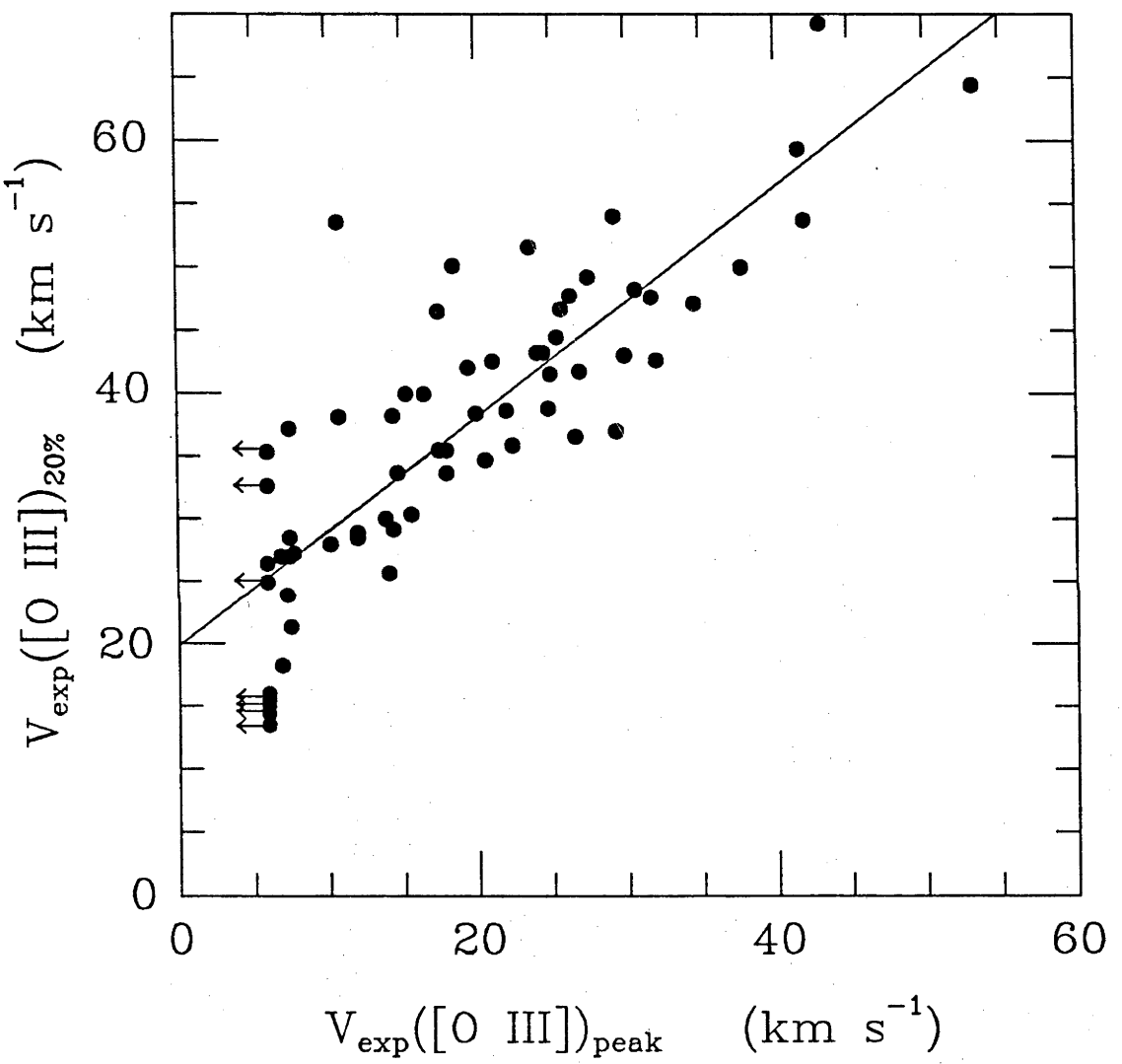
60
40
20
0
0
20
40
60
$V_{exp}([O\ III])_{20\%}$ (km s^{-1})
$V_{exp}([O\ III])_{peak}$ (km s^{-1})

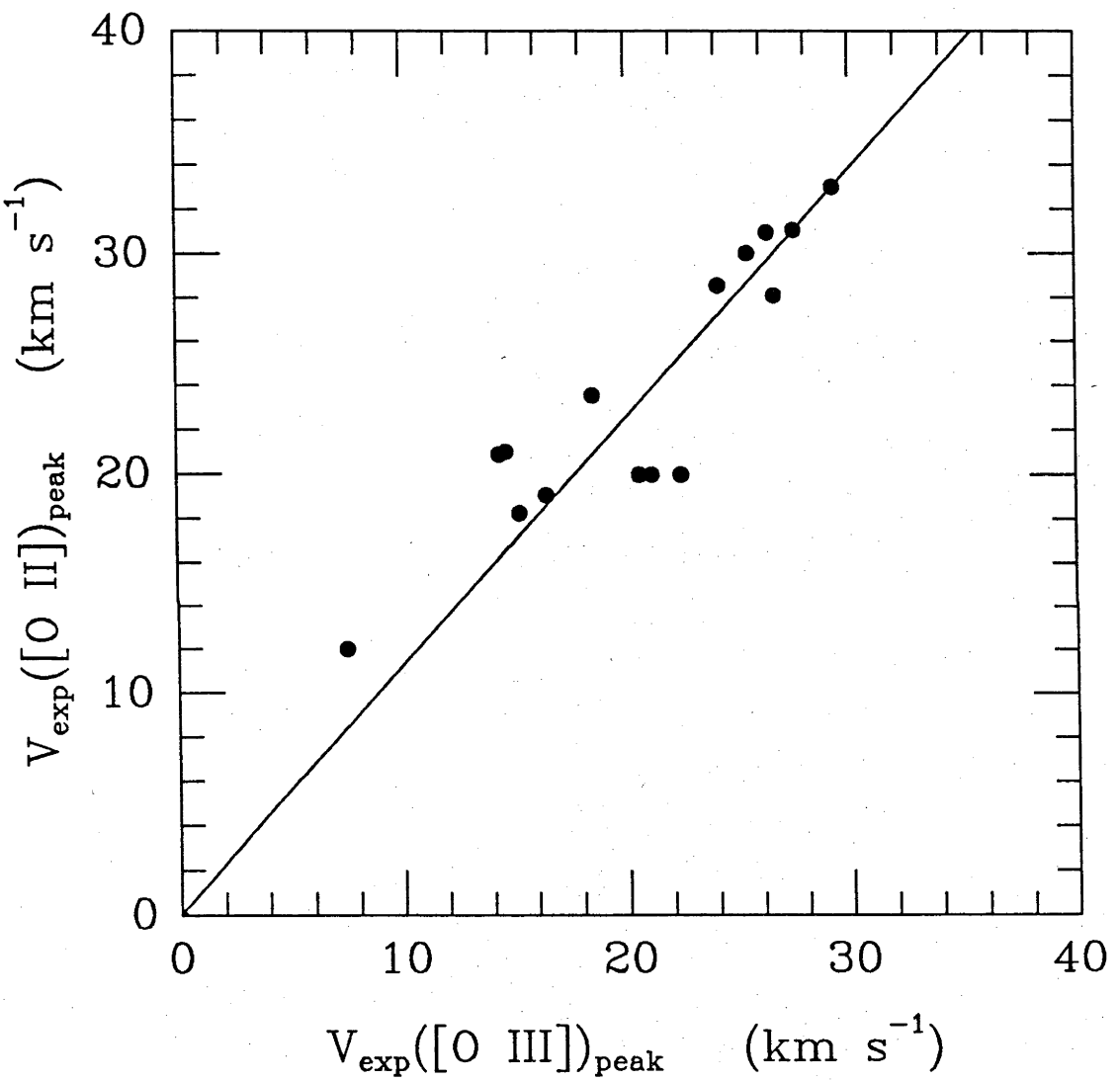
40
30
20
10
0
0
10
20
30
40
$V_{exp}([O\ II])_{peak}$ (km s^{-1})
$V_{exp}([O\ III])_{peak}$ (km s^{-1})

Figure 3. Correlation between the [O II] and [O III] expansion velocities. The line of best fit indicates a fractional thickness of the ionized region of $\Delta R/R_{neb} \approx 0.13$.

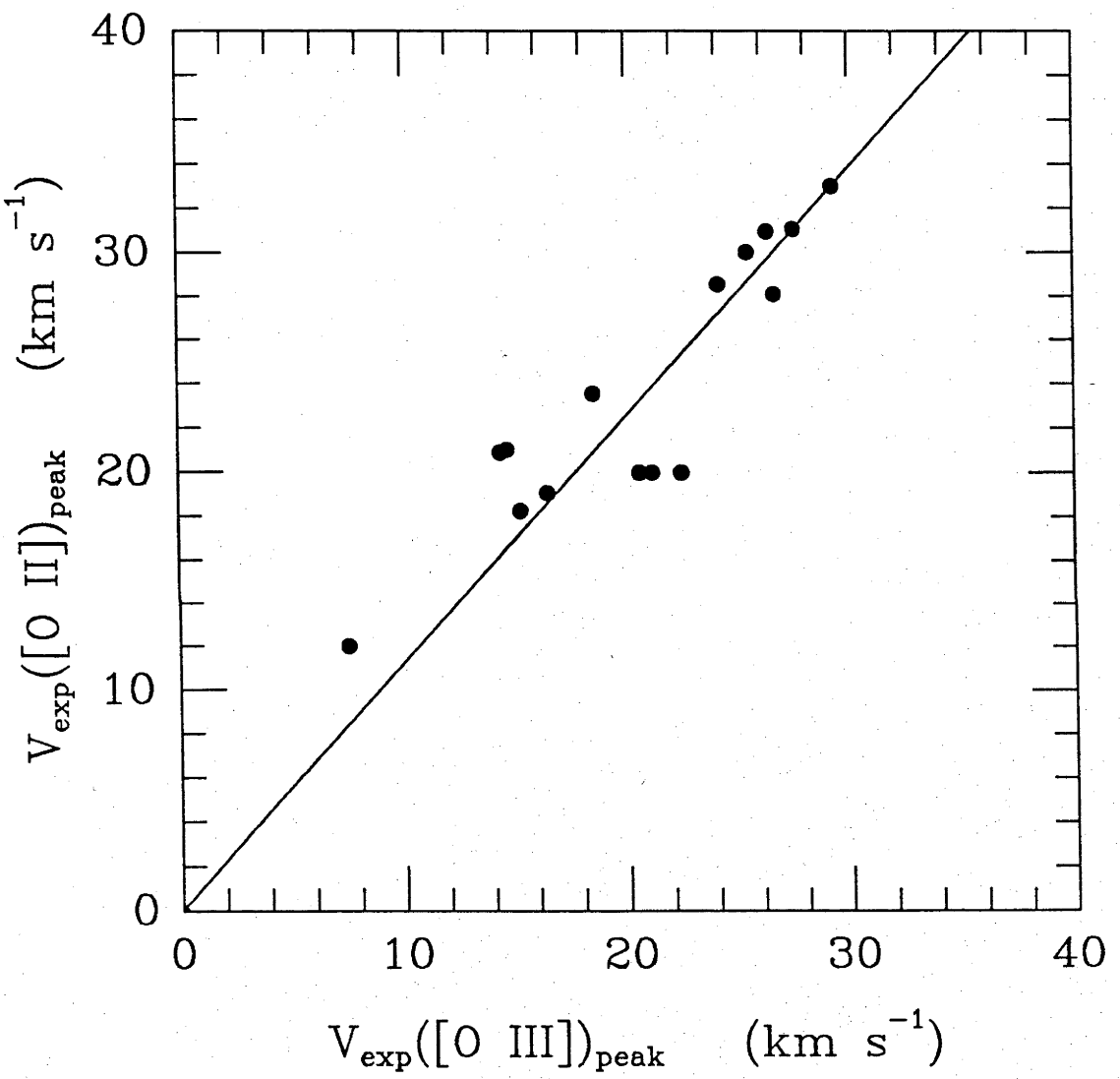
40
30
20
10
0
0
10
20
30
40
$V_{exp}([O\ II])_{peak}$ (km s^{-1})
$V_{exp}([O\ III])_{peak}$ (km s^{-1})

TABLE 2

EXPANSION VELOCITIES

Object Name	$2V_{exp}$ (km s^{-1}) [O III]	[O II]	He II
NGC2022	42.5	...	48.7
NGC2346	< 12.0	< 12.0	...
NGC2438	44.9	40.0	29.5
NGC2440	58.6	66.0	36.2
NGC2452	63.5	...	53.8
NGC2610	27.8	...	< 20.0
NGC2792	39.0	...	23.0
NGC2818	42.3	40.0	< 20.0
NGC2867	37.1	47.1	33.3
NGC2899	64.1	...	...
NGC3132	29.4	42.0	...
NGC3195	50.9	60.0	< 12.0
NGC3211	52.7	61.9	42.1
NGC3699	53.3	56.2	48.1
NGC3918	48.3	57.1	< 20.0
NGC4071	28.2	...	...
NGC4361	51.5	...	33.9
NGC5307	21.6	...	< 12.0
NGC6026	49.1	...	41.2
NGC6072	< 12.0	19.8	< 12.0
NGC6153	44.1	...	33.0
NGC6326	33.0	32.1	26.6
NGC6337	15.6	...	< 12.0
NGC6369	83.3	...	...
NGC6537	36.0	...	20.5
NGC6565	28.8	41.8	16.6
NGC6629	< 12.0	13.3	...
NGC6772	20.4	...	...
NGC6818	55.1	59.1	41.9
NGC6852	86.3	...	< 12.0
NGC7009	41.2	40.0	34.6
A44	12.0	...	...

TABLE 2 (continued)

EXPANSION VELOCITIES

Object Name	$2V_{exp}$ (km s^{-1}) [O III]	[O II]	He II
A51	84.0	...	...
A65	21.6	...	...
A70	75.5	...	...
ESO 259–10...	24.0	...	...
Fg 1	28.8	...	< 20.0
He 2–7	30.6	36.5	< 12.0
He 2–29	47.3	...	42.1
He 2–37	61.4	...	57.0
He 2–51	< 20.0	...	...
He 2–82	40.0	...	...
He 2–103	< 12.0	...	...
He 2–111	24.0	...	23.7
He 2–114	15.0	24.0	...
He 2–120	13.8	...	...
He 2–146	< 12.0	...	...
He 2–165	14.6	...	...
He 2–198	53.9	...	...
Hf 4	< 20.0	...	...
Hf 38	< 12.0	...	...
IC418	< 12.0	< 12.0	...
IC4406	< 12.0	28.3	< 12.0
IC4642	69.2	...	56.2
IC4673	49.7	...	28.8
IC5148–50	106.7	...	...
M 1–42	15.0	< 12.0	25.0
M 1–46	13.8	...	...
M 3–39	50.0	...	...
Mz 1	< 12.0	< 12.0	< 12.0
Mz 2	36.0	...	26.9
Skwl 3–2	31.2	...	...
Sp 1	58.7	...	48.0
Th 2–A	35.0	...	...

c) Nebular Densities

Use of the [O II] $\lambda\lambda 3727, 3729$ doublet as a probe of nebular electronic density (n_e) was established by Seaton and Osterbrock (1967). Barlow (1987) has recently confirmed the [O II] doublet ratio to be an excellent density indicator. For the expected range of nebular temperatures found in most planetary nebulae the ratio of these lines is only a weak function of temperature. At densities greater than about 15000 cm^{-3} and less than 200 cm^{-3} the I(3729)/I(3727) ratio tends to finite limits, and uncertainties in the measurement of the ratio lead to successively larger errors in the density. Fortunately, the majority of PN have densities within this range. Figure 4 shows I(3729)/I(3727) as a function of the electronic density for nebular temperatures of 10000 and 20000 °K, as calculated from five level atomic models using the collision strengths of Pradhan (1976) together with the transition probabilities of Zeippen (1982).

The densities derived from the [O II] profiles are given in Table 3. One possible criticism of our densities is that they may not be representative of the mean [O II] density throughout the nebula. However, as the spectrograph slit was positioned along the major axis it is hoped that a reasonable mean value has been obtained. Comparing our densities with published [O II] densities we find very good agreement. Where published values differ wildly we generally find our density agrees with one of the published values. On the whole our [O II] densities differ by $< 15\%$ from the mean values given by all other authors.

Figure 4. Ratio of the density sensitive [O II] $\lambda\lambda 3727, 3729$ lines as a function of nebular electronic density, for electronic temperatures of 10000°K and 20000°K.

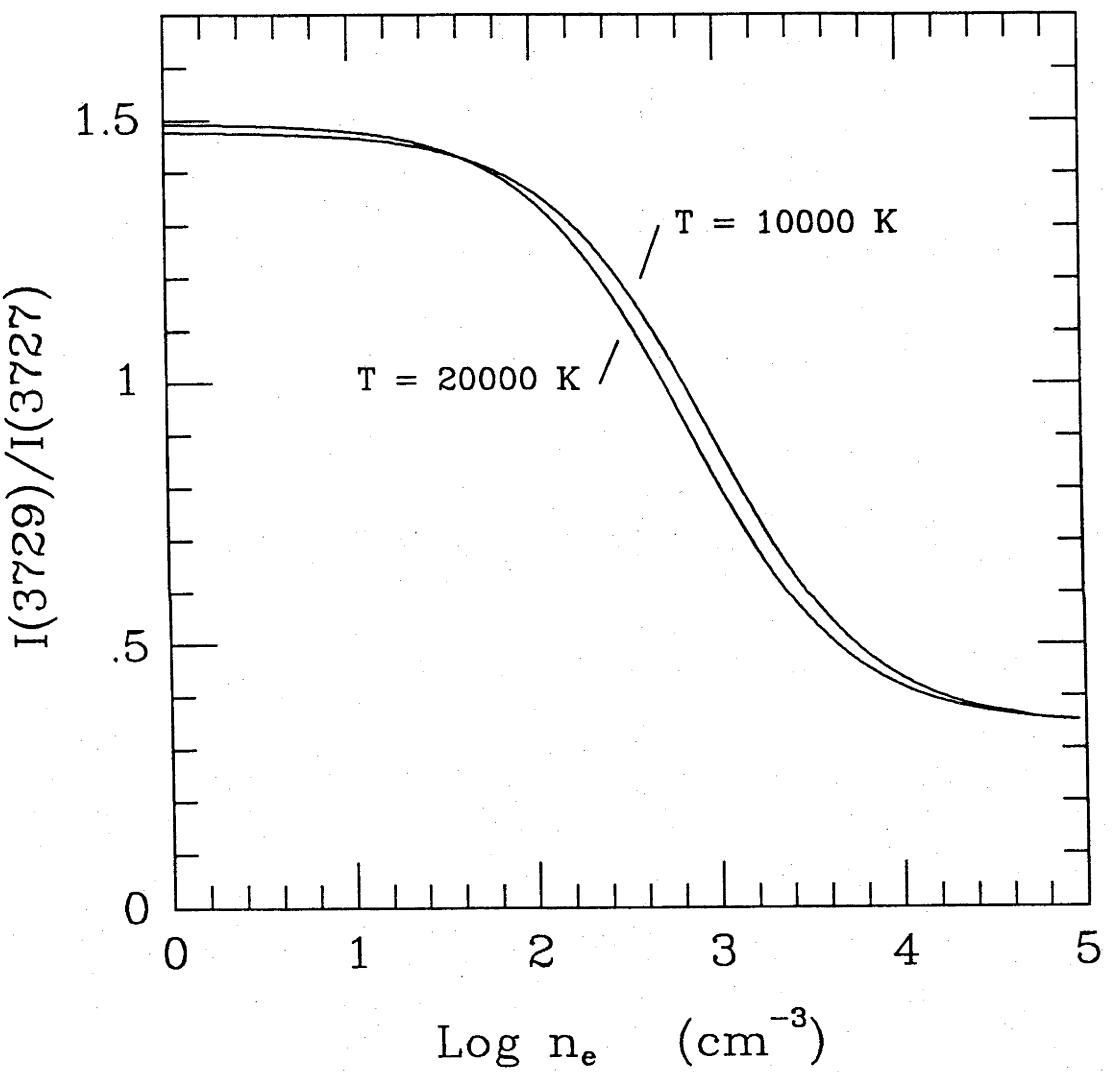
1.5
1
.5
0
0
1
2
3
4
5
I(3729)/I(3727)
Log n_e (cm^{-3})
T = 10000 K
T = 20000 K

TABLE 3

NEBULAR DENSITIES

Object Name	n_e (cm^{-3})	Object Name	n_e (cm^{-3})
NGC2346	450	NGG6326	2300
NGC2438	300	NGC6565	1550
NGC2440	1900	NGC6629	3500
NGC2818	450	NGC6818	3600
NGC2867	2200	NGC7009	5200
NGC3132	600	He 2–7	800
NGC3195	550	He 2–114	200
NGC3211	850	IC418	16000
NGC3699	200	IC4406	500
NGC3918	3200	M 1–42	750
NGC6072	220	Mz 1	400
NGC6153	1450		

IV. DISTANCES AND NEBULAR RADII

Dopita *et al.* (1988), using a sample of 43 planetary nebulae in the Large and Small Magellanic Clouds, found that their objects fell in a plane in the dynamical age / density / excitation class space defined by :

$$\log \tau_{dyn} = (4.70 \pm 0.23) + (0.0375 \pm 0.0106)E - (0.441 \pm 0.055) \log n_e$$

where E is the excitation class of the nebula and $\tau_{dyn} = R_{neb}/V_{exp}$ the dynamical age of the nebula. In this section we derive distances to individual Galactic nebulae using the above relation to determine τ_{dyn} from the observed electronic densities (n_e) and excitation classes (E); the radius is then given by $R_{neb} = V_{exp}\tau_{dyn}$, and the distance follows from the observed angular radius.

Electronic density values are taken from this paper as well as previous authors (Aller and Czyzak 1979, 1983; Kaler 1970, 1979; Martin 1981; Barker 1978; Amnuel *et al.* 1984). The idea of assigning excitation classes to planetary nebulae was first proposed and used by Feast (1968), and has since been enlarged upon by Webster (1975) and Morgan (1984). We have used Morgan's scheme together with line intensities published by Kaler (1976) to determine excitation classes for as many of our nebulae as possible. Using these data dynamical ages were calculated for a total of 33 nebulae in the sample. These ages, together with the excitation classes and densities, are listed in Table 4. The density for NGC2899 is from the [S II] $\lambda\lambda 6717, 6730$ ratio as no [O II] density has been published.

TABLE 4

DISTANCES, RADII AND MASSES

Object Name	Excitation Class	n_e (cm^{-3})	τ_{dyn} (yr)	R (pc)	r (")	D (pc)	M_{neb} ($\mathcal{M}_\odot$)
NGC2022	7	1450	3700	0.146	11.0	2740	0.126
NGC2346	7	450	6200	0.101	27.3	760	0.039
NGC2438	6	300	6800	0.264	35.2	1550	0.714
NGC2440	8	1900	3580	0.153	21.7	1450	0.907
NGC2452	7	1900	3290	0.168	11.0	3150	0.175
NGC2610	4	300	5720	0.233	19.5	2460	0.464
NGC2792	6	2040	2920	0.108	10.0	2230	0.377
NGC2818	8	470	6630	0.262	24.6	2200	0.238
NGC2867	6	2340	2750	0.103	9.6	2210	0.333
NGC2899	7	760	4920	0.218	45.0	1000	0.313
NGC3132	5	620	4530	0.125	28.0	920	0.015
NGC3195	2	400	4240	0.174	19.7	1830	0.086
NGC3211	8	870	5050	0.219	14.0	3220	1.907
NGC3699	6	200	8130	0.398	34.0	2410	0.497
NGC3918	6	3200	2390	0.100	9.4	2180	0.413
NGC4361	8	300	8080	0.318	57.0	1150	0.596
NGC5307	5	1480	3360	0.074	6.5	2340	0.059
NGC6153	4	1450	2860	0.096	12.5	1570	0.027
NGC6326	6	2300	2770	0.094	6.8	2840	0.250
NGC6369	5	4350	1780	0.108	14.5	1540	0.547
NGC6537	9	11300	1780	0.050	5.0	2040	0.175
NGC6565	5	1550	3340	0.093	5.1	3760	0.084
NGC6629	4	3500	2110	0.058	7.5	1580	0.089
NGC6772	6	230	7650	0.204	34.0	1240	0.078
NGC6818	8	3600	2700	0.121	11.0	2260	0.159
NGC7009	4	5760	1690	0.059	15.0	810	0.047
He 2–7	4	800	4050	0.120	13.0	1900	0.182
He 2–114	5	200	7460	0.239	15.0	3290	0.362
He 2–146	1	980	2620	0.063	10.0	1290	0.032
IC418	0	21900	610	0.013	6.2	440	0.002
IC4406	5	550	4780	0.148	17.3	1730	0.163
M 1–42	6	750	4540	0.080	4.0	4120	0.051
Mz 1	6	400	5990	0.180	15.0	2470	0.306

The nebular radii listed in column 5 are determined from the [O III] expansion velocity and dynamical age. It should be noted that the expansion velocities used here are not the peak to peak velocities, but are those corresponding to the Dopita *et al.* (1985) definition, and as such are systematically higher than the peak to peak values given in Table 2. Dopita *et al.* (1985, 1988) observed a large sample of PN in the Magellanic Clouds adopting a different definition of expansion velocity as very few Magellanic Cloud objects show split profiles, because the nebulae are unresolved and only bi-polar nebulae are expected to give rise to multi-component profiles. They noted that the true velocity of expansion can only be measured from half the full width at zero intensity, but such a measurement introduces too much uncertainty due to a low signal to noise in the profile wings. So they settled for a compromise measuring the half width at 10% maximum intensity. By looking at a variety of geometries and determining resultant profile shapes the 10% level was found to give a good approximation to the maximum expansion velocity for spherical shell as well as those bi-polar nebulae. It is not possible to relate their Magellanic Cloud definition directly to the more usual Galactic peak-to-peak velocities in a simple way as the exact relationship will differ for various geometries. However, in the case of a spherical shell the Magellanic Cloud definition is virtually equivalent to measuring half the full width at half maximum. We have remeasured our Galactic profiles at levels as close as possible to the Magellanic Cloud 10% definition in order to use the Dopita *et al.* formulation directly.

Nebular angular radii are given in column 6 and have been taken from the Perek and Kohoutek (1967) catalogue. For those nebulae not

appearing roughly circularly symmetric, the dimension most appropriate to the position angle for the observation was used. These angular radii agree closely with values used by other authors. Distances to the nebulae as computed from our method are given in column 7 of Table 4.

The agreement between our distances and those calculated by other authors is quite good. Figure 5 is a comparison of our distances and those obtained by Daub (1982). Named nebulae in the figure are those for which the two distances do not agree well, and possible causes are discussed below. Excluding those few nebulae for which we have reason to believe one of the distances is in error, our distances are on average, 1.07 times larger than Daub's, with a correlation coefficient of 0.95. The ratio of our distance scale to that of Maciel (1984) is 1.00 with a correlation coefficient of 0.85 (Figure 6), if we once again exclude the few nebulae which we believe to have one incorrect distance determination.

We may also compare our distances with those derived by Cahn and Kaler (1971) using the Shklovsky method. The agreement is also very good; using all 22 objects in common the Cahn and Kaler scale is found to be only some 15% bigger than ours (Figure 7). However, as the Shklovsky method relies on the assumption of constant nebular ionized mass and this has now been found to vary of several orders of magnitude, for optically thick nebulae, then distances to such nebulae will have been overestimated by Cahn and Kaler. Meatheringham *et al.* (1988b) and Barlow (1987) have recently found that Magellanic Cloud PN appear to become optically thin at densities less than about $5000-6000$ cm^{-3}. There are only three objects in this study with densities greater than 5000 cm^{-3} (NGC6537, NGC7009, IC418), and the Cahn and Kaler distances for them are between 1.6 and

Figure 5. A comparison of our distance scale with that of Daub (1982). The dashed line is a line of slope unity for comparison. Named nebulae are discussed in the text.

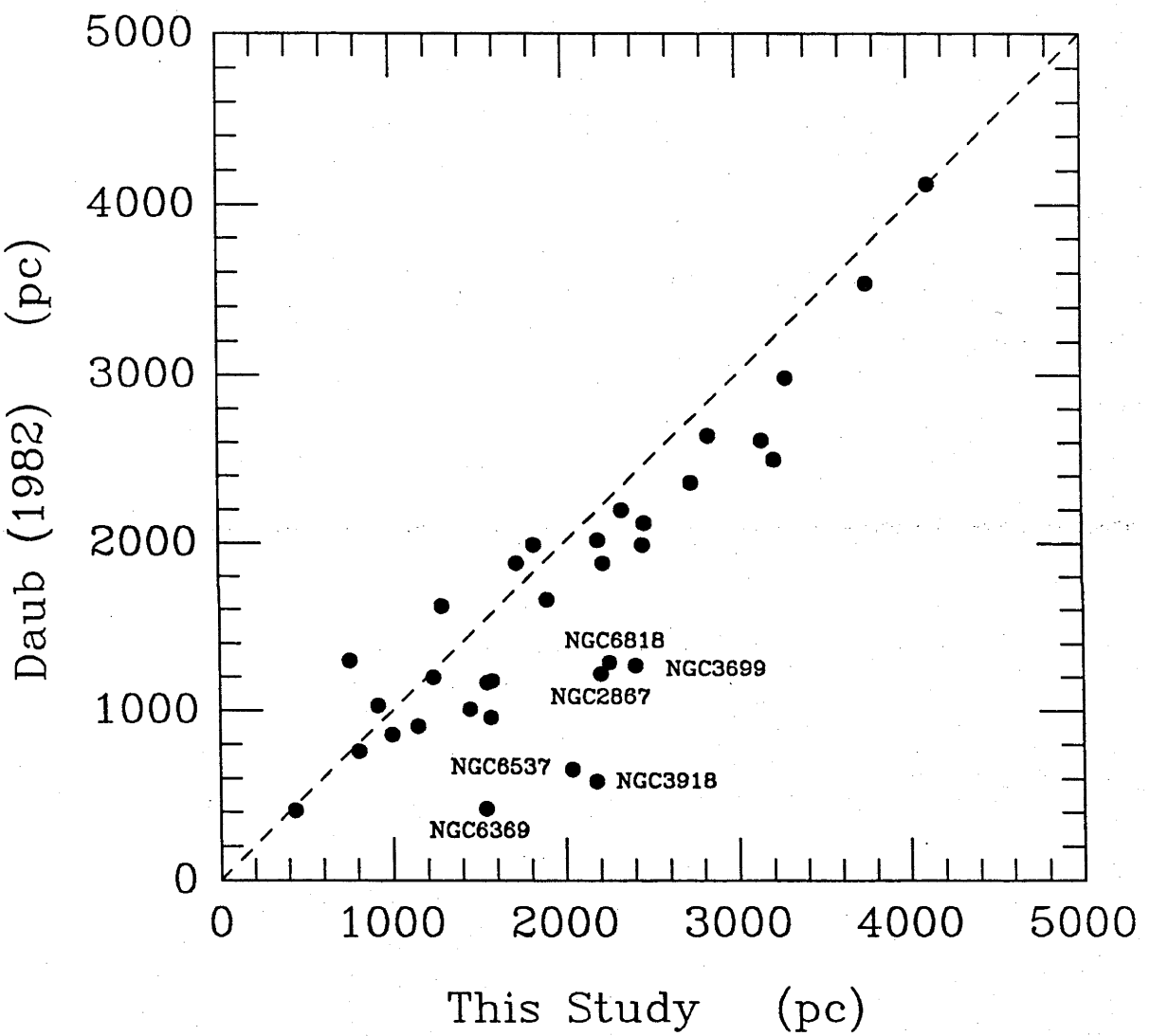
5000
4000
3000
2000
1000
0
Daub (1982) (pc)
0
1000
2000
3000
4000
5000
This Study (pc)
NGC6818
NGC3699
NGC2867
NGC6537
NGC3918
NGC6369

Figure 6. A comparison of our distance scale with that of Maciel (1984). The dashed line is a line of slope unity for comparison. Named nebulae are discussed in the text.

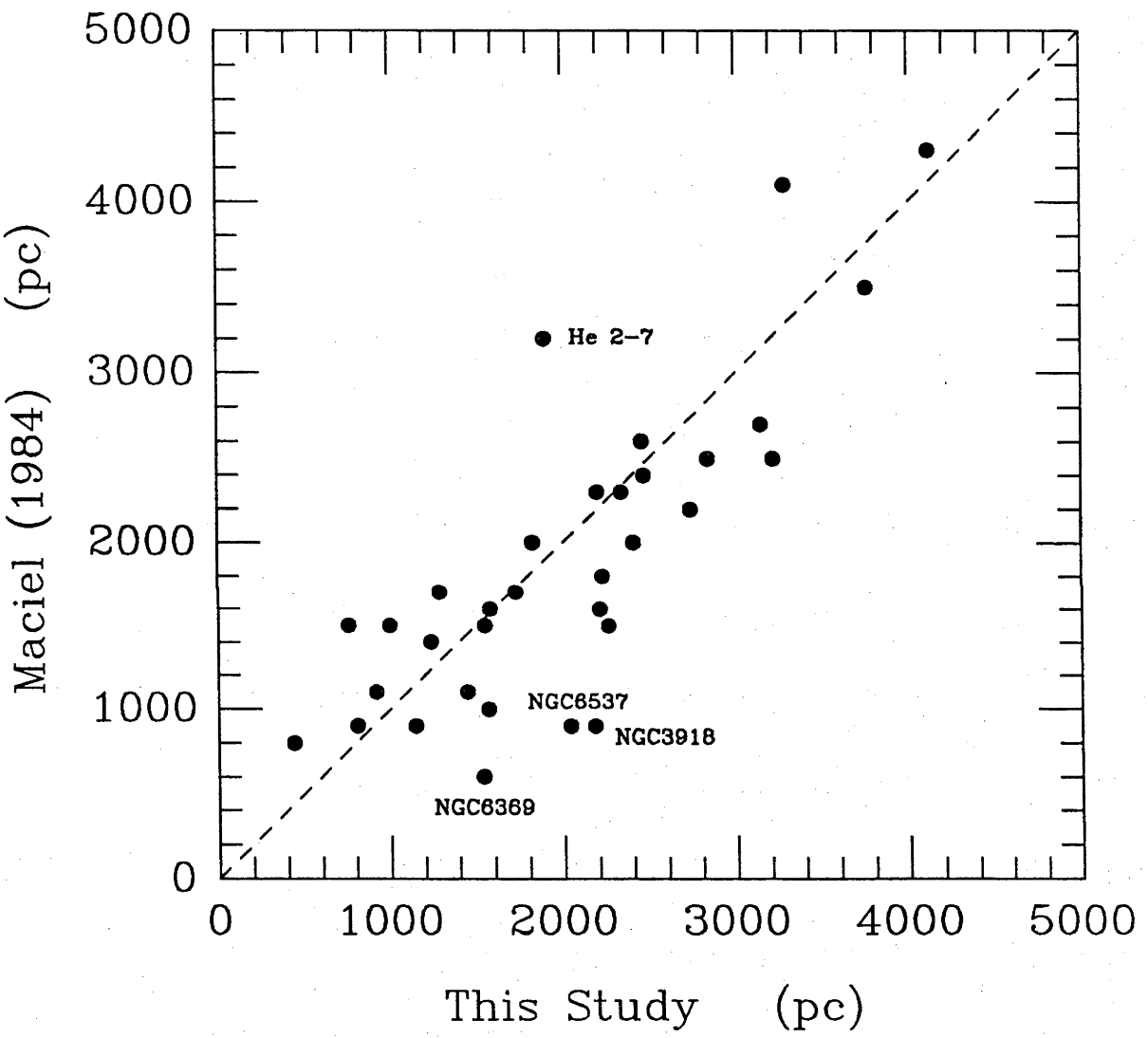
5000
4000
3000
2000
1000
0
0
1000
2000
3000
4000
5000
Maciel (1984) (pc)
This Study (pc)
He 2-7
NGC6537
NGC3918
NGC6369

Figure 7. A comparison of our distance scale with that of Cahn and Kaler (1971). The three named nebulae are believed to be optically thick. The dashed line is a line of slope unity for comparison.

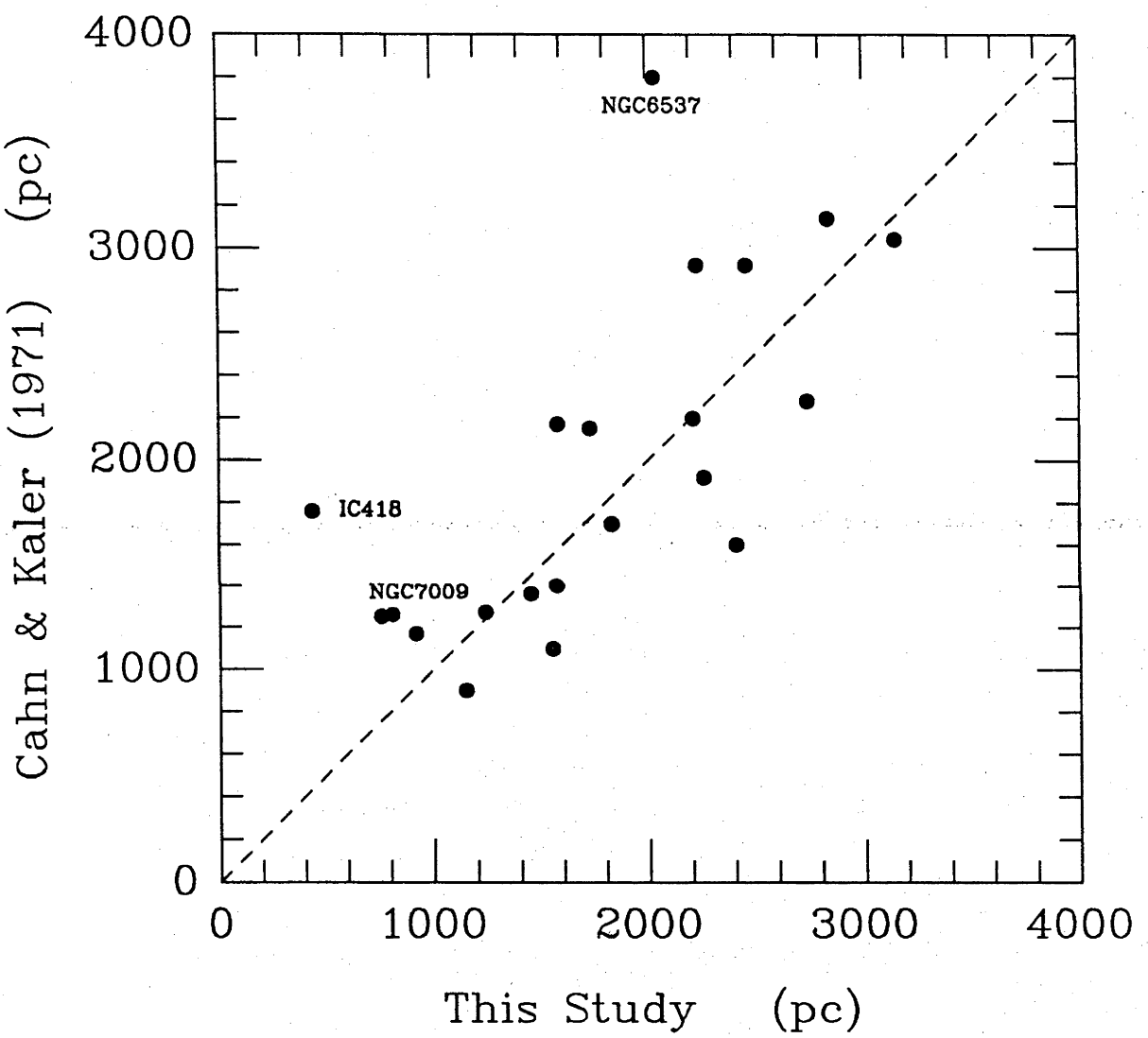
4000
3000
2000
1000
0
0
1000
2000
3000
4000
Cahn & Kaler (1971) (pc)
This Study (pc)
NGC6537
IC418
NGC7009

4 times larger than what we find. So, indeed their distances seem to be to too large for optically thick nebulae. Neglecting these three objects the ratio of the two scales is then reduced to 0.95.

This leads us to conclude that the method proposed by Dopita *et al.* (1988) using the Magellanic Cloud nebulae is a valid one for determining Galactic PN distances. However, there are a few nebulae which deserve special comment and these are :

NGC2440 : Gathier (1986a) finds a distance of 1.92 kpc (angular radius of 16 arcsec), Daub gives 1.17 kpc (angular radius of 27 arcsec), and we find 1.45 kpc (angular radius 21.7 arcsec). It is interesting to note that all these distances would be virtually the same if the one angular radius was used.

NGC2867: Our distance to this nebula (2.21 kpc) is appreciable larger than Daub's (1.22 kpc), and also larger than Maciel (1.60 kpc). However, Phillips and Pottasch (1984) using radio continuum fluxes derived a distance of 2.64 kpc, Gathier *et al.* (1986a) find the nebula to be at a distance of > 2 kpc, and others also find about 2.2 kpc (eg. O'Dell 1962; Milne and Aller 1975; Cahn 1976).

NGC3699 : Although almost twice the distance given by Daub, our value is in reasonable agreement with Maciel.

NGC3918 : Our distance of 2.18 kpc is much larger than either Daub or Maciel. However, it agrees excellently with the reddening distance of Gathier *et al.* (1986a) of 2.24 ± 0.84 kpc.

NGC6369 : Our distance of 1.54 kpc is consistent with the H I absorption

distance of Gathier *et al.* (1986b), but much larger than Daub and Maciel.

NGC6537 : This object is similar to the above two, in that our distance of 2.04 kpc disagrees with Daub and Maciel but agrees well with the H I absorption distance of 2.4 ± 0.6 kpc (Gathier *et al.* 1986b).

NGC6565 : This nebula's distance is the reverse of the above few objects, in that it agrees well with Daub and Maciel, but the reddening distance is very much smaller.

NGC6818 : Our value is in good agreement with Maciel but at odds with that given by Daub.

He 2-7 : Maciel determines a distance almost twice what we find, however, this comes about due to his using an angular size just on half of what we find.

V. NEBULAR MASSES

The ionized mass is an important nebular quantity in that it allows an investigation of possible mass–radius relations and gives information on the optical thickness / thinness of the nebula. We have used the following formula as given by Gathier (1986) to determine ionized masses for the 33 nebulae in our sample :

$$M_{neb}/\mathcal{M}_{\odot} = 1.18 \times 10^{-8} n_e D^3 \theta^3 \epsilon \left(\frac{1+4y}{1+y+xy} \right) \qquad (1)$$

with n_e in cm^{-3}, D in kpc and θ in seconds of arc. Values of the Helium

abundance y = N(He)/N(H) have been determined for many Galactic planetary nebulae and we have taken our values from Aller and Czyzak (1979), and Kaler (1970, 1979). Where no abundance was available we have assumed an average figure of $y = 0.12$. The fraction of doubly ionized Helium (x) was taken from the same literature, and where no value existed an average of $x = 0.33$ was assumed. The error in the derived mass that these assumptions introduce is relatively small considering the scatter in published values, and will amount to less than 15%. Together with our adopted densities and distances we have calculated ionized masses for the nebulae in our sample (column 8 of Table 5).

We avoided using an equation relying on the nebular Hβ flux, as many flux determinations are quite old and were done using aperture photometry. Where two or more values exist for the one nebula these often differ very significantly, and this introduces the possibility that some of the apertures were insufficiently large to measure the whole flux. This, together with uncertain reddening corrections may cause the nebular masses to be underestimated by a large amount.

Our masses compare favourably with those published by Pottasch (1980) and Gathier (1986) for the objects in common. Much of the difference in mass being due simply to different adopted distances. We may also compare the masses derived by Phillips and Pottasch (1984) (hereinafter PP) using radio continuum fluxes with our sample. The masses are, on the whole, quite different. However, the distances PP derived are often completely different to those that we find, and which other authors quote. An extreme example being IC418; PP give a distance of 5740 pc, we find 440 pc, Daub gives 412 pc, Maciel 800 pc and Gathier (1986) 580 ± 250

pc. This difference in distance is enough to account for the extremely high ionized mass ($2.04\mathcal{M}_{\odot}$) that PP give for IC418, compared to the value we find ($1.6 \times 10^{-3}\mathcal{M}_{\odot}$). Similarly for the other nebulae in common between PP and ourselves, the difference in mass can be mainly attributed to the different distance estimates.

Figure 8 is a plot of nebular radius versus ionized mass. There seems to be a general increase in ionized mass with radius, up to about $R \sim 0.2$ pc, but we have very few points with radii less than 0.06 pc. Also shown is the area occupied by PN with well-known distances, either in the Magellanic Clouds (Wood *et al.* 1987), or in the Galactic Centre (Gathier *et al.* 1983). It is clear that there is good agreement between the masses found for our objects and those determined for other PN whose distances are well known. The ionized masses range from $1.6 \times 10^{-3}\mathcal{M}_{\odot}$ up to a limit of between $0.4 - 0.6\mathcal{M}_{\odot}$. This large range in ionized mass of ~ 300 is real and cannot be attributed to errors in distance or other nebular quantities.

Figure 9 is a plot of the relationship between nebular radius and density. Barlow (1987) and Meatheringham *et al.* (1988b) found that Magellanic Cloud PN become optically thin to Hydrogen ionizing radiation at densities $n_e < 5000 - 6000$ cm^{-3}. As most of the nebulae in our sample have $n_e < 5000$ cm^{-3} it is instructive to see if the Galactic PN share this. A linear least squares fit through those objects is shown in Figure 9, and the slope is such that $n_e \propto R^{-2.8}$. This is consistent with constant nebular mass ($n_e \propto R^{-3}$) below this limiting density. Optically thin nebulae are believed to be evolving at approximately constant nebular mass and hence the Galactic PN we have looked at seem to become optically thin at similar densities to the Magellanic Cloud population.

Figure 8. Relationship between the nebular radius and ionzised mass as derived in this paper. The boxed area delineates the region occupied by Planetary Nebulae in the Magellanic Clouds (Wood *et al.* 1987), and in the Galactic Centre (Gathier *et al.* 1983).

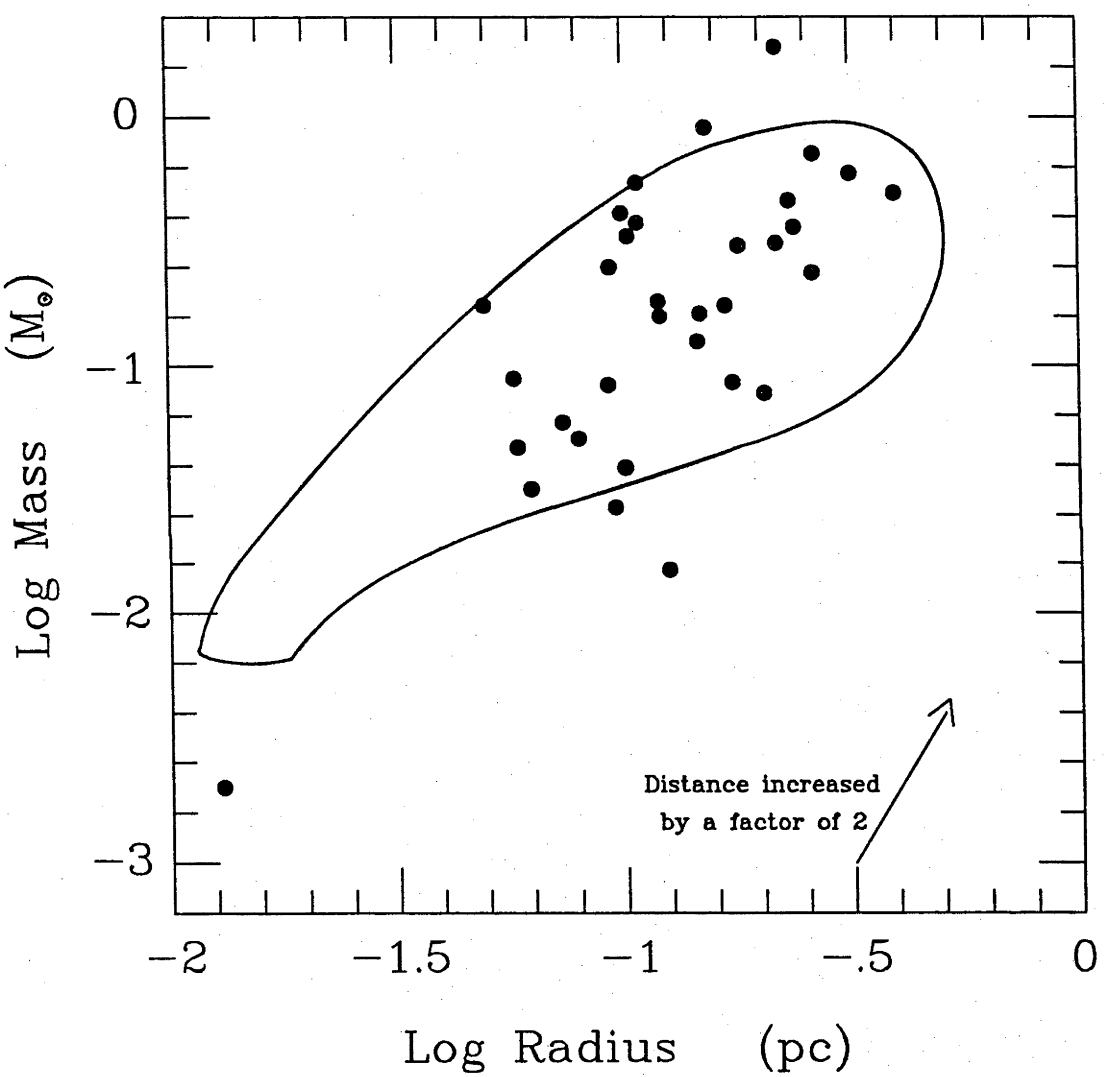
0
−1
−2
−3
Log Mass (M⊙)
−2
−1.5
−1
−.5
0
Log Radius (pc)
Distance increased
by a factor of 2

Figure 9. The correlation between nebular radius and density ($n_e <$ 5000 cm^{-3}), is such that $n_e \propto \mathrm{R}^{-2.8}$ which is very similar to what one would expect if the nebulae were evolving at constant nebular mass ($n_e \propto \mathrm{R}^{-3}$).

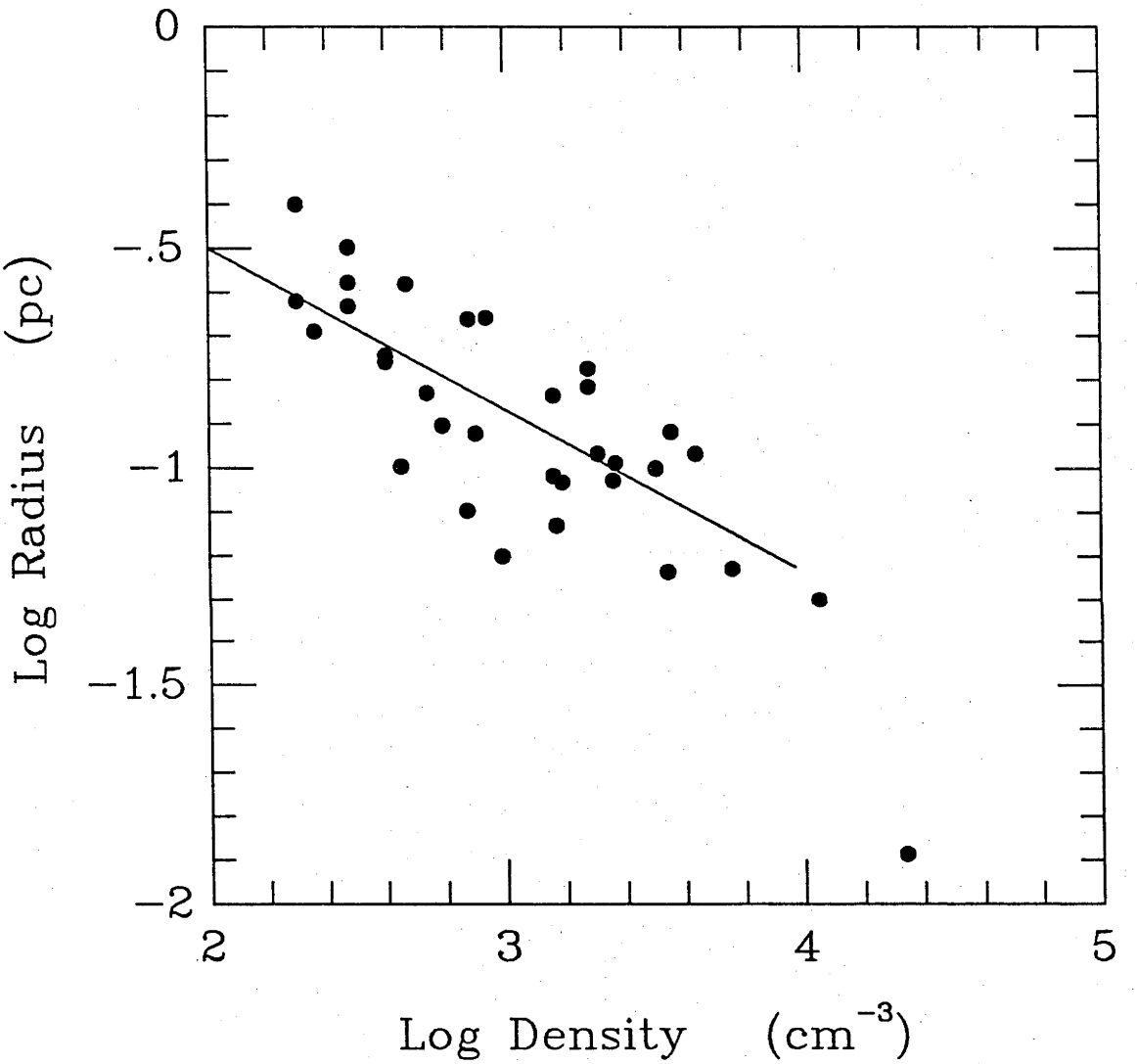
0
−.5
−1
−1.5
−2
2
3
4
5
Log Radius (pc)
Log Density (cm^{-3})

Figure 10 also serves to show that the nebulae are becoming optically thin at $n_e < 5000$ cm^{-3}. Although there is a large amount of scatter there does not seem to be any appreciable increase in ionized mass to densities less than this value. This contrasts with Pottasch (1980) who found that Galactic PN were ionization bounded to densities below 1000 cm^{-3}. Gathier (1986) plots the same diagram as our Figure 10 and reaches the same conclusion as Pottasch. However, from his figure it would appear that there is very little increase in nebular mass to densities below $n_e < 4000 - 5000$ cm^{-3}, this being in agreement with our findings.

VI. SUMMARY

We have determined radial velocities for a sample of 64 southern planetary nebulae. Expansion velocities have also been measured for these nebulae. Nebular electronic densities were derived from the [O II] $\lambda\lambda 3727, 3729$ doublet for a subset of 23 of the objects. Using a recently published correlation between density and other nebular parameters, together with published data we have measured distances to 33 of the nebulae. These distances are found to agree well with previously published values, based on the distance scales of Daub and Maciel. Using these distances we were then able to calculate the nebular ionized masses for the nebulae. The large range in ionized mass confirms again that the Shklovsky method is inappropriate for distance determinations to optically thick nebulae. This is seen directly in our sample were Cahn and Kaler found distances much larger than us to three optically thick nebulae.

Figure 10. Relation between the nebular density and ionzied mass. The majority of objects have $\log n_e < 3.6$, and as such are expected to be optically thin. There appears to be no significant increase in ionized mass at densities less than the limiting value.

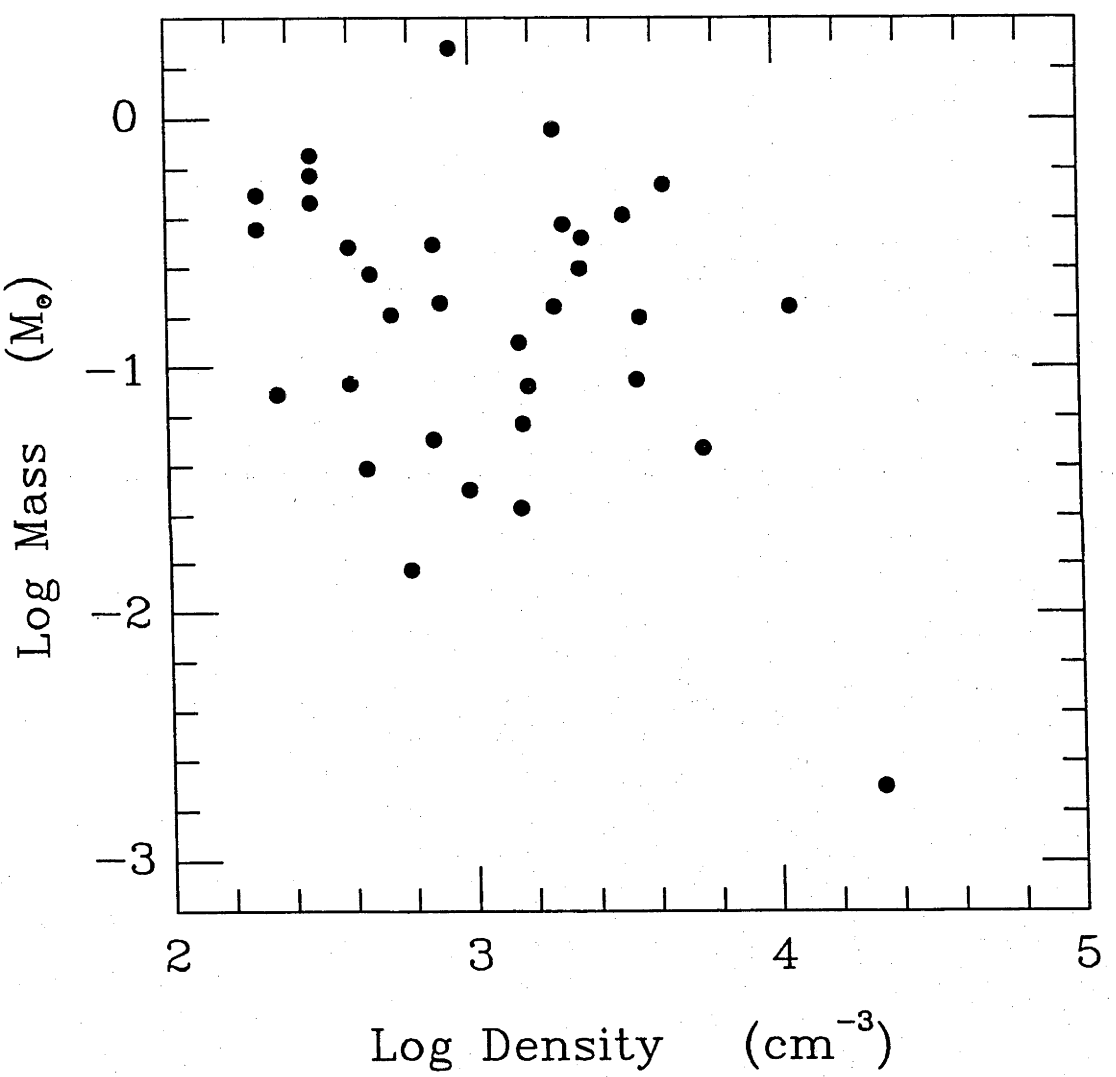
0
−1
−2
−3
2
3
4
5
Log Mass (M⊙)
Log Density (cm^{-3})

Evolutionary correlations between nebular parameters have been examined, and lead to the conclusion that the transition from being optically thick to thin occurs at densities considerably greater than previous work has suggested, and that the optically thin nebulae evolve at an approximately constant nebular mass.

REFERENCES

Aller, L.H., and Czyzak, S.J. 1979, *Ap. Space Sci.*, **62**, 397.

Aller, L.H., and Czyzak, S.J. 1983, *Ap. J. Suppl.*, **51**, 211.

Amnuel, P.R., Guseinov, O.H., Novruzova, H.I., and Rustamov, Yu.S., 1984, *Ap. Space Sci.*, **107**, 19.

Barker, T. 1978, *Ap. J.*, **219**, 914.

Barlow, M. 1987, *M.N.R.A.S.*, **227**, 161.

Bevington, P.R. 1969, *"Data Reduction and Error Analysis for the Physical Sciences"*.

Cahn, J.H. 1976, *Astron. J.*, **81**, 407.

Cahn, J.H. and Kaler, J.B. 1971, *Ap. J. Suppl.*, **22**, 319.

Chu, Y-H, Kwitter, K.B., Kaler, J.B. and Jacoby, G.H. 1984, *Pub. A.S.P.*, **96**, 598.

Daub, C.T. 1982, *Ap. J.*, **260**, 612.

Dopita, M.A., Ford, H.C., Lawrence, C.J. and Webster, B.L. 1985, *Ap. J.*, **296**, 390.

Dopita, M.A., Meatheringham, S.J., Wood, P.R., Ford, H.C., Webster, B.L., and Morgan, D.H. 1987a, *Ap. J. (Letters)*, **315**, L107.

Dopita, M.A., Meatheringham, S.J., Ford, H.C., and Webster, B.L. 1988, *Ap. J.*, in press (April 15).

Feast, M.W. 1968, *M.N.R.A.S.*, **140**, 345.

Gathier, R. 1986, ESO preprint, number 474.

Gathier, R., Pottasch, S.R., and Pel, J.W. 1986a, *Astr. Ap.*, **157**, 171.

Gathier, R., Pottasch, S.R., and Goss, W.M. 1986b, *Astr. Ap.*, **157**, 191.

Kaler, J.B. 1970, *Ap. J.*, **160**, 887.

Kaler, J.B. 1976, *Ap. J. Suppl.*, **31**, 517.

Kaler, J.B. 1979, *Ap. J.*, **228**, 163.

Maciel, W.J. 1984, *Astr. Ap. Suppl.*, **55**, 253.

Maciel, W.J., and Pottasch, S.R. 1980, *Astr. Ap.*, **88**, 1.

Martin, W. 1981, *Astr. Ap.*, **98**, 328.

Meatheringham, S.J., Dopita, M.A., Ford, H.C., and Webster, B.L. 1988a, *Ap. J.*, in press (April 15).

Meatheringham, S.J., Dopita, M.A., and Morgan, D.H. 1988b, *Ap. J.*, in press (June 1).

Milne, D.K., and Aller, L.H. 1975, *Astr. Ap.*, **38**, 183.

Morgan, D.H. 1984, *M.N.R.A.S.*, **208**, 633.

O'Dell, C.R. 1962, *Ap. J.*, **135**, 371.

Osterbrock, D.E. 1974, *"Astrophysics of Gaseous Nebulae"* (San Francisco : Freeman).

Osterbrock, D.E., Miller, J.S. and Weedman, D.W. 1966, *Ap. J.*, **145**, 697.

Perek. L. and Kohoutek, L. 1967, *"Catalog of Galactic Planetary" Nebulae"* (Prague : Czechoslovakian Acad. of Sci.).

Phillips, J.P. 1984, *Astr. Ap.*, **137**, 92.

Phillips, J.P., and Pottasch, S.R. 1984, *Astr. Ap.*, **130**, 91.

Pottasch, S.R. 1980, *Astr. Ap.*, **89**, 336.

Pradhan, A.K. 1976, *M.N.R.A.S.*, **177**, 31.

Robinson, G.J., Reay, N.K. and Atherton, P.D. 1982, **199**, 649.

Sabbadin, F. 1984, *Astr. Ap. Suppl.*, **58**, 273.

Sabbadin, F., Gratton, R.G., Bianchini, A. and Ortolani, S. 1984, *Astr. Ap.*, **136**, 200.

Sabbadin, F., Strafella, F., and Bianchini, A. 1986, *Astr. Ap. Suppl.*, **65**, 259.

Schneider, S.E., Terzian, Y., Purgathofer, A. and Perinotto, M. 1983,

Ap. J. Suppl., **52**, 399.

Seaton, M.J., and Osterbrock D.E. 1967, *Ap. J.*, **125**, 66.

Shklovsky, I.S. 1956, Astr. Zh., **33**, 222,315.

Stapinski, T.E., Rodgers, A.W and Ellis, M.J. 1984, *Pub. A.S.P.*, **93**, 242.

Webster, B.L. 1975, *M.N.R.A.S.*, **173**, 437.

Weedman, D.W. 1968, *Ap. J.*, **153**, 49.

Wilson, O.C. 1950, *Ap. J.*, **111**, 279.

Wood, P.R., Meatheringham, S.J., Dopita, M.A., and Morgan, D.H. 1987, *Ap. J.*, **320**, 178.

Zeippen, C.J. 1982, *M.N.R.A.S.*, **198**, 111.

DISCUSSION AND CONCLUSIONS

This dissertation has presented a study of the kinematics of the planetary nebula (PN) population in the Large Magellanic Cloud (LMC). It has determined evolutionary relationships between various observable nebular parameters from a large sample of nebulae in both the Large and Small Clouds, and shown the basis for a possible solution to the distance scale problem for Galactic PN. Finally, new data is given for a sample of southern Galactic nebulae. The detailed results of this study are discussed in each of the five papers that comprise this thesis and will not be repeated here at length. However, the major contributions of this work are summarized below, together with indications of areas which will profit from further research.

Radial velocities for a total of 97 PN in the LMC have been measured. Using these data the kinematics of the PN an old population in the LMC have been analyzed, by a comparison with the young H I. To do this the extensive H I survey of the LMC due to Rohlfs *et al.* (1984) was examined. The large angular diameter and transverse velocity of the LMC ensure a substantial velocity gradient in the direction of motion. The best solution found for this transverse velocity is 275 ± 65 km s^{-1}, in agreement with previously assumed values. Once the effects of this velocity gradient have been subtracted from the H I velocity data a rotation curve can be obtained. Due to the bar of the LMC a pure exponential disk is not a good fit to the rotation curve. A better fit is obtained in the inner region if solid body rotation is assumed, with an exponential disk outside that. If the exponential disk continues out to a radius of 6 degrees then a mass of $6 \times 10^9 \mathcal{M}_\odot$ is implied. This value is consistent with that obtained in a

study by Feitzinger (1979). The method used by Freeman *et al.* (1983) to study the old clusters in the LMC has been adopted to analyze the PN radial velocity data. The rotation solutions obtained for the PN and the H I are found to be the same, with the exception of a much larger vertical velocity dispersion for the PN. The increased vertical velocity dispersion can be explained as a consequence of a greater age. The observations are found to be consistent with the hypothesis that this increase is a result of stellar orbital diffusion processes, and that these processes operate in a similar manner to in the local solar neighbourhood.

The possibility that the PN and H I share the same kinematics was alluded to by Freeman *et al.* (1983) and must be reconciled with their finding that the old clusters ($> (1-2) \times 10^9$ years) have a rotation axis whose position angle differs from the younger populations by some 50°. The age of the PN population is such that twisting due to the close encounter of the LMC with the SMC some 2×10^8 years can be excluded. The most important follow-up research that presents itself is a new determination of the rotation solution for a large sample of old clusters with ages greater than $\sim 10^9$ years, to check the reality and cause of the twisting of the rotation axis of these clusters. Other interesting work would involve a study of stellar populations of different ages in the LMC, similar to that by Wielen (1977) for the solar neighbourhood, and a derivation of accurate diffusion coefficients.

Expansion velocities, absolute Hβ fluxes and nebular electronic densities have been measured for a large sample of PN in both the Large and Small Magellanic Clouds. These data are presented in papers two, three and four. Together with excitation classes determined by Morgan (1984), a number

of new evolutionary correlations have been determined.

Measurement of absolute Hβ nebular fluxes for the majority of known PN in the Magellanic Clouds has now been carried out from this study and that of Wood *et al.* (1987). These fluxes, in conjunction with electronic densities derived from the [O II] density sensitive doublet for about half this number has permitted a determination of ionized nebular masses for these objects. The range of masses is in the range from less than $0.01\mathcal{M}_{\odot}$ up to about $0.4\mathcal{M}_{\odot}$, and this is in agreement with the finding of Gathier (1983) for a sample of Galactic centre nebulae. Nebular evolutionary relationships between Hβ flux, density and mass point to a limiting density of order $5000 - 6000$ cm^{-3} below which the nebulae begin to become optically thin to Hydrogen ionizing radiation. This is in excellent agreement with the result found by Barlow (1987) for his sample of Magellanic Cloud PN using a different approach. The data also imply a nebular mass–radius relation of the form $M_{neb} \propto R^{3/2}$ for optically thick nebulae, while optically thin nebulae evolve at approximately constant or possibly even decreasing ionized mass.

Dopita *et al.* (1985) found a relationship between excitation class and expansion velocity for 44 PN in the Small Magellanic Cloud. Such a correlation also exists for the LMC nebulae, however, a much tighter correlation is found when the Hβ flux is included. In the event that the PN are optically thick the $\log F_{\mathrm{H}\beta}$: excitation class plane represents a transformed Hertzsprung–Russell (HR) diagram for the central stars, as excitation class is related to the Zanstra temperature of the nuclear star and Hβ flux counts the number of ionizing photons. But without detailed nebular modelling the relationship to the true HR diagram cannot

be determined. Detailed photo-ionization modelling would also be of assistance in determining a more "physical" understanding of excitation class and its relation to Zanstra temperature, since at the moment excitation is determined purely from a set of nebular emission line ratios (Morgan 1984). This will not be a straightforward task as excitation class depends not only on stellar temperature, but also the chemical composition of the central star (eg. Hydrogen or Helium rich), as well as nebular density.

A very direct evolutionary relationship was found connecting dynamical age, nebular mass and expansion velocity. This implies a relation between the net momentum and dynamical age of the ionizyed shell, and such a result is consistent with a theoretical model in which the energy content of the nebula increases rapidly with time and drives the expansion down the density gradient from the precursor Asymptotic Giant Branch star.

Adopting the relation between momentum and dynamical age as true allows a determination of age for all those nebulae with expansion velocities and ionized masses. The dynamical age is found to be strongly correlated with both excitation class and density. This dual correlation implying that the PN population forms a 2-parameter family with little intrinsic scatter appears to be of considerable interest in solving the question of distances to Galactic PN, as it implies that a distance can be determined from a knowledge of excitation class and density, together with the expansion velocity and angular size of a given nebula. All these parameters are independent of reddening and should be able to be measured accurately.

This question of distances to Galactic nebulae is addressed in the final paper. A sample of 64 southern nebulae has been observed and

radial velocities, expansion velocities, and where possible, densities derived. Together with published data on densities, and angular sizes, this permitted a calculation of dynamical ages, radii, distances, and nebular masses. The distances are found to be in good agreement with both the Daub (1982) and Maciel (1984) scales. Ionized masses determined for the Galactic PN in this sample exhibit the same range as found for the Magellanic Cloud objects, and cover the same area on a nebular mass–radius diagram.

The imminent launch of the Hubble Space Telescope (HST) will be the next major boost to the understanding of planetary nebulae, and especially so for the Magellanic Cloud nebulae. Its imaging capabilities will permit the angular resolution of many more nebulae, and this will allow the evolutionary relationships presented in this work to be verified and better determined. Ultraviolet spectra from the HST together with the large amount of ground-based data now existing will surely increase the understanding of planetary nebulae as the important link between Asymptotic Giant Branch evolution and the white dwarfs.

REFERENCES

Barlow, M.J. 1987, *M.N.R.A.S.*, **227**, 161.

Dopita, M.A., Ford, H.C., Lawrence, C.J. and Webster, B.L., 1985a, *Ap. J.*, **296**, 390.

Daub, C.T., 1982, *Ap. J.*, **260**, 612.

Feitzinger, J.V. 1979 Doctoral Thesis: Astronomisches Institut der Ruhr-Universitt, Bochum.

Freeman, K.C., Illingworth, G., and Oemler, A. 1983, *Ap. J.*, **272**, 488.

Gathier, R., Pottasch, S.R., Goss, W.M., and van Gorkom, J.H., 1983, *Astr. Ap.*, **128**, 325.

Maciel, W.J., 1984, *Astr. Ap. Suppl.*, **55**, 253.

Morgan, D.H., 1984, *M.N.R.A.S.*, **208**, 633.

Pottasch, S.R. 1980, *Astr. Ap.*, **89**, 336.

Rohlfs, K., Kreitschmann, J., Siegmann, B.C., and Feitzinger, J.V. 1984, *Astr. Ap.*, **137**, 343.

Wielen, R. 1977, *Astr. Ap.*, **60**, 263.

Wood, P.R., Meatheringham, S.J., Dopita, M.A., and Morgan, D.H., 1987, *Ap. J.*, **320**, 178.